Comments to the author by Co-Editor:
Three Anonymous Referees provided comments for your ACPD manuscript; two of them requested major revisions and the third one requested rejection. Therefore, I nominated the same three referees again to have a look at your revised ACPD submission. However, one of the three (who had requested major revisions) missed the nomination deadline. The other two provided comments; the one who had requested major revisions now requests minor revisions, but the one who recommended rejection still asks for rejection. I therefore invited a new third Referee; he/she requests major revisions.
Considering the comments of the three Referees for your revised ACPD submission, I request major revisions for it. I suggest that you take the comments of the three Anonymous Referees seriously into consideration and that you submit a newly revised manuscript.

Dear Prof. Dr. Maenhaut,

Thank you for giving us this opportunity to resubmit our manuscript. We appreciate the comments of the three anonymous referees to improve this paper, and have prepared our responses accordingly.

Anonymous Referee #2

Response to Reviewer #2

We kindly thank the referee for considering our manuscript and we value the comments raised to improve the manuscript. A point-to-point response (in regular typeset) to the reviewers' remarks (in italic typeset) follows. Changes to the manuscript are indicated in blue font. In the following, page and lines references refer to the previous version of the manuscript reviewed by anonymous referee #2.

The manuscript has improved considerably and can be published if the remarks listed below are implemented.

Comment #1
In the methodological section it must be clarified the total apportioned variable is the sum of the 14 trace elements. This is not obvious as SA studies, including some of those cited by the authors (Liu et al, 2019; Ji et al., 2018), most commonly apportion the total PM on the basis of elements and other chemical components. Similarly, in section 4.2, the sentence "In this section the final results of the elemental PM10 source apportionment are presented and validated" must be reworded to clarify the total variable is only the sum of the 14 elements used for the analysis. The same applies to Figure 2 where it must be stated that the average concentration is the sum of the elements.

We agree with reviewer #2 and we have modified the text in Abstract as follows:

We conducted source apportionment by positive matrix factorization (PMF) of the elemental mass measurable by the Xact (i.e., major elements heavier than Al), defined here as PM_{10el}.

Eight different sources were identified in PM_{10el} (elemental PM_{10}) mass driven by the sum of 14 elements.

We also added the following line in section 4.2 (page 11 line 4):
In this section, the results of the PM_{10el} mass driven by the sum of 14 elements are presented and validated.

Accordingly, we modified Figure 3 caption as follows:

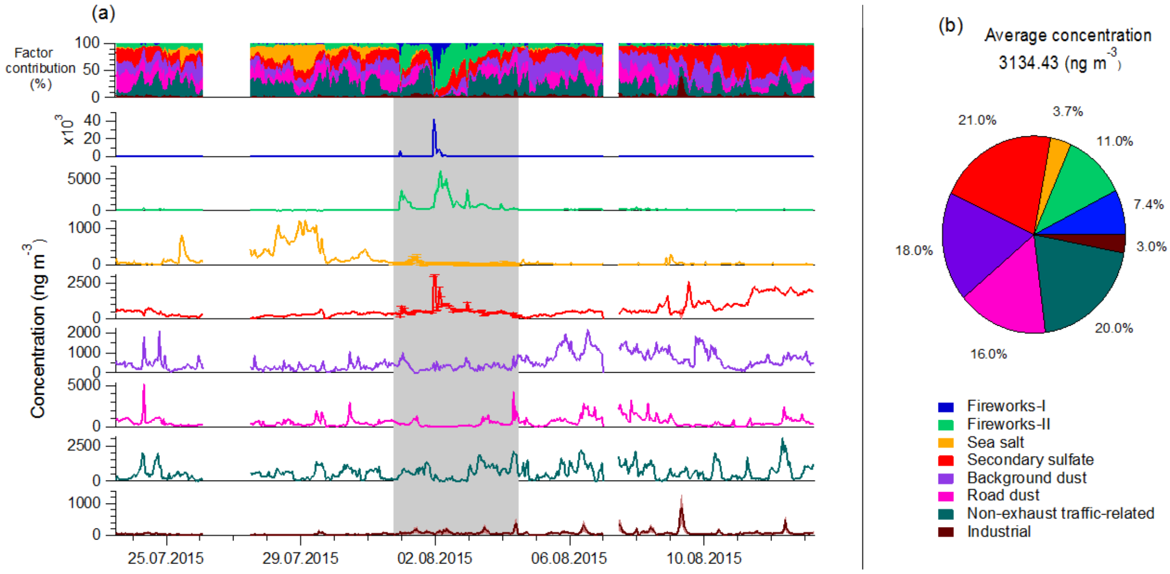

Figure 3: (a) Time series of the PM_{10el} sources and relative contributions of the different sources over time; shaded areas indicate the uncertainties (interquartiles) of selected bootstrap runs; grey background color represents the fireworks period; the estimated uncertainties of the secondary sulfate (± 5%) and the sea salt factors (± 42%) during the fireworks period are added as error bars; (b) Mean relative contributions of PM_{10el} sources. The average concentration represents the mean value of apportioned sources in PM_{10el} which is the sum of 14 elements.

Comment #2

Combining measurements obtained with different size cuts (in the fine fraction) introduces an additional degree of uncertainty but also gives the chance to handle a wider range of information at once. The additional uncertainty due to using different sizes could be modelled with PMF/ME-2. However, I agree that in this case it would be challenging to combine elemental data in the fine + coarse fractions with those of other components in the fine fraction only.

We appreciate the reviewer’s feedback on this issue.

Comment #3

There are other recent source apportionment studies using Xact 620/625 data than the six listed in Page 3 line 11 (you find some suggested papers in the references below).

Done.

Comment #4

The discussion about road salt is more convincing now. However, the composition of the deicing products may vary considerably between countries. It would be more appropriate to check with European rather than US data.

We have adopted the European deicing salt composition. We modified the text as follows:

The measured Cl / Ca ratio (0.33) from Xact does not lie in the range of de-icing salt composition (5.27) measured in northern Germany (Pernigotti et al., 2016).

Comment #5

The characterization of the industrial source is still rather vague. The authors should support their statement about the similarity with the profiles in the literature better. Two of the cited emission sources, smelter and coal combustion process, are pretty different from each other. In Ostrava, Vossler et al. identified two point sources associated with coal combustion: a power plant (Coal Power) and a "dirty" industrial profile (Industry 1) with high content of typical biomass burning components (K and Rb). None of these is a good representative of the industry sources.

We agree with reviewer #2 for concerning the wish for better literature to support the industrial factor. Since different workshops and ateliers surround the sampling site, small contributions from metal workshops can be expected. However, we have already mentioned some other references (Crilley et al., 2016; Richard et al., 2011) in the manuscript which have likewise retrieved a similar source profile without a direct link to a specific point source.

We have modified the text by removing the above citations (Amato et al., 2010; Dall'Osto et al. 2013; Vossler et al., 2016).

Comment #6

The conclusion that traffic is the main source of PM10 elements in a traffic site is weak as outcome of a source apportionment study. I suggest putting more emphasis on the influence of other sources (fireworks, as suggested by the authors) or background levels on the elemental composition at a traffic site.

We added the following text in the conclusions (page 15 line 29):

The outcome of this study emphasizes the significant influence of regional background secondary sulfate and local background dust apart from non-exhaust traffic emissions at the sampling location.

Anonymous Referee #3

Response to Reviewer #3

We kindly thank the referee for considering our manuscript and we value the comments raised to improve the manuscript. A point-to-point response (in regular typeset) to the reviewers' remarks (in italic typeset) follows. Changes to the manuscript are indicated in blue font. In the following, page and line references refer to the previous version of the manuscript reviewed by anonymous referee #3.

The authors of the paper ACP-2018-1229 performed a huge job to revise the paper and they partially answered the concerns risen during the discussion phase. The reviewer appreciated their efforts, which gave a better explanation of data treatment helping the reader to follow the analysis. Nevertheless, in the reviewer's opinion the procedure presented here is not fully convincing and it is still affected by a degree of subjectivity whose impact cannot be evaluated. Thus, in the reviewer's opinion it does not meet the scientific standards for publication in Atmospheric Chemistry and Physics.
More in detail:

Comment #1
The authors define the fireworks hour FH as July 31st 21:00 to August 1st 7:00. They run PMF on such database to constrain fireworks profile. The period includes 10 hours – i.e. 10 time slots. The authors state that they performed PMF on such data. At the reviewer's knowledge, 14 variables and 10 time slots used to resolve 5 factors by PMF should lead to scarcely reliable results due to lack of statistics (see https://source-apportionment.jrc.ec.europa.eu/Docu/european%20_guide_SA_RMs_revision_2019.pdf). Please consider that the results of the analysis are used to constrain fireworks profile in the final solution. Whether deriving constraints within a dataset is in principle possible (as proposed by Sofowote et al. 2015, http://dx.doi.org/10.1016/j.atmosenv.2015.02.045) in that case a very high number of samples was available to identify the constraints.

We agree that the appropriateness of an input dataset for PMF analysis is an important consideration. The number of time points required for such analysis is strongly dataset-dependent. To quote the PMF guidelines cited by the reviewer (https://source-apportionment.jrc.ec.europa.eu/Docu/european%20_guide_SA_RMs_revision_2019.pdf, p. 37):

> *"In practice, the minimum number of samples required to detect the latent variables cannot be established a priori as it depends on the amount of information contained in the dataset. If the relative contribution of sources were the same in all samples, analysing new samples would not add any new information to the model. Therefore, there should be enough samples to catch the variability of the sources, including samples where some sources are absent or negligible."*

This excerpt highlights the fact that the number of points itself is not the determining factor, but whether the dataset contains sufficient variability for the factors to be distinguished. The approximate rules for dataset size referenced by the reviewer are developed for application to typical ambient datasets. Such datasets are fundamentally different from analysis of the FH period, where the input PMF matrix is selected specifically to maximize the variability of a specific factor. As a result, far fewer time points are required to resolve the dominant (fireworks) factor.

This does still leave the question of how many points are too few. We test this issue with a bootstrap (BS) analysis on the FH dataset, which resamples 11 data points randomly by repeating or removing data points from the original 11 data points. If number of time points in the dataset were too small, one would expect a high degree of variability in the output solutions. The stability of the fireworks factor profile was assessed by investigation of 1000 random BS runs on the FH dataset (see more details below). Solutions were accepted based on a K / S ratio in the fireworks factor of 2.76 ± 0.5, consistent with black powder composition (Dutcher et al., 1999) and the concentration peak between 40-45 µg m^{-3} on 1 August 23:00 LT in the factor time series. This criterion yielded an acceptance rate of 21.3 %, with an average Q/Q_{exp} of 1.3. The results of the BS analysis are provided in Fig. S6, where we show the fractional composition of the fireworks factor profiles from: (a) FH BS analysis (blue color); (b) 5-factor constrained FH PMF analysis (base case, in red color). The data and their corresponding uncertainty are given as box-whisker plot (bottom to top: p10-p25-p50-p75-p90) of selected 213 solutions out of 1000 BS runs. The displayed error bars for the base case correspond to the a-value of 0.1 used to constrain fireworks profile in the complete dataset PMF analysis. This figure shows that the variation in fireworks profiles retrieved from the bootstrap analysis is relatively stable despite the small number of data points; indeed, it generally denotes a smaller range of values than those allowed by the constrained fireworks profile in the full dataset PMF. Further, the resolved fireworks profile from FH BS solution agrees well with the base case, and the Q/Q_{exp} values are reasonable. Taken together, these results suggest that the FH dataset contains sufficient variability to allow retrieval of a robust fireworks profile.

We fully agree that *if* analysis of the FH period were intended to quantitatively resolve *non-fireworks* factors, the number of time points in the dataset would be almost certainly insufficient. However, extraction of the fireworks factor from the specially constructed FH dataset is a different case that does not fall within the class of datasets considered in formulating general rules for PMF. Indeed, our FH analysis is conceptually similar to a simple subtraction of background aerosol from a plume in order to obtain the profile of the plume emissions source; the implementation of such a subtraction through PMF merely allows the subtraction to be more adaptive. This concept also motivates the independent estimation and constraint of the sea salt profile and time series during FH analysis, which further reduces the number of points required to resolve the FH profile.

Finally, we note that the general strategy of deriving an anchor profile from analysis of selected time points from a full dataset has been performed successfully on several occasions. Most similar to the current study are the examples of Froehlich et al. (2015), in which short-duration spikes in organic aerosol concentration were combined into a sub-dataset to determine an anchor profile related to local cigarette smoke, and Visser et al. (2015), in which a subset of a trace element dataset with high residuals was analysed separately to retrieve a factor profile related to industrial emissions.

We agree that it is important for the reader to be aware of the fundamental differences between analysis of a typical ambient dataset and a constructed one such as FH. Therefore we have added the following paragraph to section 3.2 (Page 8 line 31):

Note that the number of time points contained in the input matrices for the data subsets (as opposed to the full dataset) are in some cases smaller than typical recommendations for ambient PMF (Olivier et al., 2019). This is most extreme in the case of the FH dataset, where only 11 time points are used. However, there are two important differences between PMF analyses of these sub-datasets and typical ambient PMF: (1) the sub-datasets are constructed to maximize variability of a factor or set of factors; and (2) we are concerned only with accurately characterizing the profile(s) of these selected major factors. These two points work together to greatly reduce the number of time points required for the analysis (Fig. S6). A similar approach has been successfully applied by Froehlich et al. (2015), in which short-duration spikes in organic aerosol concentration were combined into a sub-dataset to determine an anchor profile related to local cigarette smoke, and Visser et al. (2015), in which a subset of a trace element dataset with high residuals was analysed separately to retrieve a factor profile related to industrial emissions.

We added the following text and figure in the supplement (page 2 line 3):

The stability of the fireworks factor profile was assessed by investigation of 1000 random BS runs on the FH dataset (see more details below). Solutions were accepted based on a K / S ratio in the fireworks factor of 2.76 ± 0.5, consistent with black powder composition (Dutcher et al., 1999) and the concentration peak between 40 - 45 µg m^{-3} on 1 August 23:00 LT in the factor time series. This criterion yielded an acceptance rate of 21.3 %, with an average Q/Q_{exp} of 1.3. The results of the BS analysis are provided in Fig. S6, where we show the fractional composition of the fireworks factor profiles from: (a) FH BS analysis (blue color); (b) five-factor constrained FH PMF analysis (base case, in red color). The data and their corresponding uncertainty are given as box-whisker plot (bottom to top: p10-p25-p50-p75-p90) of selected 213 solutions out of 1000 BS runs. The displayed error bars for the base case correspond to the a-value of 0.1 used to constrain fireworks profile in the complete dataset PMF analysis. This figure shows that the variation in fireworks profiles retrieved from the bootstrap analysis is relatively stable despite the small number of data points; indeed, it generally denotes a smaller range of values than those allowed by the constrained fireworks profile in the full dataset PMF. Further, the resolved fireworks profile from FH BS solution agrees well with the base case, and the Q/Q_{exp} values are reasonable. Taken together, these results suggest that the FH dataset contains sufficient variability to allow retrieval of a robust fireworks profile.

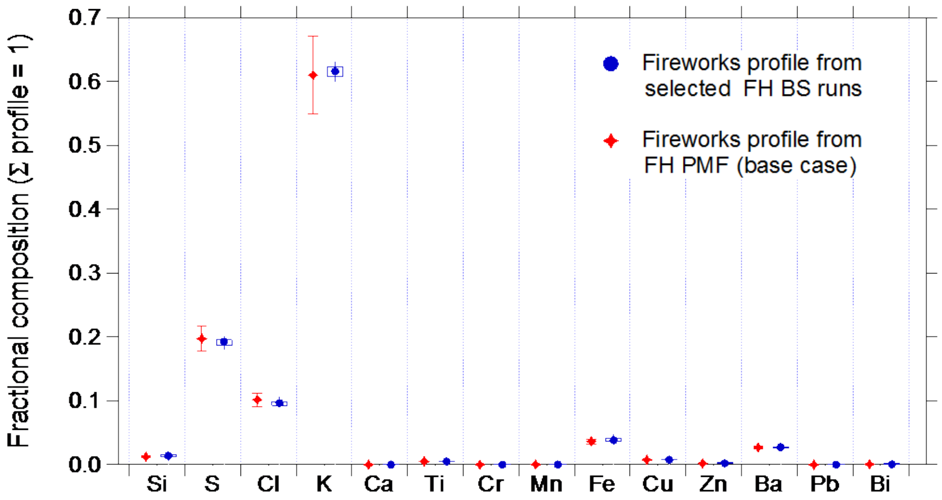

Figure S6: Fireworks factor profiles from: (a) FH BS analysis (blue color); (b) 5-factor constrained FH PMF analysis (base case, red color). The data and their corresponding uncertainties are given as box-whisker plot (bottom to top: p10-p25-p50-p75-p90) of selected 213 solutions from 1000 BS runs in blue color. Base case uncertainties are given ± 10 % as error bar by considering that *a*-value 0.1 is applied to constrain fireworks profile in complete dataset PMF analysis. Y-axis represents the fractional composition of the factor profile in row-wise for each factor in ng ng^{-1}.

Comment #2

No discussion on the Q increase due to the constraints is carried out. Opposite, this should be used to support the reliability of the imposed constraints. Excessive increase of Q may indicate an excess of subjectivity in the solution (Paatero and Hopke, 2009 DOI: 10.1002/cem.1197).

We agree that the effect of the constraints on the residuals for the FH dataset should be addressed. This can be done in a broad sense by investigation of constraint effects on *Q*, as suggested by the reviewer. However, because the purpose of this analysis is not a full description of the FH dataset but rather the fireworks component, it makes sense to also investigate the explained variation (EV) and unexplained variation (UEV) on an element-by-element basis. Finally, an additional consideration is that the application of constraints changes which factors are resolved and in what order as the number of factors in a solution increases. Specifically, while the five-factor constrained FH solution contains secondary sulfate, sea salt, fireworks, dust-related, and mixed K-rich/traffic factors, the five-factor unconstrained FH solution contains three factors related to fireworks, 1 mixed fireworks/traffic factor, and a dust-related factor. This significantly decreases the residuals but would be rejected in any normal PMF analysis due to a non-interpretable explanation of the data (i.e., excessive factor splitting/mixing). We therefore compare three solutions: (1) constrained five-factor FH, used in the paper to derive the fireworks profile; (2) unconstrained five-factor FH, and (3) unconstrained three-factor FH (which represents the most interpretable unconstrained FH solution.

As shown in Fig. S4, the constrained five-factor Q/Q_{exp} is 1.5, which is ~3 times higher than the unconstrained 5-factor Q/Q_{exp} but same as unconstrained five-factor Q/Q_{exp} (1.52). The increase in Q is significant over the constrained five-factor FH PMF and unconstrained three-factor because its UEV for each variable is between 2 % to 16 % (average ~10 %), while is it between 1.5 % to 15 % (average ~5 %) (see Fig. S5). The three-factor unconstrained FH PMF analysis validates the five-factor constrained FH PMF analysis, which suggests that both methods are working fine, and gives us more confidence to identify the fireworks factor profile.

We modified the text on page 8 line 30 as follows:

The unconstrained FH PMF analysis was also performed for two to five factors with different seeds. As shown in Fig. S4, the constrained five-factor Q/Q_{exp} is 1.5, which is ~3 times higher than the unconstrained five-factor Q/Q_{exp} but same as unconstrained 3-factor Q/Q_{exp} (1.52). The increase in Q is significant over the constrained five-factor FH PMF and unconstrained five-factor because its UEV for each variable is between 2 % to 16 % (average ~10 %), while is it between 1.5 % to 15 % (average ~5 %) (see Fig. S5). The three-factor unconstrained FH PMF analysis validates the five-factor constrained FH PMF analysis, which suggests that both methods are working fine, and gives us more confidence to identify the fireworks factor profile.

We have added the following text and figures in the supplement on page 2 line 3:

The unexplained variation (UEV, Paatero et al., 2004; Canonaco et al., 2013) which is a dimensionless quantity, describes how much of the measured variation (time or variable) is not explained by each PMF factor (Eq. S1, for variable j):

$$UEV_{j,k,real} = \frac{\sum_{i=1}^{n}\left(\left|e_{i,j}\right|/s_{i,j}\right)}{\sum_{i=1}^{n}\left(\left(\sum_{k=1}^{p}\left|g_{i,k}f_{k,j}\right|+\left|e_{i,j}\right|\right)/s_{i,j}\right)} \quad \text{for } k = 1, \ldots \ldots, p \text{ for } \left(x_{i,j}/s_{i,j}\right) > 2 \qquad \text{(S1)}$$

Where $f_{k,j}$ are the factor profiles and $g_{i,k}$ represent their time-dependent contributions. The index i represents a specific point in time (up to n), j is the variable, and k is a factor (up to p). $e_{i,j}$ are the PMF-residuals, $x_{i,j}$ the input data and $s_{i,j}$ the measurement uncertainties. The UEV presented here is the real UEV for high S/N threshold >2, otherwise UEV will be considered as noisy UEV.

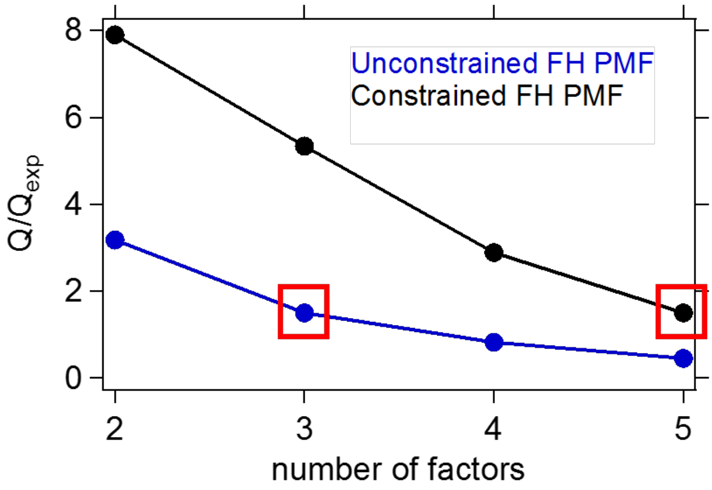

Figure S4: Q/Q_{exp} as a function of the number of factors for FH PMF analyses.

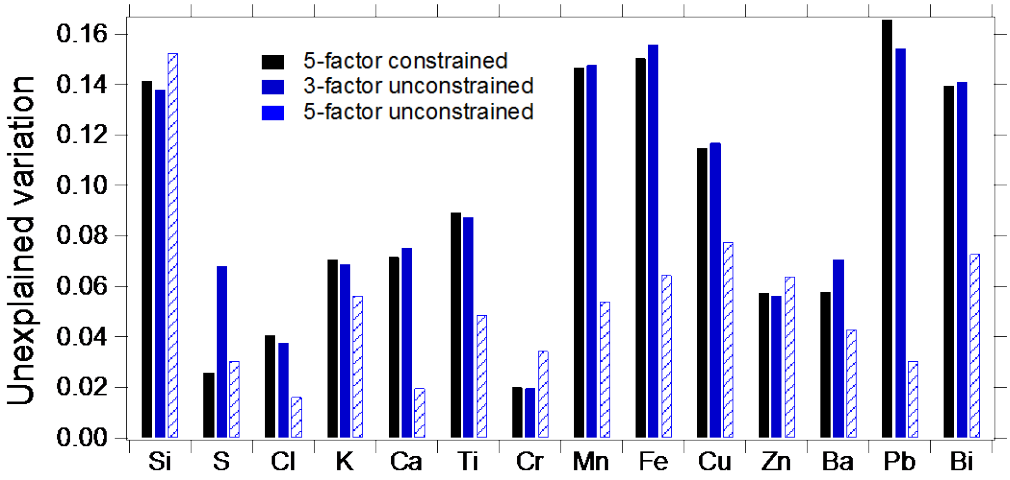

Figure S5: Unexplained variation for each variable in FH PMF solutions: (1) constrained 5-factor (black color); (2) unconstrained 5-factor (semi filled blue color); and (3) unconstrained 3-factor (blue color).

Comment #3

Implemented constraints e.g. to FD and FH analyses arise from different solutions from the same dataset. It is noteworthy that 9-factor unconstrained PMF on NFD was used to constrain the sulphate factor, whereas sea-salt was constrained using the 7-factor solution from the same dataset. In the reviewer's opinion, only one solution from the same dataset should be used as reference for constraints, as the sea-salt solution could have been impacted by the increase of factors needed to derive the sulphate one. Furthermore, the authors performed also background concentration interpolation of the concentrations before and after fireworks to obtain background levels during the episode. The absence of a detailed analysis of the Q-value increases compared to FD and FH unconstrained solutions do not allow to detect the degree of subjectivity in all these assumptions.

We believe the reviewer’s concern lies with the supposed derivation of factor constraints from two solutions to the same dataset having different numbers of factors. However, this is not done in the current analysis. On page 7 line 25, we state that the secondary sulfate factor was derived from a 9-factor unconstrained PMF on the complete dataset, whereas the sea salt profile was derived from a 7-factor unconstrained PMF solution from the NFD (non-fireworks days) dataset. However, we found a typo mistake on page 8 line 11, which should be “complete data set” instead of “NFD dataset”. This may have created misunderstanding to the reviewer. We apologise for that. Because these analyses are performed on different datasets, the set of factor(s) that can be cleanly extracted from each analysis also differs.

Based on the suggested changes due to comment #2, we believe that we have also answered the last part of the comment (*Q*-value for FH PMF). Since we did not use any solution from FD (fireworks days) PMF analysis, we do not want to discuss its *Q*-value in the manuscript. However, we have mentioned in the manuscript that we performed PMF on this dataset (test case) to resolve a fireworks profile, but we were not able to resolve a clean fireworks factor profile.

Comment #4

The authors report scaled residuals for the sulphate source in the range [-0.45, 0.85] for the unconstrained 9-factor NFD analysis: it is asymmetric and far from expected [-3, 3]. This unique factor merit to be commented more in detail.

Although the range of reported S scaled residuals [-0.45, 0.85] appears asymmetric, these endpoints are merely the minimum/maximum values recorded and do not reflect the shape of the overall distribution. The scaled residual distribution is nearly symmetric. This distribution has been added to the manuscript as Fig. S3 (and included below). We agree that the range of observed values for the scaled residuals are surprisingly close to zero. However, this is consistent with the overall Q/Q_{exp} (0.4) rather than a specific feature of the S variable, and suggests that the Xact uncertainties are systematically overestimated. As discussed in the text, we currently utilize a generic error model, although development of an instrument-specific formulation (that might give more accurate results) would certainly be of interest in the future

We have modified the text in the manuscript on page 7 line 28 as follows:

The scaled residual (over the time series) of S in this solution was within the range of ± 3 with very small values, as shown in Fig. S3. The strong influence of fireworks in this solution yielded small values of the scaled residual for S which are consistent also with lower-than-expected Q/Q_{exp} (0.4) values, suggesting an overestimation of uncertainties by the generic error model used herein (see Eqs. 6 and 7).

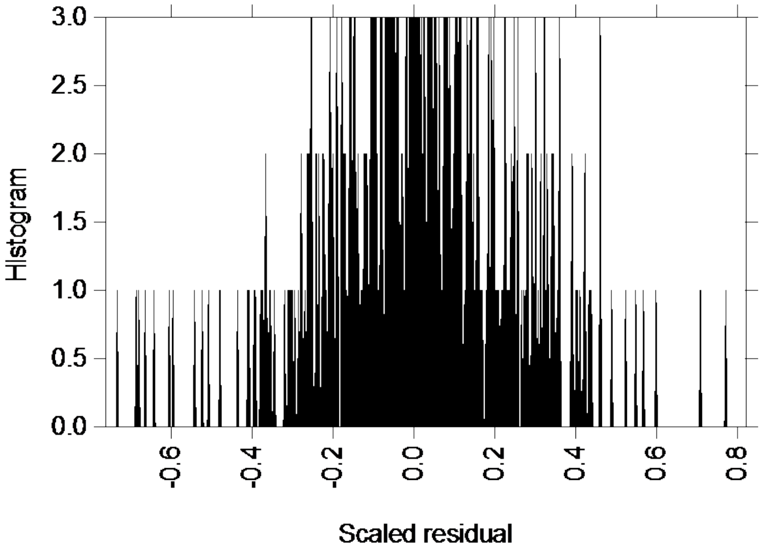

Figure S3: Histograms of the scaled residuals (e_{ij}/s_{ij}) for S in the nine-factor unconstrained PMF solution on the complete dataset.

Comment #5

Performing ten pseudorandom run is quite limited to explore possible multiple minima. Especially for the chosen solutions, the reviewer would expect more runs (30-50). Moreover, *it is now evident from the text that only in one case out of ten the authors were able to identify the unique factor sulphate mentioned above. Nevertheless, no comments on being the solution with the lowest Q or not. If not, what is the value compared with the lowest Q obtained in the ten pseudorandom runs?*

We agree, and have extended this analysis to 100 random seeds. We identified the secondary sulfate factor profile for 24 seeds out of 100 seeds. Note that the fraction of seeds yielding a given solution is unrelated to the mathematical quality or environmental interpretability of the solution. The distributions of the Q/Q_{exp} for 24 seeds (where the secondary sulfate factor was resolved) and the remaining 76 seeds are shown in Fig. S2 below. The distributions are not significantly different.

We have modified the text in manuscript on page 7 line 26 as follows:

The identified secondary sulfate factor time series correlated very well with ACSM sulfate (r^2 = 0.91) (Fig. S1) at 24 seeds out of 100 seeds while r^2 was ≤ 0.88 for the remaining 76 seeds. The Q/Q_{exp} values for all 100 seeds were in the range of 0.41- 0.45 (Fig. S2).

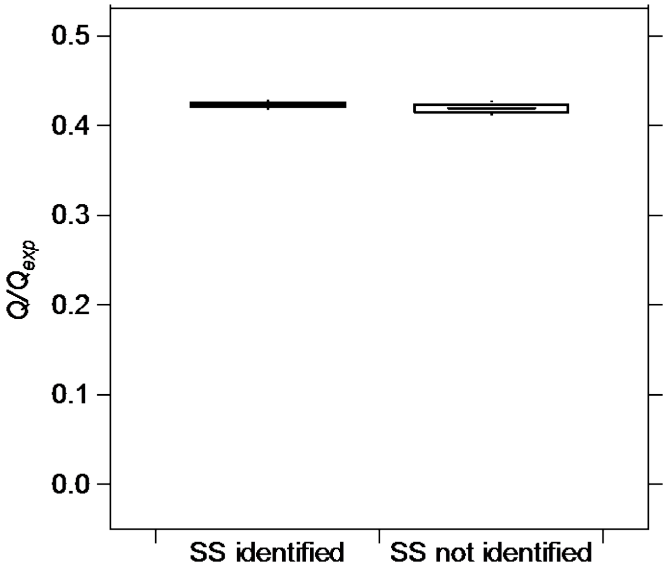

Figure S2: Box-whisker plots of Q/Q_{exp} for the seed analysis of the 9-factor unconstrained PMF on the full dataset. Shown separately are the 24 solutions in which a secondary sulfate (SS) factor was identified ("SS identified") and the 76 solutions where it was not ("SS not identified").

Comment #6

Mass apportionment: the reviewer is still convinced that an attempt to insert PM10 TEOM data to provide more information on PM10 source apportionment should be performed and commented.

The reviewer's suggestion could be a valid approach if PM_{10} were dominantly composed of sources identifiable from PMF analysis of the Xact data. However, this is clearly not the case. For example, secondary organic aerosol, a major PM_1 constituents, comprises a significant fraction (~60%) of PM_{10} (Richard et al., 2011), and has no direct relationship to any of the resolved sources. This is also the case for NO_3^- and primary organic aerosol from biological and cooking sources, while major constituents such as NH_4^+, black carbon, and other primary organics derive from sources that are only partly represented by species measured by the Xact (e.g., NH_4^+ is related to both S, which the Xact can measure, and NO_3^-, which it cannot). Unlike in chemical mass balance, where the ratios of the apportioned quantity to tracers are predetermined and any residual is deposited in its own factor, the PMF model will attempt to maximize apportionment of PM_{10} across all factors. In the present case, where it is expected that PM_{10} contains a significant contribution from sources to which the Xact is entirely blind, such an analysis will yield incorrect results. Further, it is not possible to assess the nature of the biases, e.g. whether the erroneously included PM_{10} mass were to be apportioned uniformly across all factors, predominantly to a single factor, or in a time-dependent way. As a result, we do not consider the addition of PM_{10} mass to the Xact PMF matrix to be a valid analysis strategy.

One could argue that the Xact and ACSM data should be combined in a PMF analysis. While we agree this would be a potentially useful strategy, it is also highly complex as demonstrated by previous combined PMF analyses (e.g. Slowik et al., 2010; Crippa et al., 2013). Given the already complex nature of the Xact-only PMF, we contend that this would need to be addressed in a standalone manuscript and is beyond the scope of the current study.

Anonymous Referee #4

Response to Reviewer #4

We kindly thank the referee for considering our manuscript and we value the comments raised to improve the manuscript. A point-to-point response (in regular typeset) to the reviewers' remarks (in italic typeset) follows. Changes to the manuscript are indicated in blue font. In the following, page and line references refer to the previous version of the manuscript reviewed by anonymous referee #4.

Comment #1

Regarding the manuscript entitled "Source apportionment of highly time resolved trace elements during a firework episode from a rural freeway site in Switzerland". The study is very interesting as the authors are using an approach that it is commonly used for the organic fraction of PM to a "portion" of the inorganic fraction of PM. The methodology that is used is thoroughly explained, the study is brilliantly written and the results are interesting. As it happens in every case that a new approach is tried, there are some fundamental assumptions that the authors need to make in order to use it. In my opinion there are some important questions to be answered before the study is published.

I understand that the authors aim to perform source apportionment analysis not on the full PM10 mass, but on the identified/used elements only. My first minor comment regarding this, is that it should be made very clear from the beginning of the manuscript and in the Abstract. In line 14 of the Abstract, the term "elemental PM10" is used to probably describe that approach. In my opinion this term is unclear and wrong. In line 17 the term "PM10 elemental *mass" is used, which is much more accurate but still unclear. It must be stated clearly that the work is representative of PM10 mass that corresponds to the used variables (around 20% of the total).*

We agree with reviewer #4 that our terminology may be misleading. We have modified it on page 1 line 12 as follows:

We conducted source apportionment by positive matrix factorization (PMF) of the elemental mass measurable by the Xact (i.e., major elements heavier than Al), defined here as PM_{10el}. Eight different sources were identified in PM_{10el} (elemental PM_{10}) mass driven by the sum of 14 elements.

Comment #2

My main concern and the question that rises, is even when the target is clear, is it possible to perform source apportionment analysis without major PM components? In principle you can perform SA in any type of dataset and the results will be representative of that mass. As the authors state correctly, when you do SA in organics, the results are representative for the organic mass only. The problem is that when the organics are used, all the possible (or at least most of them) organics compounds are taken into account. Here only a small fraction of the inorganics is used. My concern in this case, is not (only) the mass that it is missing when the ions and EC are not taken into account, but the tracers that are not present. For example, you can run PMF for the organics without m/z 43, 44, 55, 57 and 60 (or some of them), you still have enough mass to apportion, but you are missing key tracers that will help resolve the factors. It is the same as trying to identify traffic without EC. The authors should thoroughly discuss those limitations in the manuscript and explain why by the way the methodology is implemented the limitations are resolved. For example, in the conclusions the authors state that "We show that the rotational control available in ME-2 provides a means for treating extreme events such as fireworks within a PMF analysis". Even though that is true, the authors need to explain that the fact they have to resort in so complicated methodology to get a good solution, is not only due to the nature of the environmental situation at hand, but because of the lack of data. I strongly believe that if the ions and EC/OC were available the situation would be much simpler. It is extremely important to give the right message to the readers, that they need to use full and complete datasets in order to perform good source apportionment analysis. The authors may have the experience and expertise to work around it, but this fact must not be used as an example.

We agree with the reviewer on the need to clearly define the quantity being apportioned, which we have done in response to the previous comment. In regards to the reviewer's point about source resolution, we note that the key factor is the inclusion of measured variables that fully represent source variability (e.g., source-specific tracers) rather than the amount of total mass captured. On the other hand, including variables that are only partially representative of the key sources in a dataset can impede source apportionment.

For example, the reviewer suggests to include EC to improve separation of the traffic factor. However, we note that EC is emitted directly from the tailpipe, whereas the traffic factor identified herein is attributed primarily to break wear and, crucially, is significantly influenced by resuspension. Thus inclusion of EC would be expected to either (1) degrade separation of the current traffic factor or (2) form part of an additional factor not retrievable in the current dataset. Option (2) would be an attractive outcome, but would be best implemented in the context of an integrated source apportionment of data from multiple instruments, which is highly complex and beyond the scope of the current manuscript.

Overall, we find that the currently retrieved factors are well matched with the measured variables, with the following exceptions:

1. Sea salt would benefit from inclusion of Na.
2. Fireworks would benefit from the measurement and inclusion of Sr.

We have added the following line in conclusions (page 15 line 21):

The source apportionment model performance could possibly be additionally improved by the inclusion of Na and Sr to better resolve the sea salt and fireworks factors, respectively.

Comment #3

My other fundamental concern is the use of FH PMF resolved profile for constraining the firework profile. My problem is the number of "samples" that is used to run PMF is this case (for FH). How many samples are used? Are there enough to even run PMF let alone have good statistics? It has been proved that the suggested methodology works brilliantly for a usual organic dataset where thousand of measurements are available, but I am not certain that it works just as well with 500 samples (when you split the dataset and therefore reduce the variability) and I am certain that it does not work with less than 50. One can argue that this is a PMF/CMB hybrid and in CMB you can run the model successfully with one sample in principal. The problem is that in CMB external information is used to constrain the factors (regarding the source profiles), while in this case the information is extracted by the dataset itself, which in a way recycles the uncertainty.

This issue was addressed in response to reviewer #3 (comment #1) and we refer the reader to our response there.

Comment #4

The naming of the "Road dust" and "Traffic related" factors is wrong. The authors describe the Traffic related factor as "Coarse particles from brake/disc wear…" which is the exact definition of road dust! On the other hand, they describe "Road dust" as "The sampling site is located close to the freeway and must be influenced by wear and tear of the asphalt/concrete roads because of heavy traffic". I strongly suggest that the "Traffic related" factor is renamed to Road dust and the factor named "road dust" should be named "road abrasion". The are two types of traffic related sources: road dust and exhaust emissions. Since the factor that the authors name "road dust" cannot be exhaust emissions (there is no EC and authors describe it differently), it must be road dust. The naming makes much more sense that way since in this *case Road dust contains actual tracers of road dust such as Zn and Cu, and "road abrasion" can justify the presence of only Ca in the factor.*

We appreciate the concern raised by reviewer #4. However, we do not agree with reviewer for renaming the traffic-related factor as road dust. The factor profile of traffic-related (Fe, Cr, Cu, Zn, Mn, Zn, Ba) is attributed to non-exhaust traffic emissions such as: brake/disc wear, brake lining, tire wear, brake pads etc. This factor profile contains negligible contributions of crustal elements such as Ca and Ti, which indicates that the traffic-related factor is not influenced by dust-related sources. In the absence of size-segregated elemental PM data, we cannot draw conclusions about coarse or fine particles for these elements. On the other hand, brake wear/pads related elements have been found to be predominately in the coarse fraction (Bukowiecki et al., 2009; Amato et al., 2014; Harrison et al., 2012) which brackets the reference statement "Coarse particles from brake/disc wear could appear as flakes and mainly consist of iron oxides (Wahlström et al., 2010)".

For clarity, we therefore rename the "traffic-related" factor as "non-exhaust traffic-related". The factor named road dust represents the resuspension of particles emitted from road wear/tear, vehicle wear/tear and/or mineral dust during traffic rush hours. Yet, the factor profile of the road dust is different from the traffic-related factor profile, indicating resuspension of mineral dust and/or road wear/tear particles. The separation of road wear/tear and mineral dust profiles is often difficult due to the deposition of road wear/tear particles on the road surface, which are then resuspended together with deposited mineral dust. The high contribution of Ca alone (> 80%) has been seen in previous studies (Ducret-Stich et al., 2013; Bukowiecki et al., 2010; Hueglin et al., 2005) where it was named as "road dust". Another study at a rural site in Switzerland also found the Ca rich factor in the coarse fraction where it was linked to soil resuspension (Minguillon et al., 2012). The composition of road dust has been found to be dominated by elements and compounds typically associated with crustal material. The composition, therefore, often reflects the local geology and subsequently varies greatly with location. All these studies (except Minguillon et al., 2012) reported the road dust composition at various locations in Switzerland.

We have replaced "traffic-related" with "non-exhaust traffic-related" in the manuscript and the supplement. We have added the text in manuscript on page 13 line 29 as follows:

Road dust profiles are often difficult to identify due to resuspension of materials deposited on the road surface such as mineral dust, vehicle wear/tear, and/or road surface wear/tear. However, the road dust factor profile is distinct from the non-exhaust traffic-related factor profile. It is possible that the road dust factor is related to resuspension of mineral dust and road wear/tear particles. The high contribution of Ca alone (> 80%) has been seen in previous studies (Ducret-Stich et al., 2013; Bukowiecki et al., 2010; Hueglin et al., 2005) where it was named as "road dust". Another study at a rural site in Switzerland also found the Ca rich factor in the coarse fraction where it was linked to soil resuspension (Minguillon et al., 2012).

Comment #5

"The time series of secondary sulfate exhibits peaks during the fireworks event". Does this not mean that the factors are somewhat mixed? Secondary sulfate should not be related with fireworks. Please comment about that in the manuscript.

We agree with reviewer #4 that the secondary sulfate factor yielded peaks during fireworks event. Inorganic gases (SO_2, NO_x, etc.) emitted during the fireworks events may be oxidized to secondary organic and inorganic components that may condense to the particle phase (Sarkar et al., 2010) within a very short span of time, as observed in previous studies (Wang et al., 2007; Yang et al., 2014). We monitored two parameters to explain the influence of fireworks in secondary sulfate time series: (1) mass balance for ACSM PM_1 data; (2) secondary sulfate peaks during the main fireworks hours (1 August 23:00 LT to midnight). The equivalent concentration of ammonium (NH_{4eq}) balances the sum of NO_{3eq} and SO_{4eq} during non-fireworks periods, while during fireworks peaks, the balance shifts towards the sum of NO_{3eq} and SO_{4eq}. This indicates that sulfate related to fireworks adds up to an acidic budget of particles. The excess sulfate observed from this analysis is approximately in quantitative agreement (within 20%) with the enhancement of the secondary sulfate during fireworks period. The peak in secondary sulfate at 23:00 LT is slightly offset from the main fireworks peak because secondary sulfate formed maximum peak 1 h later (00:00 LT 2 August).

Taking these two together suggests that we may have some downstream production of sulphuric acid and conversion to ammonium sulfate, which makes secondary sulfate factor time series slightly delayed relative to main fireworks plume. Because this delay is consistent with chemical processing, we consider inclusion of this temporal feature in the secondary sulfate factor to be reasonable, although we cannot completely rule out some degree of mathematical mixing with the direct fireworks emissions.

We have added the following text in manuscript on page 15 line 5:

Inorganic gases (SO_2, NO_x, etc.) emitted during the fireworks events may be oxidized to secondary organic and inorganic components that may condense to the particle phase (Sarkar et al., 2010) within a very short span of time, as observed in previous studies (Wang et al., 2007; Yang et al., 2014). We monitored two parameters to explain the influence of fireworks in secondary sulfate time series: (1) mass balance for ACSM PM_1 data; (2) secondary sulfate peaks during the main fireworks hours (1 August 23:00 LT to midnight). The equivalent concentration of ammonium (NH_{4eq}) balances the sum of NO_{3eq} and SO_{4eq} during non-fireworks periods, while during fireworks peaks, the balance shifts towards the sum of NO_{3eq} and SO_{4eq}. This indicates that sulfate related to fireworks adds up to an acidic budget of particles. The excess sulfate observed from this analysis is approximately in quantitative agreement (within 20%) with the enhancement of the secondary sulfate during fireworks period. The peak in secondary sulfate at 23:00 LT is slightly offset from the main fireworks peak because secondary sulfate formed maximum peak 1 h later (00:00 LT 2 August). Taking these two together suggests that we may have some downstream production of sulphuric acid and conversion to ammonium sulfate, which makes secondary sulfate factor time series slightly delayed relative to main fireworks plume. Because this delay is consistent with chemical processing, we consider inclusion of this temporal feature in the secondary sulfate factor to be reasonable, although we cannot completely rule out some degree of mathematical mixing with the direct fireworks emissions.

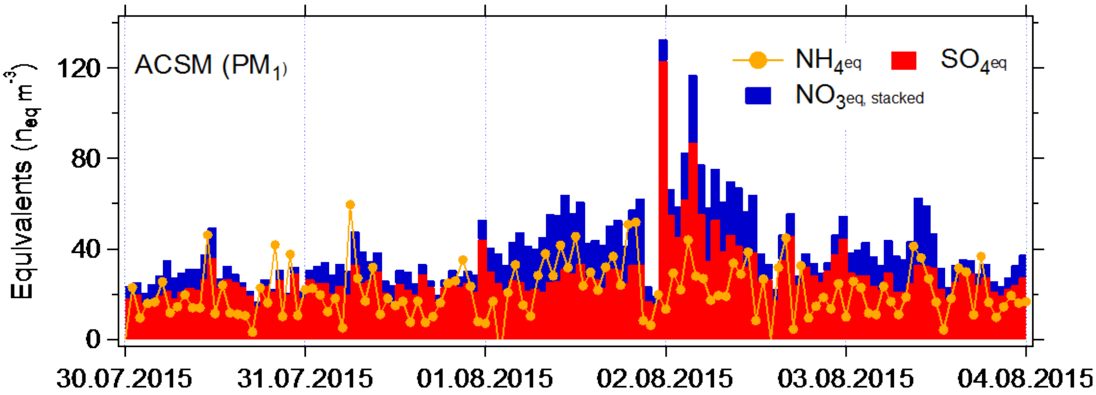

Figure S22: Time series of equivalents concentrations of the ACSM (PM$_1$) NH_{4eq}, and NO_{3eq} and +2*SO_{4eq}. The NO_{3eq} is stacked on 2*SO_{4eq}.

References

Amato, F., Nava, S., Lucarelli, F., Querol, X., Alastuey, A., Baldasano, J. M., and Pandolfi, M.: A comprehensive assessment of PM emissions from paved roads: Real-world emission factors and intense street cleaning trials, Sci. Total Environ., 408, 4309–4318, https://doi.org/10.1016/j.scitotenv.2010.06.008, 2010.

Amato, F., Alastuey, A., de la Rosa, J., Sánchez de la Campa, A. M., Pandolfi, M., Lozano, A., Contreras González, J., and Querol, X.: Trends of road dust emissions contributions on ambient air particulate levels at rural, urban and industrial sites in southern Spain, Atmos. Chem. Phys., 14, 3533–3544, https://doi.org/10.5194/acp-14-3533-2014, 2014.

Belis, C.A., Pikridas, M., Lucarelli, F., Petralia, E., Cavalli, F., Calzolai, G., Berico, M., and Sciare, J.: Source apportionment of fine PM by combining high time resolution organic and inorganic chemical composition datasets, Atmos, Environ., 3, 100046. https://doi.org/10.1016/j.aeaoa.2019.100046, 2019.

Bukowiecki, N., Lienemann, P., Hill, M., Figi, R., Richard, A., Furger, M., Rickers, K., Falkenberg, G., Zhao, Y., Cliff, S. S., Prévôt, A. S. H., Baltensperger, U., Buchmann, B., and Gehrig, R.: Real-world emission factors for antimony and other brake wear related trace elements: size-segregated values for light and heavy duty vehicles, Environ. Sci. Technol., 43, 8072–8078, https://doi.org/10.1021/es9006096, 2009.

Bukowiecki, N., Lienemann, P., Hill, M., Furger, M., Richard, A., Amato, F., Prévôt, A. S. H., Baltensperger, U., Buchmann, B., and Gehrig, R.: PM_{10} emission factors for non-exhaust particles generated by road traffic in an urban street canyon and along a freeway in Switzerland, Atmos. Environ., 44, 2330–2340, https://doi.org/10.1016/j.atmosenv.2010.03.039, 2010.

Canonaco, F., Crippa, M., Slowik, J. G., Baltensperger, U., and Prévôt, A. S. H.: SoFi, an IGOR-based interface for the efficient use of the generalized multilinear engine (ME-2) for the source apportionment: ME-2 application to aerosol mass spectrometer data, Atmos. Meas. Tech., 6, 3649–3661, https://doi.org/10.5194/amt-6-3649-2013, 2013.

Crilley, L. R., Lucarelli, F., Bloss, W. J., Harrison, R. M., Beddows, D. C., Calzolai, G., Nava, S., Valli, G., Bernardoni, V., and Vecchi, R.: Source apportionment of fine and coarse particles at a roadside and urban background site in London during the 2012 summer ClearfLo campaign, Environ. Pollut., 220, 766–778, https://doi.org/10.1016/j.envpol.2016.06.002, 2016.

Crippa, M., Canonaco, F., Slowik, J. G., El Haddad, I., De-Carlo, P. F., Mohr, C., Heringa, M. F., Chirico, R., Marchand, N., Temime-Roussel, B., Abidi, E., Poulain, L., Wiedensohler, A., Baltensperger, U., and Prévôt, A. S. H.: Primary and secondary organic aerosol origin by combined gas-particle phase source apportionment, Atmos. Chem. Phys., 13, 8411–8426, https://doi.org/10.5194/acp-13-8411-2013, 2013.

Dall'Osto, M., Querol, X., Amato, F., Karanasiou, A., Lucarelli, F., Nava, S., Calzolai, G., and Chiari, M.: Hourly elemental concentrations in PM2.5 aerosols sampled simultaneously at urban background and road site during SAPUSS – diurnal variations and PMF receptor modelling, Atmos. Chem. Phys., 13, 4375–4392, https://doi.org/10.5194/acp-13-4375-2013, 2013.

Ducret-Stich, R. E., Tsai, M.-Y., Thimmaiah, D., Kunzli, N., Hopke, P. K., and Phuleria, H. C.: PM10 source apportionment in a Swiss Alpine valley impacted by highway traffic, Environ. Sci. Pollut. Res., 20, 6496–6508, https://doi.org/10.1007/s11356-013-1682-1, 2013.

Dutcher, D. D., Perry, K. D., Cahill, T. A., and Copeland, S. A.: Effects of indoor pyrotechnic displays on the air quality in the Houston Astrodome, J. Air Waste Manage. Assoc., 49, 156–160, https://doi.org/10.1080/10473289.1999.10463790, 1999.

Fröhlich, R., Cubison, M. J., Slowik, J. G., Bukowiecki, N., Canonaco, F., Croteau, P. L., Gysel, M., Henne, S., Herrmann, E., Jayne, J. T., Steinbacher, M., Worsnop, D. R., Baltensperger, U., and Prévôt, A. S. H.: Fourteen months of on-line measurements of the non-refractory submicron aerosol at the Jungfraujoch (3580 m a.s.l.) – chemical composition, origins and organic aerosol sources, Atmos. Chem. Phys., 15, 11373–11398, https://doi.org/10.5194/acp-15-11373-2015, 2015.

Harrison, R. M., Jones, A. M., Gietl, J., Yin, J., and Green, D. C.: Estimation of the Contributions of Brake Dust, Tire Wear, and Resuspension to Non-exhaust Traffic Particles Derived from Atmospheric Measurements, Environ. Sci. Technol., 46, 6523−6529, https://doi.org/10.1021/es300894r, 2012.

Hueglin, C., Gehrig, R., Baltensperger, U., Gysel, M., Monn, C., and Vonmont, H.: Chemical characterisation of $PM_{2.5}$, PM_{10} and coarse particles at urban, near-city and rural sites in Switzerland, Atmos. Environ., 39, 637–651, https://doi.org/10.1016/j.atmosenv.2004.10.027, 2005.

Jeong, C.-H., Wang, J. M., Hilker, N., Debosz, J., Sofowote, U., Su, Y., Noble, M., Healy, R. M., Munoz, T., Dabek-Zlotorzynska, E., Celo, V., White, L., Audette, C., Herod, D., and Evans, G. J.: Temporal and spatial variability of traffic-related $PM_{2.5}$ sources: Comparison of exhaust and non-exhaust emissions, Atmos. Environ., 198, 55–69, https://doi.org/10.1016/j.atmosenv.2018.10.038, 2019.

Minguillon, M. C., Querol, X., Baltensperger, U., and Prévôt, A. S. H.: Fine and coarse PM composition and sources in rural and urban sites in Switzerland: local or regional pollution?, Sci. Total Environ., 427–428, 191–202, https://doi.org/10.1016/j.scitotenv.2012.04.030, 2012.

Olivier, F., Belis, C. A., Amato, F., Decesari, S., Diapouli, E., El Haddad, I., Gilardoni, S., Harrison, R. M., Hopke, P. K., Larsen, B. R., Manousakas, M., Mocnik, G., Mooibroek, D., Nava, S., Paatero, P., Paglione, M., Prévôt, A. S. H., Quass, U., Salvador, P., Takahama, S., Vecchi, R., Viana, M., and Vratolis, S: European guide on air pollution source apportionment with receptor models revision 2019, https://source-apportionment.jrc.ec.europa.eu/Docu/european%20_guide_SA_RMs_revision_2019.pdf.

Paatero, P.: User’s guide for positive matrix factorization programs PMF2 and PMF3, 2004.

Pernigotti, D., Belis, C. A., and Spanó, L.: SPECIEUROPE: The European data base for PM source profiles, Atmos. Pollut. Res., 7 (2), 307–314, https://doi.org/10.1016/j.apr.2015.10.007, 2016.

Richard, A., Gianini, M. F. D., Mohr, C., Furger, M., Bukowiecki, N., Minguillón, M. C., Lienemann, P., Flechsig, U., Appel, K., DeCarlo, P. F., Heringa, M. F., Chirico, R., Baltensperger, U., and Prévôt, A. S. H.: Source apportionment of size and time resolved trace elements and organic aerosols from an urban courtyard site in Switzerland, Atmos. Chem. Phys., 11, 8945–8963, https://doi.org/10.5194/acp-11-8945-2011, 2011.

Sarkar, S., Khillare, P. S., Jyethi, D. S., Hasan, A., and Parween, M.: Chemical speciation of respirable suspended particulate matter during a major firework festival in India, J. Hazard. Mater., 184, 321–330, https://doi.org/10.1016/j.jhazmat.2010.08.039, 2010.

Slowik, J. G., Vlasenko, A., McGuire, M., Evans, G. J., and Abbatt, J. P. D.: Simultaneous factor analysis of organic particle and gas mass spectra: AMS and PTR-MS measurements at an urban site, Atmos. Chem. Phys., 10, 1969–1988, https://doi.org/10.5194/acp-10-1969–2010, 2010.

Sofowote U. M., Healy R. M., Su Y., Debosz J., Noble M., Munoz A., Jeong C.-H., Wang J. M., Hilker N., Evans G.J, and Hopke P. K.: Understanding the $PM_{2.5}$ imbalance between a far and near road location: Results of high temporal frequency source apportionment and parameterization of black carbon, Atmos. Environ., 173, 277–288., https://doi.org/10.1016/j.atmosenv.2017.10.063, 2018.

Visser, S., Slowik, J. G., Furger, M., Zotter, P., Bukowiecki, N., Canonaco, F., Flechsig, U., Appel, K., Green, D. C., Tremper, A. H., Young, D. E., Williams, P. I., Allan, J. D., Coe, H., Williams, L. R., Mohr, C., Xu, L., Ng, N. L., Nemitz, E., Barlow, J. F., Halios, C. H., Fleming,

Z. L., Baltensperger, U., and Prévôt, A. S. H.: Advanced source apportionment of size-resolved trace elements at multiple sites in London during winter, Atmos. Chem. Phys., 15, 11291–11309, https://doi.org/10.5194/acp-15-11291-2015, 2015.

Vossler, T., Černikovský, L., Novák, J., and Williams, R.: Source apportionment with uncertainty estimates of fine particulate matter in Ostrava, Czech Republic using positive matrix factorization, Atmos. Pollut. Res., 7, 503–512, https://doi.org/10.1016/j.apr.2015.12.004, 2016.

Wang, Y., Zhuang, G. S., Xu, C., and An, Z. S.: The air pollution caused by the burning of fireworks during the lantern festival in Beijing, Atmos. Environ., 41, 417–431, https://doi.org/10.1016/j.atmosenv.2006.07.043, 2007.

Yang, L. X., Gao, X. M., Wang, X. F., Nie, W., Wang, J., Gao, R., Xu, P. J., Shou, Y. P., Zhang, Q. Z., and Wang, W. X.: Impacts of firecracker burning on aerosol chemical characteristics and human health risk levels during the Chinese New Year Celebration in Jinan, China, Sci. Total Environ., 476–477, 57–64, https://doi.org/10.1016/j.scitotenv.2013.12.110, 2014.

Source apportionment of highly time resolved ~~trace~~ elements during a firework episode from a rural freeway site in Switzerland

Pragati Rai[1], Markus Furger[1], Jay G. Slowik[1], Francesco Canonaco[1], Roman Fröhlich[1], Christoph Hüglin[2], María Cruz Minguillón[3], Krag Petterson[4], Urs Baltensperger[1] and André S.H. Prévôt[1]

[1]Laboratory of Atmospheric Chemistry, Paul Scherrer Institute, Villigen PSI, 5232, Switzerland
[2]Laboratory for Air Pollution / Environmental Technology, Empa, 8600 Dübendorf, Switzerland
[3]Institute of Environmental Assessment and Water Research (IDAEA), CSIC, 08034 Barcelona, Spain
[4]Cooper Environmental Services (CES), 9403 SW Nimbus Avenue, Beaverton, OR 97008, USA

Correspondence to: André S. H. Prévôt (andre.prevot@psi.ch) and Markus Furger (markus.furger@psi.ch)

Abstract. ~~Trace~~ The ~~element~~ measurement~~s~~ of elements in PM_{10} were performed with 1 h time resolution at a rural freeway site during summer 2015 in Switzerland using the Xact 625 multi-metals monitor. On average the Xact elements (without accounting for oxygen and other associated elements) make up about 20 % of the total PM_{10} mass (14.6 µg m^{-3}). We conducted source apportionment by positive matrix factorization (PMF) of the elemental mass measurable by the Xact (i.e., major elements heavier than Al), defined here as PM_{10el}. Eight different sources were identified in PM_{10el} (elemental PM_{10}) mass driven by the sum of 14 elements~~Subsequently, a source apportionment by positive matrix factorization (PMF) implemented via the Source Finder software (SoFi Pro version 6.2, PSI, Switzerland) was applied. Eight different sources were identified for elemental~~ ~~PM_{10}~~ (notable elements in brackets): fireworks-I (K, S, Ba, Cl), fireworks-II (K), sea salt (Cl), secondary sulfate (S), background dust (Si, Ti), road dust (Ca), ~~traffic-related~~non-exhaust traffic-related (Fe) and industrial (Zn, Pb). The major components were secondary sulfate and ~~traffic-related~~non-exhaust traffic-related followed by background dust and road dust factors, explaining 21 %, 20 %, 18 % and 16 % of the analysed PM_{10} elemental mass, respectively, with the factor mass not corrected for oxygen content. Further, there were minor contributions (on the order of a few percent) of sea salt and industrial sources. The regionally influenced secondary sulfate factor showed negligible resuspension, and concentrations were similar throughout the day. The significant loads of the ~~traffic-related~~non-exhaust traffic-related and road dust factors with strong diurnal variations highlight the continuing importance of vehicle-related air pollutants at this site. Enhanced control of PMF implemented via the Source Finder software (~~using~~ SoFi Pro version 6.2, PSI, Switzerland) allowed for a successful apportionment of transient sources such as the two firework factors and sea salt, which remained mixed when analysed by unconstrained PMF.

1 Introduction

Ambient particulate matter (PM) plays a major role in affecting human health and air quality. Trace elements represent a minor fraction of the atmospheric aerosol on a mass basis, but they can act as specific markers for several emission sources.

The short- or long-term exposure of ambient particulate matter (PM) has significant negative effects on human health (Dao et al., 2012; Ancelet et al., 2012; Zhao and Hopke, 2004; Pope and Dockery, 2006; Dockery et al., 1993; Zhou et al., 2018). Cakmak et al. (2014) found significant association of acute changes in cardiovascular and respiratory physiology with $PM_{2.5}$ metals in Ontario, Canada. In Stockholm, Meister et al. (2012) estimated a 1.7 % increase in the daily mortality per 10 µg m^{-3} increase in the coarse fraction of PM. Metallic components of PM, especially the fine fraction of elements such as Fe, Ni, Cu, V, Pb and Zn, appear to be a significant cause of both pulmonary and cardiovascular diseases (Kelly and Fussell, 2012). Airborne particles and associated (trace) elements originate from various emission sources, such as motor vehicles, power plants, construction activities, in a broad size range. Among them, traffic-related emissions are of particular interest (Brauer et al., 2002). Traffic-derived PM has a high risk of respiratory illness, asthma and cardiovascular diseases, resulting in an increased rate in mortality (Kelly and Fussell, 2011). Traffic-related PM is emitted mainly as exhaust emissions (tailpipe exhaust from gasoline and diesel engines) and non-exhaust emissions (resuspension of road dust and brake and tire wear emissions) (Lawrence et al., 2013; Lin et al., 2015; Thorpe and Harrison, 2008; Zhou et al., 2018; Grigoratos and Martini, 2015; Amato et al., 2014b; Bukowiecki et al., 2010). Exhaust emissions are predominantly in the fine fraction of PM, whereas non-exhaust emissions contribute mostly to the coarse fraction (Amato et al., 2011; Thorpe and Harrison, 2008). Exhaust emission-related elements are comprised of Pb, Zn, Ni and V (Lin et al., 2015; Minguillon et al., 2012), while the non-exhaust emissions are dominated by Fe, Cu, Ba, Ca, Sb, Sn, Cr and Zn from brake lining and tire wear. The presence of Fe in brake lining can reach up to 60 % by weight (Chan and Stachowiak, 2004; Schauer et al., 2006). Brake pads are usually filled with $BaSO_4$, while Sb, Sn and Mo sulfides are often added as lubricants, and Cu, Cr and Zn are major additives to lubricating oils and normally used to improve friction (Thorpe and Harrison, 2008; Amato et al., 2014a). Sb has been identified as a major tracer of brake wear, due to significant (1–5 %) percentage of Sb in brake linings in the form of stibnite (Sb_2S_3) (Grigoratos and Martini, 2015; Bukowiecki et al., 2009). It has been reported that asphalt pavement-induced particles were characterized mainly by high concentrations of Cu, Cr, Ni, As and Pb (Yu, 2013) as well as Ca, Si, Mg, Al, Fe, P, S, Cl, K, V, Mn, Na (Fullova et al., 2017). Therefore, it is important to monitor traffic emissions for health risk assessment, the study of which relies heavily on the source apportionment (SA) of PM using chemically speciated data (Zhou et al., 2018).

Source quantification and characterization is an important step in understanding the relationship between source emissions, ambient concentrations, and health and environmental effects. SA by receptor models has been widely used in recent years to identify and apportion the contributions of various sources to the airborne PM concentrations. Positive Matrix Factorization (PMF) is one of the most widely used receptor models for SA of trace elements (Rahman et al., 2011; Ancelet et al., 2012; Cesari et al., 2014; Ducret-Stich et al., 2013; Kim et al., 2003; Rai et al., 2016; Zhang et al., 2013; Harrison et al., 2011; Hedberg et al., 2005). However, a very limited number of studies are available for trace elements emission sources with high time resolution (hourly or sub-hourly) (Visser et al., 2015; Crilley et al., 2016; Bukowiecki et al., 2010; Richard et al., 2011; Dall'Osto et al., 2013; Manousakas et al., 2015; Jeong et al., 2019; Wang et al., 2018, among others). Hourly elements data can be used to explore the diurnal patterns of emissions from traffic, biomass burning and industrial sources, thereby yielding more accurate and exposure-relevant SA results. Currently, there are very few offline instruments available for field sampling of elements with high time resolution, such as the rotating drum impactor (RDI) (Bukowiecki et al., 2008), the streaker sampler (PIXE International Corporation) (Lucarelli et al., 2011) and the semi-continuous elements in aerosol sampler (SEAS) (Kidwell and Ondov, 2001). The large quantity of samples generated by these samplers requires a labour intensive and time consuming offline analysis. These offline analyses require high precision and low detection limit techniques such as synchrotron radiation induced X-ray fluorescence spectrometry (SR-XRF) of aerosol samples collected with a RDI, particle induced X-ray emission (PIXE) with the streaker sampler, and graphite furnace atomic absorption spectrometry (GFAAS) with the SEAS. In practice, the offline samplers lead to undesirable trade-offs between time resolution and data coverage even for short duration field campaigns, whereas highly time-resolved long-term measurements are impractical. A recently introduced online high time resolution instrument can collect samples and perform analysis for elements simultaneously in a near real time scenario for long-term measurements without waiting for laboratory analysis. The XRF-based Xact 620, 625 and the newer 625i ambient metals monitors (Cooper Environmental Services, Beaverton, Oregon, USA) have been developed in recent years and have been used in several field studies (Fang et al., 2015; Cooper et al., 2010; Furger et al., 2017; Park et al., 2014; Phillips-Smith et al., 2017; Tremper et al., 2018; Chang et al., 2018; Liu et al., 2019). However, only 10~~six~~ studies included SA on Xact data (Park et al., 2014; Fang et al., 2015; Phillips-Smith et al., 2017; Chang et al., 2018; Liu et al., 2019; Ji et al., 2018; Sofowote et al., 2018; Jeong et al., 2019; Belis et al., 2019; Cui et al., 2019).

The main focus of this work is the exploration of the use of the Xact for source apportionment in Europe where the concentrations are considerably lower than in polluted areas in Asia. In the present study, we conducted SA using PMF to characterize the source contributions of highly time-resolved metals during a three-week campaign at a traffic-influenced site in Härkingen, Switzerland. PMF was implemented through the multilinear engine-2 (ME-2) solver and controlled via SoFi, which allows for a comprehensive and systematic exploration of the solution space (Bozzetti et al., 2016; Canonaco et al., 2013). The rotational control available in ME-2 provides a means for treating extreme events such as fireworks within a PMF analysis. Such events are often excluded from the PMF input matrix to avoid modelling errors due to the pulling of a solution by outliers (Ducret-Stich et al., 2013; Norris et al., 2014). Although a few studies have already been carried out in the past at this location (Lanz et al., 2010; Hueglin et al., 2006; Furger et al., 2017), none of them have reported SA on elements.

2 Experimental setup and data analysis

2.1 Sampling location

PM_{10} sampling was performed from 23 July until 13 August 2015 in Härkingen, Switzerland, a permanent station of the Swiss Air Pollution Monitoring Network (NABEL) (Fig. 1). Extreme firework episodes were captured during the Swiss National Day Celebration (1 August). The site is situated next to the A1 freeway, which is the main traffic route between eastern (Zurich) and western (Bern) Switzerland. The measurement site is bordered by agricultural areas to the west and north while there are villages in the south and east direction. There is a metal processing company to the south-east across the freeway which manufactures wheels for passenger cars and commercial vehicles, and some small scale industrial buildings to the north-west. The emissions reaching the measurement site depend on wind direction. The site is strongly influenced by local road traffic emissions when winds come from the southern sector, while the northern wind sector represents the air constituents from a rural area. A detailed description of the sampling site can be found in previous studies (Furger et al., 2017; Hueglin et al., 2006)

2.2 Sampling and analysis

Sampling and analysis was conducted with an Xact 625 ambient metals monitor equipped with a PM_{10} inlet. The instrument was set up to quantify 24 elements (Si, S, Cl, K, Ca, Ti, V, Cr, Mn, Fe, Co, Ni, Cu, Zn, As, Se, Cd, Sn, Sb, Ba, Pt, Hg, Pb and Bi) with 1 h time resolution. In addition, 24-h PM_{10} samples were collected by a HiVol sampler (Digitel DA-80H, DIGITEL Hegnau, Switzerland) with quartz fiber filters (Pallflex XP56 Tissuquartz 2500QAT-UP, Pall, AG, Switzerland). Ten of these 24-h PM_{10} samples were analysed by inductively coupled plasma optical emission spectrometry (ICP-OES) for the concentrations of Na, Mg, Al, P, S, K, Ca, Ti and Fe. Moreover, the station was equipped with other instruments such as a tapered element oscillating microbalance filter dynamics measurement system (TEOM FDMS 8500, Thermo Fischer Scientific, MA, USA) for 10 min PM_{10} mass concentration measurements, a multi angle absorption photometer (MAAP, Thermo 5012, Thermo Fischer Scientific, MA, USA) for balck carbon (BC) measurements in $PM_{2.5}$ and standard meteorological sensors (temperature, wind speed and direction, precipitation). The trace gases were measured with conventional instruments by the Swiss National Air Pollution Monitoring Network, NABEL (Empa, 2011). The time resolution of all these instruments was 1 h. The station also provided hourly traffic counts for the freeway in the form of total number of vehicles, number of heavy-duty vehicles (HDV), and the number of light-duty vehicles (LDV). NO_x was measured by chemiluminescence spectroscopy (Horiba APNA 370). Specifically for the campaign, a quadrupole aerosol chemical speciation monitor (Q–ACSM 140-145, Aerodyne Inc, Billerica, MA, USA) with vacuum aerodynamic diameters smaller than 1µm (non-refractory-PM_1) was deployed (Ng et al., 2011; Crenn et al., 2015) and the data were used for comparison of the factors during the SA analysis.

2.3 PMF using ME-2

Positive matrix factorization is one of the most common receptor models based on a weighted least squares fit (Paatero and Tapper, 1994). It is used to describe the variability of a multivariate dataset as the linear combination of a set of constant factor profiles and their corresponding time series as shown in Eq. (1) in cell notation:

$$x_{ij} = \sum_{k=1}^{p} g_{ik} f_{kj} + e_{ij} , \qquad (1)$$

where **X**, **G**, **F** and **E** represent the data matrix, factor time series, factor profiles and residual matrices, respectively, while *i*, *j* and *k* indices denote time, element, and factor number. The index *p* represents the total number of factors in the PMF solution. The PMF model iteratively solves Eq. (1) by minimizing the object function (Q), defined as:

$$Q = \sum_i \sum_j \left(\frac{e_{ij}}{s_{ij}}\right)^2 , \qquad (2)$$

Here, s_{ij} corresponds to the measurement uncertainty (error matrix) for the input point *ij*.

The PMF algorithm was solved using ME-2 (Paatero, 1999), which enables an efficient exploration of the solution space by introducing *a priori* information to **G** and / or **F** into the PMF model. Using the constraining technique of the *a*-value, one or more factor profile/factor time series can be confined by the scalar a ($0 \leq a \leq 1$), which can be applied to the entire profile/time series or to individual variables/data points of the profile/time series. The scalar a defines how much the resolved factors are allowed to deviate from the input profile/time series, according to:

$$f'_{kj} = f_{kj} \pm a \times f_{kj} , \qquad (3)$$

$$g'_{ik} = g_{ik} \pm a \times g_{ik} , \qquad (4)$$

where the subscript *j* varies between 0 and the number of variables and *i* varies between 0 and the number of measured data points in time. f_{kj} and g_{ik} are the starting value used as a *priori* knowledge from the base case solution in this SA study, and f'_{kj} and g'_{ik} are the resulting values in the solution. Normalization in Eq. (3) and (4) can lead to the resulting values slightly outside the specified *a*-value boundaries. This method reduces the available solution space and directs the solution towards an optimized and environmentally meaningful solution. The ~~Source Finder software~~ SoFi Pro (Canonaco et al., 2013) which is coded in the Igor Pro software environment (Wavemetrics, Inc., Portland, OR, USA) was used for the PMF configuration and analysis.

2.4 Conditional bivariate polar function (CBPF) plots

CBPF is a data analysis tool to identify the direction of source contributions and was applied to the PMF source factors. Polar plots are used to present the CBPF analyses, where the number of events with a concentration greater than the ith percentile (0 to 100) is plotted as a function of both wind speed and direction, as shown in Eq. (5):

$$CBPF = \frac{m_{\theta,r}}{n_{\theta,r}} , \qquad (5)$$

where $m_{\theta,r}$ is the number of samples in wind sector θ and wind speed sector r with a concentration greater than the ith percentile and $n_{\theta,r}$ is the total number of samples with the same wind direction and speed (Carslaw and Beevers, 2013). The resultant CBPF polar plots present the probability that high concentrations of a pollutant correspond to a particular wind direction and speed and can give insight into the contributions from local and regional sources.

3 SA method and solutions selection

3.1 PMF input preparation

In our study, the PMF input consists of a data matrix and an error matrix of hourly element measurements, where the rows represent the time series (456 points with 1 h steps) and the columns contain the elements (14 variables). The input preparation of PMF was done by excluding some specific elements for better source apportionment results. A common approach for the choice of species to include in the PMF input depends on: 1) the percentage of data below detection limit (Polissar et al., 1998), and 2) Xact data comparison with offline 24-h PM_{10} filters (Pearson coefficient of determination r^2). The minimum detection limits (MDL), r^2 and data points below MDL of Xact elements are listed in Furger et al. (2017). The MDLs were given by the manufacturer and were calculated by using the sensitivity of the element and counts in the region of interest of a blank section of the tape from where 1σ interference-free detection limits are reported. Elements (% of data points below MDL, r^2 value) which had more than 50 % of data points below MDL and low r^2 (< 0.5) between Xact and offline data were not included in the PMF input, such as: V (98 %, 0.57), Co (100 %, 0.05), Ni (32 %, 0.22), As (96 %, 0.5), Se (62 %, 0.3), Cd (87 %, 0.18), Sn (15 %, 0.27), Sb (6%, 0.42), Hg (13 %, 0.12) and Pt (98 %, not measured on the filters)-. The element Bi (93% data points below MDL) was an exception to include in the PMF input due to an excellent correlation between Xact and offline data (r^2 = 0.98) during fireworks peaks. The detailed description of the Xact data quality is given in the previous study (Furger et al., 2017). Missing data points in time (e.g. a power failure during sampling or a filter tape change) were removed from the data and error matrices. In the present work, if the element concentration was less than or equal to the MDL provided, the error matrix element s_{ij} was calculated using the Eq. (6), and if the concentration was greater than the MDL provided, the error matrix element s_{ij} was calculated using Eq. (7) (Reff et al., 2007; Tian et al., 2016; Polissar et al., 1998):

$$s_{ij} = \frac{5}{6} \times MDL_j \,, \qquad (6)$$

$$s_{ij} = \sqrt{(p_j \times x_{ij})^2 + (MDL_j)^2} \,, \qquad (7)$$

where **X** indicates the data matrix, while subscripts i and j are indices for time and elements. In this study, an estimated analytical uncertainty (p_j) of 10 % was used to derive the error matrix data set (Kim et al., 2005; Kim and Hopke, 2007; Tian et al., 2016; Ji et al., 2018), which did not change the PMF solution. The metal-specific analytical uncertainty was also considered from the previous studies (Jeong et al., 2016; Phillips-Smith et al., 2017), where it was calculated on the basis of high/medium-concentration metal standards laboratory experiments and the additional 5-10% flow rate accuracy, which yielded similar PMF solutions compared to an overall 10 % analytical uncertainty.

3.2 PMF setup

An important step in the PMF analysis is the selection of the number of factors by the user, as mathematical diagnostics alone are insufficient for choosing the correct number of factors (Ulbrich et al., 2009; Canonaco et al., 2013). The selection of factors is often based on an analysis of total Q or Q/Q_{exp}, scaled residuals (e_{ij}/s_{ij}), comparison of time series of the factor with external tracers, as well as diurnal patterns, and the evaluation of the residual time series as a function of the number of resolved factors.

In a first step, we examined a range of solutions with three to 10 factors at 10 seeds (number of PMF repeats) from unconstrained runs. The unconstrained PMF solution resulted in mixed factors, such as sea salt mixed with fireworks, even for higher numbers of factors (Fig. S1). This is likely because of the very high concentration and variation in composition of fireworks emissions during the fireworks period. Because the signal-to-noise is very high, imperfections in the model description exert a strong influence on Q, and the model therefore tries to compensate by assigning fireworks mass to other factors. This was particularly evident for the sea salt and secondary sulfate factors, where constraints on factor profiles and/or time series were necessary to obtain clean separation. Here we discuss the method for achieving this separation.

The input data set was divided into two parts: fireworks days (FD; 31 July–4 August) and non-fireworks days (NFD; all days except 31 July–4 August). To obtain a specific fireworks profile, we further selected only fireworks hours (FH; 31 July 21:00–1 August 07:00 LT) as input data. The PMF analysis was performed on the NFD, FD, FH and the complete datasets separately for three to 10 factors, with each of these solutions investigated with ~~ten~~ different seeds (each seed represents a different ~~pseudo~~random initialization).

The unconstrained NFD PMF analysis resolved seven factors at all ~~ten~~seeds such as sea salt, secondary sulfate, ~~traffic-related~~non-exhaust traffic-related, road dust, background dust, industrial and a K-rich factor. The sea salt factor profile shows excellent correlation (r^2= 0.99) between the Cl and the identified sea salt factor time series. Solutions with less than seven factors showed significant scaled residuals for elements and time series, while solutions with more than seven factors revealed a split of the ~~traffic-related~~non-exhaust traffic-related, industrial and background dust factors. The NFD analysis therefore provides a sea salt profile that can be used as a constraint in the complete dataset.

The unconstrained PMF analysis of the complete dataset identified a secondary sulfate factor (most of the S is apportioned in this factor, with 91 % of the factor mass) in the nine-factor solution (Fig. S1). The identified secondary sulfate factor time series correlated very well with ACSM sulfate (r^2 = 0.91) (Fig. S1) at 24 seeds out of 100 seeds while r^2 was ≤ 0.88 for the remaining 76 seeds. The Q/Q_{exp} values for all 100 seeds were in the range of 0.41- 0.45 (Fig. S2). ~~The identified secondary sulfate factor time series correlated very well with ACSM sulfate (r^2 = 0.91) (Fig. S1) at one seed out of ten seeds while r^2 was ≤ 0.88 for the remaining nine seeds~~. The scaled residual (over the time series) of S in this solution was within the range of ± 3 with very small values, as shown in Fig. S2. The strong influence of fireworks in this solution yielded small values of the scaled residual for S which are consistent also with lower-than-expected Q/Q_{exp} (0.4) values, suggesting an overestimation of uncertainties by the generic error model used herein (see Eqs. 6 and 7). ~~The scaled residual (over time series) of S in this solution was within the range of -0.46 to 0.85.~~ Although these r^2 are quite similar, the solution characteristics are notably different. For the $r^2 = 0.91$ solution the secondary sulfate factor did not respond significantly to the fireworks event, while the other factors time series, such as the sea salt and a mixed traffic plus K-rich factors, were enhanced during the fireworks peaks. For the other nine seeds, visible contamination (i.e. concentration spikes) during the fireworks plumes were observed, suggesting mathematical mixing. S is one of the major components of fireworks emissions, the composition of which is highly variable. Because of their high sensitivity (and thus high signal-to-uncertainty ratio), imperfections in the model description of the fireworks composition yields high-signal residuals which strongly influence Q. The model responds by apportioning fireworks residuals to the other factors during the fireworks days. A similar issue also occurred for the sea salt factor due to the significant amount of Cl in the fireworks factor profile. Therefore, such events are often excluded from traditional PMF analyses (i.e., time periods removed from the input matrix), to avoid modelling errors due to the pulling of a solution by outliers. Here we take a different approach, exploiting the rotational control available in ME-2 to isolate environmentally reasonable, unmixed solutions.

We then performed the constrained PMF analysis on the FD and FH datasets. Here we constrained the secondary sulfate factor profile (*a*-value 0.1) and the time series (*a*-value 0.01) using the results of the nine-factor unconstrained PMF analysis of the ~~NFD~~ complete dataset. We tested several approaches for the secondary sulfate constraint: a) constraining factor profile only; b) constraining the factor time series during fireworks days only; c) constraining both the factor profile and the entire factor time series; d) constraining the factor profile and the factor time series during fireworks days only. Of the above methods, only c and d yielded secondary sulfate factors without visible mixing from the fireworks period. The approach d was used for PMF analysis as it provides maximum freedom to the algorithm.

In the FD and FH PMF analyses, the sea salt factor profile (*a*-value 0.1) was also constrained from the NFD unconstrained seven-factor PMF analysis. To resolve the unmixed sea salt factor time series from the fireworks, the background Cl concentration was calculated for the fireworks data points (K > 220 ng m^{-3}) only. A Cl concentration < 30 ng m^{-3} was considered as a background Cl concentration, and the fireworks data points were replaced with the linear interpolation between the background Cl concentrations adjacent to the fireworks peaks. In this way 42 % of the data points were interpolated during the fireworks days. The calculated background Cl during the FD was constrained (with *a* -value 0.01) in the sea salt factor time series. After applying all the above four constraints, the FH PMF analysis identified the fireworks factor profile on the basis of the K / S elemental concentration ratio (~2.76) in black powder (Dutcher et al., 1999), and the concentration peak of 42 µg m^{-3}, which is close to the total elemental concentration peak of 48.4 µg m^{-3} on 1 August 23:00 LT in the factor time series. The FD PMF analysis also identified fireworks factor but the highest peak was 30 µg m^{-3} on 1 August 23:00 LT in the factor time series and the K / S elemental concentration ratio was 2.55 in the factor profile. Therefore, the fireworks factor profile from FH PMF analysis was considered for the final complete dataset PMF analysis. The FD and FH PMF analyses resolved a five-factor solution with secondary sulfate, sea salt, fireworks, background dust and a K-rich factor with fireworks related elements. In the K-rich factor, the K / S ratio was slightly higher (3.56) than the black powder ratio. ~~The common factors resolved by FD, FH and NFD PMF were comparable in terms of factor time series and factor profile.~~ The unconstrained FH PMF analysis was also performed for two to five factors with different seeds. As shown in Fig. S4, the constrained five-factor Q/Q_{exp} is 1.5, which is ~3 times higher than the unconstrained five-factor Q/Q_{exp} but same as unconstrained 3-factor Q/Q_{exp} (1.52). The increase in Q is significant over the constrained five-factor FH PMF and unconstrained five-factor because its UEV for each variable is between 2 % to 16 % (average ~10 %), while is it between 1.5 % to 15 % (average ~5 %) (see Fig. S5). The three-factor unconstrained FH PMF analysis validates the five-factor constrained FH PMF analysis, which suggests that both methods are working fine, and gives us more confidence to identify the fireworks factor profile.

Note that the number of time points contained in the input matrices for the data subsets (as opposed to the full dataset) are in some cases smaller than typical recommendations for ambient PMF (Olivier et al., 2019). This is most extreme in the case of the FH dataset, where only 11 time points are used. However, there are two important differences between PMF analyses of these sub-datasets and typical ambient PMF: (1) the sub-datasets are constructed to maximize variability of a factor or set of factors; and (2) we are concerned only with accurately characterizing the profile(s) of these selected major factors. These two points work together to greatly reduce the number of time points required for the analysis (Fig. S6). A similar approach has been successfully applied by Froehlich et al. (2015), in which short-duration spikes in organic aerosol concentration were combined into a sub-dataset to determine an anchor profile related to local cigarette smoke, and Visser et al. (2015), in which a subset of a trace element dataset with high residuals was analysed separately to retrieve a factor profile related to industrial emissions.

In the final complete dataset PMF analysis, the factor profiles of fireworks, secondary sulfate and sea salt were constrained (a-value 0.1) while the time series of secondary sulfate and the calculated background Cl concentration interpolation were constrained during the fireworks period only (a-value 0.01). The solution that best represented the input data was an eight-factor solution, consisting of factors interpreted as sea salt, secondary sulfate, ~~traffic-related~~non-exhaust traffic-related, industrial, two dust-related and fireworks-related (two factors).

Residual analysis (Q-contribution over time series) of the PMF runs showed significant structure in the residuals (Q maximum value was 15 during fireworks period as shown in Fig. S8~~3~~) for solutions having up to seven factors. Increasing the number of factors to eight gave evidence of structure removal, with mostly random errors remaining, by another fireworks-II factor which was explained by K, S, Ba, Ti, Cu, Bi, while a further increase led to a new mixed factor of ~~traffic-related~~non-exhaust traffic-related and background dust which however showed a noisy diurnal pattern (Fig. S9~~3~~). All the variables were approximately unimodal scaled residuals between ±3 (Paatero and Hopke, 2003) (Fig. S10~~5~~).

3.3 Uncertainty estimate of PMF results

The statistical and rotational uncertainties were explored by the bootstrap (BS) resampling strategy (Efron, 1979) and the exploration of the a-value space of the constrained information as well as random initialization of the unconstrained information. Briefly, the bootstrap algorithm generates new input matrices by randomly resampling variables from the original input matrix. Each newly generated PMF input matrix had a total number of samples equal to the original matrix (456 samples); although some of the original 456 samples were represented several times, while others were not represented at all. A systematic investigation of the *a*-value space in combination with each individual BS run is computationally impractical and was therefore replaced by random initialization of the *a*-value of the secondary sulfate, sea salt and fireworks-I factor profiles between 0 and 0.5 with an increment of 0.1 for 1000 BS runs. Moreover, to avoid rejection of many solutions due to mixing of the sea salt factor time series and the secondary sulfate time series with the fireworks factor peaks, both the sea salt and secondary factor time series (for the fireworks period only) were also constrained with an *a*-value 0.01. The small *a*-value (0.01) for the sea salt and the secondary sulfate factor time series (for the fireworks period only) were estimated based on sensitivity analyses on the *a*-value from 0 to 0.1 with an increment of 0.01. The time series of both factors were showing fireworks peaks during the fireworks period for *a*-values greater than 0.01. Solutions were selected and retained based on the correlation (correlation of coefficient Pearson *r*) of the time series between the factors of the base case and the factors of the BS runs. Solutions with low correlation and some solutions with high correlation have a factor of completely different type, i.e. mixed or split or otherwise altered factor profile/time series based on visual inspection. These kinds of solutions were rejected. This approach was used only for uncertainty assessment rather than uncertainty exploration to find the environmentally reasonable solution.

We also performed separate random bootstrap analyses for 1000 times on the correlation (*r*) between the time series of a base case factor and the respective external marker, e.g. the secondary sulfate factor vs ACSM sulfate, and the ~~traffic-related~~non-exhaust traffic-related factor vs NO_x to assess the acceptable uncertainty of the *r* value. The resulting correlation coefficients were represented in probability density functions (PDF) over 1000 bootstrap runs for both bootstrap analysis methods. In total 86 % of the bootstrap runs were classified as environmentally good solutions. The average *a*-value retained by the selected bootstrap runs was 0.233, 0.255 and 0.241 for the fireworks-I, sea salt and secondary sulfate factor profiles, respectively. The spread of the *a*-value for these three factors is presented as mean, median and interquartile in the supplement (Fig. S11~~6~~). The selected solutions factor profiles are represented as box whisker plot in the sequence of p10 (10th percentile), p25 (25th percentile), p50 or median (50th percentile), p75 (75th percentile) and p90 (90th percentile) in Fig. 2.

During the non-fireworks period, uncertainties in the source apportionment results are assessed by a bootstrap analysis as described above. However, this approach cannot be used to assess uncertainties in the sea salt and secondary sulfate factors during the fireworks period, as during this period these factor time series are constrained with an artificially low *a*-value selected to optimize deconvolution. For these two factors, uncertainties during the fireworks period are determined by our ability to accurately predict the factor time series. The secondary sulfate and sea salt factors cases are discussed separately below.

Secondary sulfate concentrations during the fireworks period were estimated from the linear fit of the secondary sulfate factor to ACSM sulfate during the entire non-fireworks period. Uncertainties of ±5 % were calculated as the standard deviation of the actual secondary sulfate concentrations to the predicted values and included for the fireworks period only in Fig. 3a.

As described above, the sea salt factor time series during the four-day fireworks period was investigated to determine measurements that were affected or not affected by fireworks, where the measurements determined to be affected were replaced with a linear interpolation between the nearest good points. To determine the uncertainties of this approach, we applied this calculation to random segments of the non-fireworks data. Specifically, the four day-long sequence of affected/non-affected time points determined during the fireworks period was applied to a randomly chosen segment of data, and the standard deviation of measurement data to the estimated values calculated by interpolation was determined. This analysis was repeated for 38 randomly selected locations through the non-fireworks data, and a mean standard deviation of ±42 % was determined. This value is used as the uncertainty of the sea salt factor time series (during the fireworks period only) in Fig. 3a

4 Results and discussion

4.1 Overview of retrieved factors

The solution that best represented the input data was the eight-factor solution. The eight factors from the PMF results are as follows:

1. Two fireworks factors with prominent relative contributions of Bi, Ba, K, S, Ti, Cu and Cl, which are important components of fireworks (Kong et al., 2015; Vecchi et al., 2008);
2. A sea salt factor explaining a large fraction of Cl in the PM_{10} fraction;
3. A secondary sulfate factor mostly dominated by S and highly correlated with ACSM sulfate; (Fig. S1);
4. Two dust factors, one dominated by Ca and showing traffic rush hours peaks, and the other dominated by Si without a clear diurnal pattern;
5. A ~~traffic-related~~non-exhaust traffic-related factor characterized by Fe, Cr, Cu, Mn, Zn and Ba;
6. An industrial factor showing relatively high contributions of Pb and Zn.

4.2 Detailed factor description

In this section, the results of the PM_{10el} mass driven by the sum of 14 elements ~~In this section the final results of the elemental PM_{10} source apportionment~~ are presented and validated. Fig. 2 represents the fractional composition of the factor profile ($f_{kj}/\sum_j f_{kj}$) (left y-axis; colored box whisker plots for each factor) and relative contribution ($\sum_i g_{ik} f_{kj}/\sum_k \sum_i g_{ik} f_{kj}$) of each factor to each variable (right y-axis; black box whisker plots). Fig. 3a shows the time series of the factors contributions in ng m^{-3} (bottom panels) and of the relative contributions (top panel) of the retrieved ~~elemental~~ PM_{10e} factors. The variability of these time series across all good solutions was relatively low. Fig. 3b reports the averaged total PM_{10}

elemental mass (excluding the fireworks factors) and relative contributions of the PM$_{10e}$ ~~elemental~~ sources. The reported variabilities/uncertainties (which correspond to the interquartile range among selected bootstrap runs) are an indication of the high stability of the solution. The diurnal variations of the absolute concentrations of the identified factors and some of their corresponding external tracers are presented in Fig. 4. CBPF analysis was performed at 90th percentile (Fig. 5) as well as at different percentile ranges (Fig. S12~~6~~) to validate some of the identified sources and their characterization.

Fireworks: The fireworks factor profiles and time series are shown in Fig. 2 and Fig.3a respectively. The fireworks factors are mostly dominated by K, S, Cl, Ti, Cu, Ba and Bi, which are the chemical elemental species of fireworks (Moreno et al., 2007; Wang et al., 2007; Vecchi et al., 2008; Perrino et al., 2011; Tian et al., 2014; Kong et al., 2015; Lin, 2016; Pongpiachan et al., 2018). Ba and Cu compounds are used to produce green and blue fireworks. The presence of Cl in fireworks-I suggests that the chloride salt might be the main chemical form in the fireworks, such as barium chloride. K is one of the major components of fireworks, which contain 74 % of KNO$_3$ in black powder as the oxidizing agent for the burning process (Drewnick et al., 2006). The ACSM inorganics concentrations during the fireworks episodes indicate that neither particulate nitrate nor ammonium is generated in the fireworks in significant amounts (Fig. S13~~7~~). Consistent with previous measurements of submicron fireworks aerosol (Drewnick et al., 2006; Vecchi et al., 2008; Jiang et al., 2015), nitrate was not enhanced during the fireworks period, suggesting conversion of KNO$_3$ to other forms of nitrogen. The NO$_2$ / K mass ratio (1.66) on the main fireworks hour (1 August 23:00 LT) (see Fig. S13~~7~~) is close to the atomic ratio of NO$_2$ / K (1.17). This measured ratio is also in agreement with the NO$_2$ / K$^+$ (2.03) ratio observed during Chinese Spring Festival in Shanghai (Yao et al., 2019). However, the NO$_2$ and/or NO$_x$ variation was not significant during the fireworks peaks in the present study (Fig. S13~~7~~), which is in agreement with the former studies (Vecchi et al., 2008; Retama et al., 2019; Yao et al., 2019). The K / S ratio of 2.72 in the fireworks-I factor profile is in good agreement with the K / S elemental concentration ratio (~2.76) in black powder (Dutcher et al., 1999). Other K compounds in black powder can be in the form of perchlorate or chlorate (Wang et al., 2007). Bi is used in crackling stars (Dragon's eggs) in the form of bismuth trioxide or subcarbonate as a non-toxic substitute for toxic lead compounds (Perrino et al., 2011). The Ba / K ratio of 0.031-0.054 for fireworks-I and fireworks-II is close to the value 0.057 reported in (Pongpiachan et al., 2018). Fireworks particles are usually present in large amounts in the fine fraction, staying longer in the atmosphere (Richard et al., 2011; Moreno et al., 2007). A pronounced increase in both fireworks factor time series is observed when the fireworks traditionally begin. The diurnal patterns of the fireworks-related elements exhibit a peak at 23:00 LT (or CEST) during the fireworks period (Furger et al., 2017) in accordance with the fireworks-I diurnal variation (Fig. 4c). Both fireworks factors contain two sharp peaks. The fireworks-I factor concentration started to increase on 31 July 2015 22:00 LT and formed the extreme peak within 1 h at 23:00 LT (~5 µg m^{-3}). After that it decayed quickly (10 times lower concentration than maximum fireworks concentration) within 1 h and remained more or less constant until 1 August 2015 21:00 LT. It again started to increase from 22:00 LT and formed a second sharp peak on 1 August 2015 23:00 LT, followed by a gradual decay over the next 6 to 10 h. Fireworks-II presents a slightly different pattern in its time series. It started to increase from 31 July 2015 22:00 LT and depicted its highest peak at

00:00 LT (~3.6 µg m^{-3}) with a quite slow decay until 1 August 2015 06:00 LT. The concentration remained slightly higher than fireworks-I over daytime. It then started to increase again from 1 August 2015 17:00 LT and yielded the highest peak on 2 August 04:00 LT with 6.7 µg m^{-3}. It remained higher until 2 August 2015 08:00 LT and slowly decayed until the afternoon, followed by further prominent peaks at 23:00 LT on 2 August and 3 August. Chemical reactions of KCl with H_2SO_4 will result in a release of gaseous HCl and may explain the absence of particulate Cl in the fireworks-II factor profile. The time series variations in both fireworks suggest that fireworks-I might be related to the main fireworks celebration while fireworks-II might result from burning of leftover crackers after the main fireworks day, as well as the influence of other sources such as bonfires, which are a common activity during Swiss National Day celebrations. Another possibility could be the advection of fireworks clouds from nearby cities where grand firework displays and bonfires are carried out at large scale to celebrate the Swiss National Day. The average relative contributions of fireworks-I and fireworks-II to the analysed mass were 7.4 % and 11 % respectively (Fig. 3b). Fig. S14~~8~~ represents an estimate of overall fireworks composition and temporal variability, complementing the PMF results. A K concentration > 220 ng m^{-3} was used as the criterion to separate fireworks data points (65 data points) from the whole data set. The detailed description is mentioned in the supplement. Most of the elements are well captured by two fireworks factors, such as S, K, Fe, Cu, Ba etc., since they lie within the fireworks data distribution. In contrast, there are some elements that are not contributing to fireworks, e.g. Ca and Cr, while some elements are explained by only one firework, e.g., Si, Cl and Pb. This indicates that a single fireworks factor is not enough to represent the fireworks data variability.

Sea salt: The sea salt factor was mainly composed of Cl (81 % of the factor mass) as shown in the factor profile (Fig. 2), with no diurnal pattern (Fig. 4e). The average relative contribution of the sea salt factor to the analysed mass was 3.7 % (Fig. 3b). Sea salt also includes Na and Mg, which were not measured by the Xact but analysed by ICP-OES for 24-h offline filters. Based on the high correlation of Na and Cl in a previous study, Cl alone can be used as a marker for sea salt particles (Vallius, 2005). The existence of sea salt particles was confirmed by a low Mg / Na ratio in the filter data, equalling 0.13 and 0.16 for 28 July and 30 July, respectively, in line with a ratio of 0.132 to 0.185 for marine aerosol (Chesselet et al., 1972). For the remaining 8 filter samples Mg / Na was higher than 0.18, probably due to absence of sea salt (Fig. S15~~0~~). A comparison with ACSM data revealed that Cl was mainly present in the fine fraction (PM_1) during firework days, while during the rest of the campaign it was in PM_{10} (Fig. S16~~1~~). The measured ~~Cl / K and~~ Cl / Ca ratio~~s~~ (~~0.27 and~~ 0.33 ~~respectively~~) from Xact does not lie in the range of de-icing salt composition (5.27) measured in northern Germany (Pernigotti et al., 2016)~~do not lie in the range of road salt snow samples (150±39 and 103±22, respectively) collected near the roadside (≤50 m) in USA (Williams et al., 2000)~~, which validates our interpretation as a sea salt factor. In addition, the highest Cl concentrations were observed only in the last week of July, with westerly winds at higher wind speed (5–8 m s^{-1}) (Fig. S16~~1~~, S17~~2~~). This result is in agreement with the CBPF plot where the high concentration of the sea salt factor dominates for westerly winds with high wind speed (Figs. 5~~4~~, S12~~6~~), and confirms previous studies (Visser et al., 2015; Twigg et al., 2015).

Dust: The PMF analysis resolved two dust-related factors, i.e., a road dust (Ca-rich) and a background dust (Si-rich) factor, with average relative contributions to the analysed mass of 18 % and 16 %, respectively (Fig. 3b). The road dust factor was mainly composed of Ca (68 % of the factor mass) followed by Si (26 %), with relative contributions of 89 % to Ca, 19 % to Si and 12 % to Mn, while the background dust factor highly contributed to Ti, Si, Mn, Fe and Ca, with 65 %, 58 %, 22 %, 16 % and 6 %, respectively. The two dust factors together explain 95 % of Ca, while the remaining factors explain only 5% of Ca. The solution with two dust factors resulted in reduced scaled residuals for Si and Ca compared to a solution with one dust factor (Fig. S18~~3~~). The scatter plot of the absolute concentrations of Si and Ca also indicates the presence of two different sources (Fig. S19~~4~~). The high relative contribution of Ca in road dust has also been found in other source apportionment studies (Ducret-Stich et al., 2013; Bukowiecki et al., 2010). In general, Ca and Si are commonly associated with mineral dust, construction activities, vehicular emissions and iron/steel plants (Lee and Pacyna, 1999; Vega et al., 2001; Bukowiecki et al., 2010; Crilley et al., 2016; Maenhaut, 2017). Iron/steel plants produce furnace slacks, a glass-like by-product which consists of Ca, Si, Mg and Al oxides. The higher fraction of crustal elements such as Ca and Si in road dust might be a consequence of the widespread use of asphalt/concrete to make roads (Fullova et al., 2017; Li et al., 2004). The sampling site is located close to the freeway and must be influenced by wear and tear of the asphalt/concrete roads because of heavy traffic. Ca has been associated with construction activities in previous studies (Bernardoni et al., 2011; Crilley et al, 2016), which have been found to peak during the day and decreased to almost zero outside of normal working times (08:00 until 17:00 LT). This evidence is not supported by the road/background dust factor diurnal pattern in this study. Further evidence of non-construction activity is found in the Xact elemental ratio of Ca / S (0.62) which is not in the agreement with the pure gypsum Ca / S ratio (1.25) used for construction work (Hassan et al., 2014), where they are the main constituents. Road dust profiles are often difficult to identify due to resuspension of materials deposited on the road surface such as mineral dust, vehicle wear/tear, and/or road surface wear/tear. However, the road dust factor profile is distinct from the non-exhaust non-exhaust traffic-related factor profile. It is possible that the road dust factor is related to resuspension of mineral dust and road wear/tear particles. The high contribution of Ca alone (> 80%) has been seen in previous studies (Ducret-Stich et al., 2013; Bukowiecki et al., 2010; Hueglin et al., 2005) where it was named as “road dust”. Another study at a rural site in Switzerland also found the Ca rich factor in the coarse fraction where it was linked to soil resuspension (Minguillon et al., 2012). The background dust factor profile exhibits elements associated with mineral dust, such as Ti, Si and Fe. These and other terrestrial elements are commonly present in soil as oxides (Rudnick and Gao, 2003). The background dust factor also contains a significant fraction of the measured Mn, which is one of the most abundant compounds in the earth’s crust, where it occurs in the form of MnO_2 (Taylor and McLennan, 1995). Since the sampling site is adjacent to agricultural fields in the north and west directions, the contribution of these elements to this factor can be expected. A similar background factor with high contributions of Si, Ti and Ca was found by Richard et al. (2011) at an urban site in Switzerland.

The separation of two dust factors is in line with Amato et al. (2009), where ME-2 yielded a road dust factor distinct from a mineral dust factor. The CBPF plot shows that higher concentrations of the road dust factor are associated with the southern wind sector, while the background dust factor is influenced by the southwest and northeast wind sectors (Figs. 5, S12~~6~~). The diurnal pattern of the road dust factor shows morning rush hour traffic peaks similar to NO_x, BC, HDV count and ~~traffic-related~~non-exhaust traffic-related factor (Fig. 4a, 4b) indicating resuspension of road dust is due to the vehicle fleet. A similar relationship between road dust and the ~~traffic-related~~non-exhaust traffic-related source was observed in a previous study (Amato et al., 2009). Resuspension of road dust in the early morning traffic is not triggered by wind speed (Fig. S20~~15~~), but by the traffic fleet, whereas in the afternoon, an increase in wind speed leads to resuspension of dust deposited on the road as well as resuspension of agricultural soil dust near the sampling site. Therefore, meteorology plays a vital role for the contribution of the background dust factor.

~~Traffic-related~~Non-exhaust traffic-related: The ~~traffic-related~~non-exhaust traffic-related factor profile was mostly dominated by Fe (73 % of the factor mass) and contributed strongly to Cr (96 %), Fe (76 %), Cu (71 %), Mn (50 %), Zn (31 %), Ba (26 %) and Si (12 %). Its average relative contribution to the analysed mass was 20 % (Fig. 3b). Coarse particles from brake/disc wear could appear as flakes and mainly consist of iron oxides (Wahlström et al., 2010). The higher fraction of Fe in the ~~traffic-related~~non-exhaust traffic-related source has been found in several previous studies (Visser et al., 2015; Amato et al., 2014a; Bukowiecki et al., 2010; Dall'Osto et al., 2013; Crilley et al., 2016). However, the ratio of Fe to other elements is variable between studies. Fe, Cr, Cu, Zn, Mn and Ba are the most abundant trace elements in brake pads, brake lining and thus attributed to tire/brake wear (Thorpe and Harrison, 2008; Grigoratos and Martini, 2015; Gianini et al., 2012) and engine wear. Si is one of the brake lining components used as abrasive to increase friction, and as fillers to reduce manufacturing costs, respectively (Thorpe and Harrison, 2008; Grigoratos and Martini, 2015). This factor is characterized by a strong diurnal peak coinciding with the morning rush hour at 08:00 LT, similar to NO_x and BC (Fig. 4b). The LDV and HDV counts start to increase from 05:00 LT (Fig. 4a), unlike the primary traffic emission NO_x and BC. The similar diurnal pattern of this factor might be due to the high braking load for vehicles during peak traffic hours, resulting in increased emissions of vehicle wear particles.

Secondary sulfate: This source is characterized by sulfur (S) and is most likely due to the regional background contribution of secondary sulfate due to conversion of SO_2 to SO_4^{2-}, consistent with the results of many previous source apportionment studies (Dall'Osto et al., 2013; Richard et al., 2011). It explains the highest fraction of S (91 % of the factor mass) with relative contributions to S (73%) and Pb (30%) (Fig. 2). The average relative contribution of this factor to the analysed mass is 21 % (Fig. 3b). Similar factor profiles were found in previous studies (Visser et al., 2015; Dall'Osto et al., 2013). This factor correlates well with ACSM SO_4^{2-} measurements ($r^2 = 0.91$), suggesting a dominant contribution from the submicron fraction and thus a slow rate of dry deposition. Combined with SO_2 oxidation processes occurring on timescales of hours to days, it is thus reasonable that the secondary sulfate factor does not exhibit a clear diurnal variation (Fig. 4f) and is consistent with regional rather than local sources. The time series of secondary sulfate exhibits peaks during the fireworks event (Fig. 3a), in agreement with the ACSM SO_4^{2-} time series (Fig. S21~~9~~). Inorganic gases (SO_2, NO_x, etc.) emitted during the fireworks events may be oxidized to secondary organic and inorganic components that may condense to the particle phase

(Sarkar et al., 2010) within a very short span of time, as observed in previous studies (Wang et al., 2007; Yang et al., 2014). We monitored two parameters to explain the influence of fireworks in secondary sulfate time series: (1) mass balance for ACSM PM_1 data; (2) secondary sulfate peaks during the main fireworks hours (1 August 23:00 LT to midnight). The equivalent concentration of ammonium (NH_{4eq}) balances the sum of NO_{3eq} and SO_{4eq} during non-fireworks periods, while during fireworks peaks, the balance shifts towards the sum of NO_{3eq} and SO_{4eq}. This indicates that sulfate related to fireworks adds up to an acidic budget of particles. The excess sulfate observed from this analysis is approximately in quantitative agreement (within 20%) with the enhancement of the secondary sulfate during fireworks period. The peak in secondary sulfate at 23:00 LT is slightly offset from the main fireworks peak because secondary sulfate formed maximum peak 1 h later (00:00 LT 2 August). Taking these two together suggests that we may have some downstream production of sulphuric acid and conversion to ammonium sulfate, which makes secondary sulfate factor time series slightly delayed relative to main fireworks plume. Because this delay is consistent with chemical processing, we consider inclusion of this temporal feature in the secondary sulfate factor to be reasonable, although we cannot completely rule out some degree of mathematical mixing with the direct fireworks emissions. ~~The secondary sulfate factor and the ACSM SO_4^{2-} capture the highest peak at midnight on 2 August 2015, while fireworks-I formed a peak at 23:00 LT on 1 August 2015.~~ The time series of ACSM SO_4^{2-} and ACSM NH_4^+ show significant correlation (Fig. S21~~9~~), indicating the formation of ammonium sulfate particles except for the main fireworks peaks.

Industrial: This factor is characterised by high relative contributions to Zn (50 %) and Pb (63 %), with a low contribution to the analysed mass (in the order of 3 %, Fig. 3b). The profile is shown in Fig. 2 and the time series in Fig. 3a. The time series contains a few spikes after 4 August, when the wind was predominantly from the south and south-east sector, suggesting an industrial emission. A similar factor profile was observed in previous source apportionment studies (Crilley et al., 2016; Richard et al., 2011) from local point source emissions without any link to specific industrial activities. ~~Amato et al. (2010) and Dall'Osto et al. (2013) also reported a PMF factor with high concentrations of Zn and Pb and attributed it to emissions from smelters in Barcelona, while Vossler et al. (2016) reported a similar factor profile from coal combustion processes in Ostrava.~~ Industrial emissions play a minor role in this study area, as it is surrounded by only a few small scale industrial buildings (logistics businesses approximately 500 m to the north-west, and a wheel manufacturing company to the south-east across the freeway). The CPBF plot confirms the dominance of high concentrations in the south-east direction (Fig. 5). The diurnal cycle shows a clear peak at 10:00 LT (Fig. 4g) which is related to a few peaks.

5 Conclusion

A source apportionment study of 14 elements in PM_{10} measured at a traffic-influenced site in Härkingen, Switzerland; during the summer of 2015 was conducted using the ME-2 implementation of PMF. The PMF model was able to resolve and evaluate the contributions and compositions of eight sources: two fireworks factors, sea salt, secondary sulfate, background dust, road dust, ~~traffic-related~~non-exhaust traffic-related, and an industrial source. The use of ME-2 allowed the use of constraints via the *a*-value approach, which improved the factor resolution relative to conventional PMF. We show that the rotational control available in ME-2 provides a means for treating extreme events such as fireworks within a PMF analysis.. This was only achievable when controlling problematic factors, i.e., factors that tend to mix within the constraining technique. Two dust factors with different time profiles and two fireworks factors were identified by the PMF model resulting in better representation of data variability. An S-rich (secondary sulfate) factor, which can typically be attributed to regional background/transported secondary sulfate, was correlated with fine mode non-refractory sulfate measured by an ACSM. The ~~traffic-related~~non-exhaust traffic-related factor followed the diurnal pattern of traffic rush hours similar to NO_x and BC with concentrations up to 4 times higher during daytime relative to night-time. The outcome of this study emphasizes the significant influence of regional background secondary sulfate and local background dust apart from non-exhaust traffic emissions at the sampling location.~~This result emphasizes the large influence of highway traffic on the composition of elemental PM_{10}~~. The small contribution of the industrial factor confirms the low influence of local daily activities from the surroundings.

The source apportionment model performance could possibly be additionally improved by the inclusion of Na and Sr to better resolve the sea salt and fireworks factors, respectively. It was shown that high time resolution elements data sets enable a fully resolved SA, with considerable improvements compared to 24-h filter analysis, where the attribution to specific sources is possible only on a larger time scale and is mostly based on seasonal variations.

Data availability

The datasets are available upon request to the corresponding author.

Author contribution

PR performed SA analysis and wrote the manuscript. MF, RF and CH performed measurement. MF and RF analysed data for Xact and ACSM, respectively. FC and JGS provided expertise on software for SA analysis. MCM provided ICP-MS and ICP-AES analysis data. KP lent Xact® 625 for measurement. UB, ASHP, MF, FC and JGS were involved with the supervision and conceptualisation. All authors commented on the paper and assisted in the interpretation of the results.

Competing interests

Krag Petterson is employed by Cooper Environmental Services, the manufacturer of the Xact® 625.

Acknowledgements

This study has been funded by the Swiss National Science Foundation (SNSF grants 200021_162448/1 and BSSGI0_155846), and by the Swiss Federal Office for the Environment (FOEN). We thank René Richter and Roland Scheidegger of PSI for their technical support during the measurement campaign. We are grateful to Chris Koch and Varun Yadav of Cooper Environmental Services for instructions on the instrument and numerous technical discussions. We thank the operators of the NABEL station for providing all kinds of support during the measurements.

References

Amato, F., Pandolfi, M., Escrig, A., Querol, X., Alastuey, A., Pey, J., Perez, N., and Hopke, P. K.: Quantifying road dust resuspension in urban environment by Multilinear Engine: A comparison with PMF2, Atmos. Environ., 43, 2770–2780, https://doi.org/10.1016/j.atmosenv.2009.02.039, 2009.

~~Amato, F., Nava, S., Lucarelli, F., Querol, X., Alastuey, A., Baldasano, J. M., and Pandolfi, M.: A comprehensive assessment of PM emissions from paved roads: Real-world emission factors and intense street cleaning trials, Sci. Total Environ., 408, 4309–4318, https://doi.org/10.1016/j.scitotenv.2010.06.008, 2010.~~

Amato, F., Pandolfi, M., Moreno, T., Furger, M., Pey, J., Alastuey, A., Bukowiecki, N., Prevot, A. S. H., Baltensperger, U., and Querol, X.: Sources and variability of inhalable road dust particles in three European cities, Atmos. Environ., 45, 6777–6787, https://doi.org/10.1016/j.atmosenv.2011.06.003, 2011.

Amato, F., Alastuey, A., de la Rosa, J., Sánchez de la Campa, A. M., Pandolfi, M., Lozano, A., Contreras González, J., and Querol, X.: Trends of road dust emissions contributions on ambient air particulate levels at rural, urban and industrial sites in southern Spain, Atmos. Chem. Phys., 14, 3533–3544, https://doi.org/10.5194/acp-14-3533-2014, 2014a.

Amato, F., Cassee, F. R., Denier van der Gon, H. A. C., Gehrig, R., Gustafsson, M., Hafner, W., Harrison, R. M., Jozwicka, M., Kelly, F. J., Moreno, T., Prevot, A. S. H., Schaap, M., Sunyer, J., and Querol, X.: Urban air quality: The challenge of traffic non-exhaust emissions, J. Hazard. Mater., 275, 31–36, https://doi.org/10.1016/j.jhazmat.2014.04.053, 2014b.

Ancelet, T., Davy, P. K., Mitchell, T., Trompetter, W. J., Markwitz, A., and Weatherburn, D. C.: Identification of particulate matter sources on an hourly time-scale in a wood burning community, Environ. Sci. Technol., 46, 4767–4774, https://doi.org/10.1021/es203937y, 2012.

Belis, C. A., Pikridas, M., Lucarelli, F., Petralia, E., Cavalli, F., Calzolai, G., Berico, M., and Sciare, J.: Source apportionment of fine PM by combining high time resolution organic and inorganic chemical composition datasets, Atmos. Environ., 3, 100046, https://doi.org/10.1016/j.aeaoa.2019.100046, 2019.

Bernardoni, V., Vecchi, R., Valli, G., Piazzalunga, A., and Fermo, P.: PM_{10} source apportionment in Milan (Italy) using time-resolved data, Sci. Total Environ., 409, 4788–4795, https://doi.org/10.1016/j.scitotenv.2011.07.048, 2011.

Bozzetti, C., Daellenbach, K. R., Hueglin, C., Fermo, P., Sciare, J., Kasper-Giebl, A., Mazar, Y., Abbaszade, G., El Kazzi, M., Gonzalez, R., Shuster-Meiseles, T., Flasch, M., Wolf, R., Křepelová, A., Canonaco, F., Schnelle-Kreis, J., Slowik, J. G., Zimmermann, R., Rudich, Y., Baltensperger, U., El Haddad, I., and Prévôt, A. S. H.: Size-resolved identification, characterization, and quantification of primary biological organic aerosol at a European rural site, Environ. Sci. Technol., 50, 3425–3434, https://doi.org/10.1021/acs.est.5b05960, 2016.

Brauer, M., Hoek, G., Vliet, P. V., Meliefste, K., Fischer, P. H., Wijga, A., Koopman, L. P., Neijens, H. J., Gerritsen, J., Kerkhof, M., Heinrich, J., Bellander, T., and Brunekreef, B.: Air pollution from traffic and the development of respiratory infections and asthmatic and allergic symptoms in children, Am. J. Respir. Crit. Care Med., 166, 1092–1098, https://doi.org/10.1164/rccm.200108-007OC, 2002.

Bukowiecki, N., Lienemann, P., Zwicky, C. N., Furger, M., Richard, A., Falkenberg, G., Rickers, K., Grolimund, D., Borca, C., Hill, M., Gehrig, R., and Baltensperger, U.: X-ray fluorescence spectrometry for high throughput analysis of atmospheric aerosol samples: The benefits of synchrotron X-rays, Spectrochim. Acta B, 63, 929–938, https://doi.org/10.1016/j.sab.2008.05.006, 2008.

Bukowiecki, N., Lienemann, P., Hill, M., Figi, R., Richard, A., Furger, M., Rickers, K., Falkenberg, G., Zhao, Y., Cliff, S. S., Prévôt, A. S. H., Baltensperger, U., Buchmann, B., and Gehrig, R.: Real-world emission factors for antimony and other brake wear related trace elements: size-segregated values for light and heavy duty vehicles, Environ. Sci. Technol., 43, 8072–8078, https://doi.org/10.1021/es9006096, 2009.

Bukowiecki, N., Lienemann, P., Hill, M., Furger, M., Richard, A., Amato, F., Prévôt, A. S. H., Baltensperger, U., Buchmann, B., and Gehrig, R.: PM_{10} emission factors for non-exhaust particles generated by road traffic in an urban street canyon and along a freeway in Switzerland, Atmos. Environ., 44, 2330–2340, https://doi.org/10.1016/j.atmosenv.2010.03.039, 2010.

Cakmak, S., Dales, R., Kauri, L. M., Mahmud, M., Ryswyk, K. V., Vanos, J., Liu, L., Kumarathasan, P., Thomson, E., Vincent, R., and Weichenthal, S.: Metal composition of fine particulate air pollution and acute changes in cardiorespiratory physiology, Environ. Pollut., 189, 208–214, https://doi.org/10.1016/j.envpol.2014.03.004, 2014.

Canonaco, F., Crippa, M., Slowik, J. G., Baltensperger, U., and Prévôt, A. S. H.: SoFi, an IGOR-based interface for the efficient use of the generalized multilinear engine (ME-2) for the source apportionment: ME-2 application to aerosol mass spectrometer data, Atmos. Meas. Tech., 6, 3649–3661, https://doi.org/10.5194/amt-6-3649-2013, 2013.

Carslaw, D. C. and Beevers, S. D.: Characterising and understanding emission sources using bivariate polar plots and k-means clustering, Environ. Modell. Softw., 40, 325–329, https://doi.org/10.1016/j.envsoft.2012.09.005, 2013.

Cesari, D., Genga, A., Ielpo, P., Siciliano, M., Mascolo, G., Grasso, F. M., and Contini, D.: Source apportionment of $PM_{2.5}$ in the harbour-industrial area of Brindisi (Italy): Identification and estimation of the contribution of in-port ship emissions, Sci. Total Environ., 497–498, 392–400, https://doi.org/10.1016/j.scitotenv.2014.08.007, 2014.

Chan, D. and Stachowiak, G. W.: Review of automotive brake friction materials, Proc Inst. Mech. Eng. Part D: J Automob. Eng., 218, 953–966, https://doi.org/10.1243/0954407041856773, 2004.

Chang, Y., Huang, K., Xie, M., Deng, C., Zou, Z., Liu, S., and Zhang, Y.: First long-term and near real-time measurement of trace elements in China's urban atmosphere: temporal variability, source apportionment and precipitation effect, Atmos. Chem. Phys., 18, 11793–11812, https://doi.org/10.5194/acp-18-11793-2018, 2018.

Chesselet, R., Morelli, J., and Buat-Menard, P.: Variations in ionic ratios between reference sea water and marine aerosols, J. Geophys. Res., 77, 5116–5131, https://doi.org/10.1029/JC077i027p05116, 1972.

Crenn, V., Sciare, J., Croteau, P. L., Verlhac, S., Fröhlich, R., Belis, C. A., Aas, W., Äijälä, M., Alastuey, A., Artiñano, B., Baisnée, D., Bonnaire, N., Bressi, M., Canagaratna, M., Canonaco, F., Carbone, C., Cavalli, F., Coz, E., Cubison, M. J., Esser-Gietl, J. K., Green, D. C., Gros, V., Heikkinen, L., Herrmann, H., Lunder, C., Minguillón, M. C., Močnik, G., O'Dowd, C. D., Ovadnevaite, J., Petit, J.-E., Petralia, E., Poulain, L., Priestman, M., Riffault, V., Ripoll, A., Sarda-Estève, R., Slowik, J. G., Setyan, A., Wiedensohler, A., Baltensperger, U., Prévôt, A. S. H., Jayne, J. T., and Favez, O.: ACTRIS ACSM intercomparison – Part 1: Reproducibility of concentration and fragment results from 13 individual Quadrupole Aerosol Chemical Speciation Monitors (Q-ACSM) and consistency with co-located instruments, Atmos. Meas. Tech., 8, 5063–5087, https://doi.org/10.5194/amt-8-5063-2015, 2015.

Crilley, L. R., Lucarelli, F., Bloss, W. J., Harrison, R. M., Beddows, D. C., Calzolai, G., Nava, S., Valli, G., Bernardoni, V., and Vecchi, R.: Source apportionment of fine and coarse particles at a roadside and urban background site in London during the 2012 summer ClearfLo campaign, Environ. Pollut., 220, 766–778, https://doi.org/10.1016/j.envpol.2016.06.002, 2016.

Cooper, J. A., Petterson, K., Geiger, A., Siemers, A., and Rupprecht, B.: Guide for developing a multi-metals, fenceline monitoring plan for fugitive emissions using X-ray based monitors, Cooper Environmental Services, Portland, Oregon, 1–42, 2010.

Cui, Y., Ji, D., Chen, H., Gao., M., Maenhaut, W., He, J., and Wang, Y.: Characteristics and sources of hourly trace elements in airborne fine particles in urban Beijing, China, J. Geophys. Res., https://doi.org/10.1029/2019JD030881, 2019.

Dall'Osto, M., Querol, X., Amato, F., Karanasiou, A., Lucarelli, F., Nava, S., Calzolai, G., and Chiari, M.: Hourly elemental concentrations in $PM_{2.5}$ aerosols sampled simultaneously at urban background and road site during SAPUSS – diurnal variations and PMF receptor modelling, Atmos. Chem. Phys., 13, 4375–4392, https://doi.org/10.5194/acp-13-4375-2013, 2013.

Dao, L., Morrison, L., and Zhang, C.: Bonfires as a potential source of metal pollutants in urban soils, Galway, Ireland, Appl. Geochem., 27, 930–935, https://doi.org/10.1016/j.apgeochem.2012.01.010, 2012.

Dockery, D. W., Pope III, C. A., Xu, X., Spengler, J. D., Ware, J. H., Fay, M. E., Ferris, B. G., and Speizer, F. E.: An association between air pollution and mortality in six U.S. cities, The New England J. Med., 329, 1753–1759, https://doi.org/10.1056/NEJM199312093292401, 1993.

Drewnick, F., Hings, S. S., Curtius, J., Eerdekens, G., and Williams, J.: Measurement of fine particulate and gas-phase species during the New Year's fireworks 2005 in Mainz, Germany, Atmos. Environ., 40, 4316–4327, https://doi.org/10.1016/j.atmosenv.2006.03.040, 2006.

Ducret-Stich, R. E., Tsai, M.-Y., Thimmaiah, D., Kunzli, N., Hopke, P. K., and Phuleria, H. C.: PM_{10} source apportionment in a Swiss Alpine valley impacted by highway traffic, Environ. Sci. Pollut. Res., 20, 6496–6508, https://doi.org/10.1007/s11356-013-1682-1, 2013.

Dutcher, D. D., Perry, K. D., Cahill, T. A., and Copeland, S. A.: Effects of indoor pyrotechnic displays on the air quality in the Houston Astrodome, J. Air Waste Manage. Assoc., 49, 156–160, https://doi.org/10.1080/10473289.1999.10463790, 1999.

Efron, B.: Bootstrap methods: Another look at the Jacknife, The Ann. Stat., 7, 1–26, 1979.

Empa: Technischer Bericht zum Nationalen Beobachtungsnetz für Luftfremdstoffe (NABEL), available at: http//www.empa.ch, 2011.

Fang, T., Guo, H., Verma, V., Peltier, R. E., and Weber, R. J.: $PM_{2.5}$ water-soluble elements in the southeastern United States: automated analytical method development, spatiotemporal distributions, source apportionment, and implications for health studies, Atmos. Chem. Phys., 15, 11667–11682, https://doi.org/10.5194/acp-15-11667-2015, 2015.

Fröhlich, R., Cubison, M. J., Slowik, J. G., Bukowiecki, N., Canonaco, F., Croteau, P. L., Gysel, M., Henne, S., Herrmann, E., Jayne, J. T., Steinbacher, M., Worsnop, D. R., Baltensperger, U., and Prévôt, A. S. H.: Fourteen months of on-line measurements of the non-refractory submicron aerosol at the Jungfraujoch (3580 m a.s.l.) – chemical composition, origins and organic aerosol sources, Atmos. Chem. Phys., 15, 11373–11398, https://doi.org/10.5194/acp-15-11373-2015, 2015.

Fullova, D., Durcanska, D., and Hegrova, J.: Particulate matter mass concentrations produced from pavement surface abrasion, MATEC Web of Conferences, 117, 00048, https://doi.org/10.1051/matecconf/201711700048, 2017.

Furger, M., Minguillón, M. C., Yadav, V., Slowik, J. G., Hüglin, C., Fröhlich, R., Petterson, K., Baltensperger, U., and Prévôt, A. S. H.: Elemental composition of ambient aerosols measured with high temporal resolution using an online XRF spectrometer, Atmos. Meas.Tech., 10, 2061–2076, https://doi.org/10.5194/amt-10-2061-2017, 2017.

Gianini, M. F. D., Fischer, A., Gehrig, R., Ulrich, A., Wichser, A., Piot, C., Besombes, J.-L., and Hueglin, C.: Comparative source apportionment of PM_{10} in Switzerland for 2008/2009 and 1998/1999 by positive matrix factorisation, Atmos. Environ., 54, 149–158, https://doi.org/10.1016/j.atmosenv.2012.02.036, 2012.

Grigoratos, T. and Martini, G.: Brake wear particle emissions: a review, Environ. Sci. Pollut. Res., 22, 2491–2504, https://doi.org/10.1007/s11356-014-3696-8, 2015.

Harrison, R. M., Beddows, D. C. S., and Dall'Osto, M.: PMF analysis of wide-range particle size spectra collected on a major highway, Environ. Sci. Technol., 45, 5522–5528, https://doi.org/10.1021/es2006622, 2011.

Hassan, A. K., Fares, S., and Abd El-Rahma, M.: Natural radioactivity levels and radiation hazards for gypsum materials used in Egypt. J. Environ. Sci. Technol., 7, 56–66, https://doi.org/10.3923/jest.2014.56.66, 2014.

Hedberg, E., Gidhagen, L., and Johansson, C.: Source contributions to PM_{10} and arsenic concentrations in Central Chile using positive matrix factorization, Atmos. Environ., 39, 549–561, https://doi.org/10.1016/j.atmosenv.2004.11.001, 2005.

Hueglin, C., Gehrig, R., Baltensperger, U., Gysel, M., Monn, C., and Vonmont, H.: Chemical characterisation of $PM_{2.5}$, PM_{10} and coarse particles at urban, near-city and rural sites in Switzerland, Atmos. Environ., 39, 637–651, https://doi.org/10.1016/j.atmosenv.2004.10.027, 2005.

Hueglin, C., Buchmann, B., and Weber, R. O.: Long-term observation of real-world road traffic emission factors on a motorway in Switzerland, Atmos. Environ., 40, 3696–3709, https://doi.org/10.1016/j.atmosenv.2006.03.020, 2006.

Jeong, C.-H., Wang, J. M., and Evans, G. J.: Source Apportionment of Urban Particulate Matter using Hourly Resolved Trace Metals, Organics, and Inorganic Aerosol Components, Atmos. Chem. Phys. Discuss., https://doi.org/10.5194/acp-2016-189, 2016.

Jeong, C.-H., Wang, J. M., Hilker, N., Debosz, J., Sofowote, U., Su, Y., Noble, M., Healy, R. M., Munoz, T., Dabek-Zlotorzynska, E., Celo, V., White, L., Audette, C., Herod, D., and Evans, G. J.: Temporal and spatial variability of traffic-related $PM_{2.5}$ sources: Comparison of exhaust and non-exhaust emissions, Atmos. Environ., 198, 55–69, https://doi.org/10.1016/j.atmosenv.2018.10.038, 2019.

Ji, D., Cui, Y., Li, L., He, J., Wang, L., Zhang, H., Wang, W., Zhou, L., Maenhaut, W., Wen, T., and Wang, Y.: Characterization and source identification of fine particulate matter in urban Beijing during the 2015 Spring Festival, Sci. Total Environ., 430–440, 628–629, https://doi.org/10.1016/j.scitotenv.2018.01.304, 2018.

Jiang, Q., Sun, Y. L., Wang, Z., and Yin, Y.: Aerosol composition and sources during the Chinese Spring Festival: fireworks, secondary aerosol, and holiday effects, Atmos. Chem. Phys., 15, 6023–6034, https://doi.org/10.5194/acp-15-6023-2015, 2015.

Kelly, F. J. and Fussell, J. C.: Air pollution and airway disease, Clin. Exp. Allergy, 41, 1059–1071, https://doi.org/10.1111/j.1365-2222.2011.03776.x, 2011.

Kelly, F. J. and Fussell, J. C.: Size, source and chemical composition as determinants of toxicity attributable to ambient particulate matter, Atmos. Environ., 60, 504–526, https://doi.org/10.1016/j.atmosenv.2012.06.039, 2012.

Kidwell, C. B. and Ondov, J. M.: Development and evaluation of a prototype system for collecting sub-hourly ambient aerosol for chemical analysis, Aerosol Sci. Technol., 35, 596–601, https://doi.org/10.1080/02786820118049, 2001.

Kim, E. and Hopke, P. K.: Source identifications of airborne fine particles using positive matrix factorization and U.S. Environmental Protection Agency positive matrix factorization, J. Air Waste Manage. Assoc., 57, 7, 811–819, https://doi.org/10.3155/1047-3289.57.7.811, 2007.

Kim, E., Hopke, P. K., and Edgerton, E. S.: Source identification of Atlanta aerosol by positive matrix factorization, J. Air Waste Manage. Assoc., 53, 731–739, https://doi.org/10.1080/10473289.2003.10466209, 2003.

Kim, E., Hopke, P. K., and Qin, Y.: Estimation of organic carbon blank values and error structures of the speciation trends network data for source apportionment, J. Air Waste Manage. Assoc., 55, 8, 1190–1199, https://doi.org/10.1080/10473289.2005.10464705, 2005.

Kong, S. F., Li, L., Li, X. X., Yin, Y., Chen, K., Liu, D. T., Yuan, L., Zhang, Y. J., Shan, Y. P., and Ji, Y. Q.: The impacts of firework burning at the Chinese Spring Festival on air quality: insights of tracers, source evolution and aging processes, Atmos. Chem. Phys., 15, 2167–2184, https://doi.org/10.5194/acp-15-2167-2015, 2015.

Lanz, V. A., Prévôt, A. S. H., Alfarra, M. R., Weimer, S., Mohr, C., DeCarlo, P. F., Gianini, M. F. D., Hueglin, C., Schneider, J., Favez, O., D'Anna, B., George, C., and Baltensperger, U.: Characterization of aerosol chemical composition with aerosol mass spectrometry in Central Europe: an overview, Atmos. Chem. Phys., 10, 10453–10471, https://doi.org/10.5194/acp-10-10453-2010, 2010.

Lawrence, S., Sokhi, R., Ravindra, K., Mao, H., Prain, H. D., and Bull, I. D.: Source apportionment of traffic emissions of particulate matter using tunnel measurements, Atmos. Environ., 77, 548–557, https://doi.org/10.1016/j.atmosenv.2013.03.040, 2013.

Lee, D. S. and Pacyna, J. M.: An industrial emissions inventory of calcium for Europe, Atmos. Environ. 33, 1687–1697, https://doi.org/10.1016/S1352-2310(98)00286-6, 1999.

Li, Z., Hopke, P. K., Husain, L., Qureshi, S., Dutkiewicz, V. A., Schwab, J. J., Drewnick, F., and Demerjian, K. L.: Sources of fine particle composition in New York city, Atmos. Environ., 38, 6521–6529, https://doi.org/10.1016/j.atmosenv.2004.08.040, 2004.

Lin, C.-C.: A review of the impact of fireworks on particulate matter in ambient air, J. Air Waste Manage. Assoc., 66, 12, 1171–1182, https://doi.org/10.1080/10962247.2016.1219280, 2016.

Lin, Y.-C., Tsai, C.-J., Wu, Y.-C., Zhang, R., Chi, K.-H., Huang, Y.-T., Lin, S.-H., and Hsu, S.-C.: Characteristics of trace metals in traffic-derived particles in Hsuehshan Tunnel, Taiwan: size distribution, potential source, and fingerprinting metal ratio, Atmos. Chem. Phys., 15, 4117–4130, https://doi.org/10.5194/acp-15-4117-2015, 2015.

Liu, Y., Zheng, M., Yu, M., Cai, X., Du, H., Li, J., Zhou, T., Yan, C., Wang, X., Shi, Z., Harrison, R. M., Zhang, Q., and He, K.: High-time-resolution source apportionment of $PM_{2.5}$ in Beijing with multiple models, Atmos. Chem. Phys., 19, 6595–6609, https://doi.org/10.5194/acp-19-6595-2019, 2019.

Lucarelli, F., Nava, S., Calzolai, G., Chiari, M., Udisti, R., and Marino, F.: Is PIXE still a useful technique for the analysis of atmospheric aerosols? The LABEC experience, X-Ray Spectrom., 40, 162–167, https://doi.org/10.1002/xrs.1312, 2011.

Manousakas, M., Diapouli, E., Papaefthymiou, H., Migliori, A., Karydas, A. G., Padilla-Alvarez, R., Bogovac, M., Kaiser, R. B., Jaksic, M., Bogdanovic-Radovic, I., and Eleftheriadis, K.: Source apportionment by PMF on elemental concentrations obtained by PIXE analysis of PM_{10} samples collected at the vicinity of lignite power plants and mines in Megalopolis, Greece, Nucl. Instr. Meth. Phys. Res. Sec. B, 349, 114–124, https://doi.org/10.1016/j.nimb.2015.02.037, 2015.

Maenhaut, W.: Source apportionment revisited for long-term measurements of fine aerosol trace elements at two locations in southern Norway, Nucl. Instrum. Methods Phys. Res. Sect. B, 417, 133–138 https://doi.org/10.1016/j.nimb.2017.07.006, 2017.

Meister, K., Johansson, C., and Forsberg, B.: Estimated short-term effects of coarse particles on daily mortality in Stockholm, Sweden, Environ. Health Perspect., 120, 431–436, https://doi.org/10.1289/ehp.1103995, 2012.

Minguillon, M. C., Querol, X., Baltensperger, U., and Prévôt, A. S. H.: Fine and coarse PM composition and sources in rural and urban sites in Switzerland: local or regional pollution?, Sci. Total Environ., 427–428, 191–202, https://doi.org/10.1016/j.scitotenv.2012.04.030, 2012.

Moreno, T., Querol, X., Alastuey, A., Minguillón, M. C., Pey, J., Rodriguez, S., Miró, J. V., Felis, C., and Gibbons, W.: Recreational atmospheric pollution episodes: Inhalable metalliferous particles from firework displays, Atmos. Environ., 41, 913–922, https://doi.org/10.1016/j.atmosenv.2006.09.019, 2007.

Ng, N. L., Herndon, S. C., Trimborn, A., Canagaratna, M. R., Croteau, P. L., Onasch, T. B., Sueper, D., Worsnop, D. R., Zhang, Q., Sun, Y. L., and Jayne, J. T.: An aerosol chemical speciation monitor (ACSM) for routine monitoring of the composition and mass concentrations of ambient aerosol, Aerosol Sci. Technol., 45, 780–794, https://doi.org/10.1080/02786826.2011.560211, 2011.

Norris, G., Duvall, R., Brown, S., and Bai, S.: EPA Positive Matrix Factorization (PMF) 5.0 fundamentals and user guide prepared for the United States Environmental Protection Agency Office of Reseach and Development, Washington DC, 2014.

Olivier, F., Belis, C. A., Amato, F., Decesari, S., Diapouli, E., El Haddad, I., Gilardoni, S., Harrison, R. M., Hopke, P. K., Larsen, B. R., Manousakas, M., Mocnik, G., Mooibroek, D., Nava, S., Paatero, P., Paglione, M., Prévôt, A. S. H., Quass, U., Salvador, P., Takahama, S., Vecchi, R., Viana, M., and Vratolis, S: European guide on air pollution source apportionment with receptor models revision 2019, https://source-apportionment.jrc.ec.europa.eu/Docu/european%20_guide_SA_RMs_revision_2019.pdf.

Paatero, P.: The Multilinear Engine – A table-driven, least squares program for solving multilinear problems, including the n-way parallel factor analysis model, J. Comput. Graph. Stat., 8, 854–888, https://doi.org/10.1080/10618600.1999.10474853-1999, 1999.

Paatero, P. and Hopke, P. K.: Discarding or downweighting high-noise variables in factor analytic models, Anal. Chim. Acta, 490, 277–289, https://doi.org/10.1016/s0003-2670(02)01643-4, 2003.

Paatero, P. and Tapper, U.: Positive matrix factorization: A non-negative factor model with optimal utilization of error-estimates of data values, Environmetrics, 5, 111–126, https://doi.org/10.1002/env.3170050203, 1994.

Park, S. S., Cho, S. Y., Jo, M. R., Gong, B. J., Park, J. S., and Lee, S. J.: Field evaluation of a near-real time elemental monitor and identification of element sources observed at an air monitoring supersite in Korea, Atmos. Poll. Res., 5, 119–128, https://doi.org/10.5094/apr.2014.015-2014, 2014.

Pernigotti, D., Belis, C. A., and Spanó, L.: SPECIEUROPE: The European data base for PM source profiles, Atmos. Pollut. Res., 7 (2), 307–314, https://doi.org/10.1016/j.apr.2015.10.007, 2016.

Perrino, C., Tiwari, S., Catrambone, M., Torre, S. D., Rantica, E., and Canepari, S.: Chemical characterization of atmospheric PM in Delhi, India, during different periods of the year including Diwali festival, Atmos. Pollut. Res., 2, 418–427, https://doi.org/10.5094/apr.2011.048, 2011.

Phillips-Smith, C., Jeong, C.-H., Healy, R. M., Dabek-Zlotorzynska, E., Celo, V., Brook, J. R., and Evans, G.: Sources of particulate matter components in the Athabasca oil sands region: investigation through a comparison of trace element measurement methodologies, Atmos. Chem. Phys., 17, 9435–9449, https://doi.org/10.5194/acp-17-9435–2017, 2017.

Polissar, A. V., Hopke, P. K., Paatero, P., Malm, W. C., and Sisler, J. F.: Atmospheric aerosol over Alaska: 2. Elemental composition and sources, J. Geophys. Res., 103, 19045–19057, https://doi.org/10.1029/98JD01212, 1998.

Pongpiachan, S., Iijima, A., and Cao, J.: Hazard quotients, hazard indexes, and cancer risks of toxic metals in PM_{10} during firework displays, Atmosphere, 9, 144, https://doi.org/10.3390/atmos9040144, 2018.

Pope III, C. A. and Dockery, D. W.: Health effects of fine particulate air pollution: Lines that connect, J. Air Waste Manage. Assoc., 56, 709–742, https://doi.org/10.1080/10473289.2006.10464485, 2006.

Rahman, S. A., Hamzah, M. S., Wood, A. K., Elias, M. S., Salim, N. A. A., and Sanuri, E.: Sources apportionment of fine and coarse aerosol in Klang Valley, Kuala Lumpur using positive matrix factorization, Atmos. Poll. Res., 2, 197–206, https://doi.org/10.5094/apr.2011.025, 2011.

Rai, P., Chakraborty, A., Mandariya, A. K., and Gupta, T.: Composition and source apportionment of PM_1 at urban site Kanpur in India using PMF coupled with CBPF, Atmos. Res., 178–179, 506–520, https://doi.org/10.1016/j.atmosres.2016.04.015, 2016.

Reff, A., Eberly, S. I., and Bhave, P. V.: Receptor modeling of ambient particulate matter data using positive matrix factorization: Review of existing methods, J. Air Waste Manage. Assoc., 57, 146–154, https://doi.org/10.1080/10473289.2007.10465319, 2007.

Retama, A., Neria-Hernández, A., Jaimes-Palomera, M., Rivera-Hernández, O., Sánchez-Rodríguez, M., López-Medina, A., and Velasco, E.: Fireworks: a major source of inorganic and organic aerosols during Christmas and New Year in Mexico city, Atmos. Environ., 2, 100013, https://doi.org/10.1016/j.aeaoa.2019.100013, 2019.

Richard, A., Gianini, M. F. D., Mohr, C., Furger, M., Bukowiecki, N., Minguillón, M. C., Lienemann, P., Flechsig, U., Appel, K., DeCarlo, P. F., Heringa, M. F., Chirico, R., Baltensperger, U., and Prévôt, A. S. H.: Source apportionment of size and time resolved trace elements and organic aerosols from an urban courtyard site in Switzerland, Atmos. Chem. Phys., 11, 8945–8963, https://doi.org/10.5194/acp-11-8945-2011, 2011.

Rudnick, R. L. and Gao, S.: Composition of the continental crust, Vol. 3, edited by: Rudnick, E., Book Section 2, 1–56, Elsevier Science, Philadelphia, 2003.

Sarkar, S., Khillare, P. S., Jyethi, D. S., Hasan, A., and Parween, M.: Chemical speciation of respirable suspended particulate matter during a major firework festival in India, J. Hazard. Mater., 184, 321–330, https://doi.org/10.1016/j.jhazmat.2010.08.039, 2010.

Schauer, J. J., Lough, G. C., Shafer, M. M, Christensen, W. C., Arndt, M. F., DeMinter, J. T., and Park, J. S.: Characterization of emissions of metals emitted from motor vehicles, Research report (Health Effects Institute), 133, 1–76; discussion 77, 2006.

Sofowote U. M., Healy R. M., Su Y., Debosz J., Noble M., Munoz A., Jeong C.-H., Wang J. M., Hilker N., Evans G. J, and Hopke P. K.: Understanding the $PM_{2.5}$ imbalance between a far and near road location: Results of high temporal frequency source apportionment and parameterization of black carbon, Atmos. Environ., 173, 277–288., https://doi.org/10.1016/j.atmosenv.2017.10.063, 2018.

Taylor, S. R. and McLennan, S. M.: The geochemical evolution of the continental crust, Rev. Geophys., 33, 241–265, 1995.

Thorpe, A. and Harrison, R. M.: Sources and properties of non-exhaust particulate matter from road traffic: A review, Sci. Total Environ., 400, 270–282, https://doi.org/10.1016/j.scitotenv.2008.06.007, 2008.

Tian, S. L., Pan, Y. P., and Wang, Y. S.: Size-resolved source apportionment of particulate matter in urban Beijing during haze and non-haze episodes, Atmos. Chem. Phys., 16, 1–19, https://doi.org/10.5194/acp-16-1-2016, 2016.

Tian, Y. Z., Wang, J., Peng, X., Shi, G. L., and Feng, Y. C.: Estimation of the direct and indirect impacts of fireworks on the physicochemical characteristics of atmospheric PM_{10} and $PM_{2.5}$, Atmos. Chem. Phys., 14, 9469–9479, https://doi.org/10.5194/acp-14-9469-2014, 2014.

Tremper, A. H., Font, A., Priestman, M., Hamad, S. H., Chung, T.-C., Pribadi, A., Brown, R. J. C., Goddard, S. L., Grassineau, N., Petterson, K., Kelly, F. J., and Green, D. C.: Field and laboratory evaluation of a high time resolution X-ray fluorescence instrument for determining the elemental composition of ambient aerosols, Atmos. Meas. Tech., 11, 3541–3557, https://doi.org/10.5194/amt-11-3541-2018, 2018.

Twigg, M. M., Di Marco, C. F., Leeson, S., van Dijk, N., Jones, M. R., Leith, I. D., Morrison, E., Coyle, M., Proost, R., Peeters, A. N. M., Lemon, E., Frelink, T., Braban, C. F., Nemitz, E., and Cape, J. N.: Water soluble aerosols and gases at a UK background site – Part 1: Controls of $PM_{2.5}$ and PM_{10} aerosol composition, Atmos. Chem. Phys., 15, 8131–8145, https://doi.org/10.5194/acp-15-8131-2015, 2015.

Ulbrich, I. M., Canagaratna, M. R., Zhang, Q., Worsnop, D. R., and Jimenez, J. L.: Interpretation of organic components from positive matrix factorization of aerosol mass spectrometric data, Atmos. Chem. Phys., 9, 2891–2918, https://doi.org/10.5194/acp-9-2891-2009, 2009.

Vallius, M.: Characteristics and sources of fine particulate matter in urban air. Ph.D. dissertation. Publications of the National Public Health Institute, Department of Environmental Health Kuopio, Finland, 2005.

Vecchi, R., Bernardoni, V., Cricchio, D., D’Alessandro, A., Fermo, P., Lucarelli, F., Nava, S., Piazzalunga, A., and Valli, G.: The impact of fireworks on airborne particles, Atmos. Environ., 42, 1121–1132, https://doi.org/10.1016/j.atmosenv.2007.10.047, 2008.

Vega, E., Mugica, V., Reyes, E., Sanchez, G., Chow, J. C., and Watson, J. G.: Chemical composition of fugitive dust emitters in Mexico City, Atmos. Environ., 35, 4033–4039, https://doi.org/10.1016/S1352-2310(01)00164-9, 2001.

Visser, S., Slowik, J. G., Furger, M., Zotter, P., Bukowiecki, N., Canonaco, F., Flechsig, U., Appel, K., Green, D. C., Tremper, A. H., Young, D. E., Williams, P. I., Allan, J. D., Coe, H., Williams, L. R., Mohr, C., Xu, L., Ng, N. L., Nemitz, E., Barlow, J. F., Halios, C. H., Fleming, Z. L., Baltensperger, U., and Prévôt, A. S. H.: Advanced source apportionment of size-resolved trace elements at multiple sites in London during winter, Atmos. Chem. Phys., 15, 11291–11309, https://doi.org/10.5194/acp-15-11291-2015, 2015.

~~Vossler, T., Černikovský, L., Novák, J., and Williams, R.: Source apportionment with uncertainty estimates of fine particulate matter in Ostrava, Czech Republic using positive matrix factorization, Atmos. Pollut. Res., 7, 503-512, https://doi.org/10.1016/j.apr.2015.12.004, 2016.~~

Wahlström, J., Olander, L., and Olofsson, U.: Size, shape, and elemental composition of airborne wear particles from disc brake materials, Tribol. Lett., 38, 15–24, 2010.Wang, Q., Qiao, L., Zhou, M., Zhu, S., Griffith, S., Li, L., and Yu, J. Z: Source apportionment of $PM_{2.5}$ using hourly measurements of elemental tracers and major constituents in an urban environment: investigation of time-resolution influence, J. Geophys. Res. : Atmos., 123, 5284–5300, https://doi.org/10.1029/2017JD027877, 2018.

Wang, Y., Zhuang, G., Xu, C., and An, Z.: The air pollution caused by the burning of fireworks during the lantern festival in Beijing, Atmos. Environ., 41, 417–431, https://doi.org/10.1016/j.atmosenv.2006.07.043, 2007.

Williams, A. L., Stensland, G. J., Peters, C. R., and Osborne, J.: Atmospheric dispersion study of deicing salt applied to roads: first progress report, Illinois State Water Surv. Contract Report, 2000-05, Champaign, IL, 2000.

Yang, L. X., Gao, X. M., Wang, X. F., Nie, W., Wang, J., Gao, R., Xu, P. J., Shou, Y. P., Zhang, Q. Z., and Wang, W. X.: Impacts of firecracker burning on aerosol chemical characteristics and human health risk levels during the Chinese New Year Celebration in Jinan, China, Sci. Total Environ., 476–477, 57–64, https://doi.org/10.1016/j.scitotenv.2013.12.110, 2014.

Yao, L., Wang, D., Fu, Q., Qiao, L., Wang, H., Li, L., Sun, W., Li, Q., Wang, L., Yang, X., Zhao, Z., Kan, H., Xian, A., Wang, G., Xiao, H., and Chen, J.: The effects of firework regulation on air quality and public health during the Chinese Spring Festival from 2013 to 2017 in a Chinese megacity, Environ. Int., 126, 96–106, https://doi.org/10.1016/j.envint.2019.01.037, 2019.

Yu, L., Wang, G., Zhang, R., Zhang, L., Song, Y., Wu, B., Li, X., An, K., and Chu, J.: Characterization and source apportionment of $PM_{2.5}$ in an urban environment in Beijing, Aerosol Air Qual. Res., 13, 574–583, https://doi.org/10.4209/aaqr.2012.07.0192, 2013.

Zhang, R., Jing, J., Tao, J., Hsu, S.-C., Wang, G., Cao, J., Lee, C. S. L., Zhu, L., Chen, Z., Zhao, Y., and Shen, Z.: Chemical characterization and source apportionment of $PM_{2.5}$ in Beijing: seasonal perspective, Atmos. Chem. Phys., 13, 7053–7074, https://doi.org/10.5194/acp-13-7053-2013, 2013.

Zhao, W. and Hopke, P. K.: Source apportionment for ambient particles in the San Gorgonio wilderness, Atmos. Environ., 38, 5901–5910, https://doi.org/10.1016/j.atmosenv.2004.07.011, 2004.

Zhou, S., Davy, P. K., Huang, M., Duan, J., Wang, X., Fan, Q., Chang, M., Liu, Y., Chen, W., Xie, S., Ancelet, T., and Trompetter, W. J.: High-resolution sampling and analysis of ambient particulate matter in the Pearl River Delta region of southern China: source apportionment and health risk implications, Atmos. Chem. Phys., 18, 2049–2064, https://doi.org/10.5194/acp-18-2049-2018, 2018.

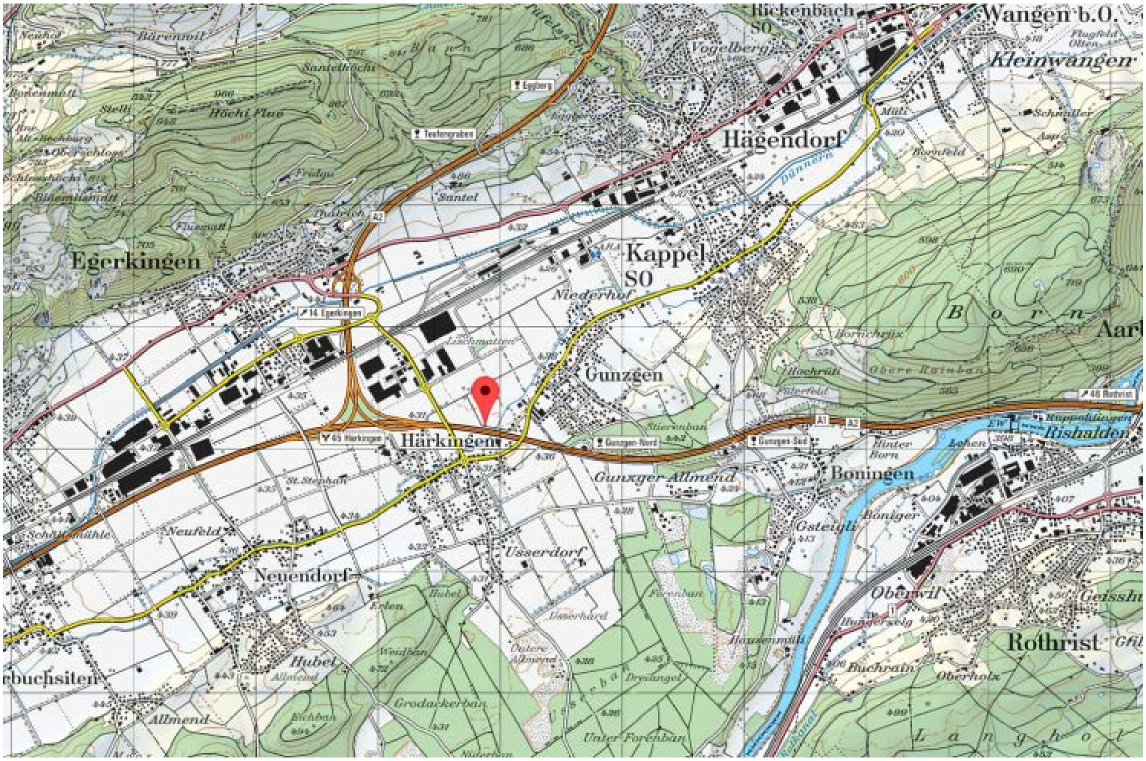

Figure 1: Map of the sampling location (NABEL site in Haerkingen), The site is marked with red google pin. Map reproduced by permission of swisstopo (JA100119).

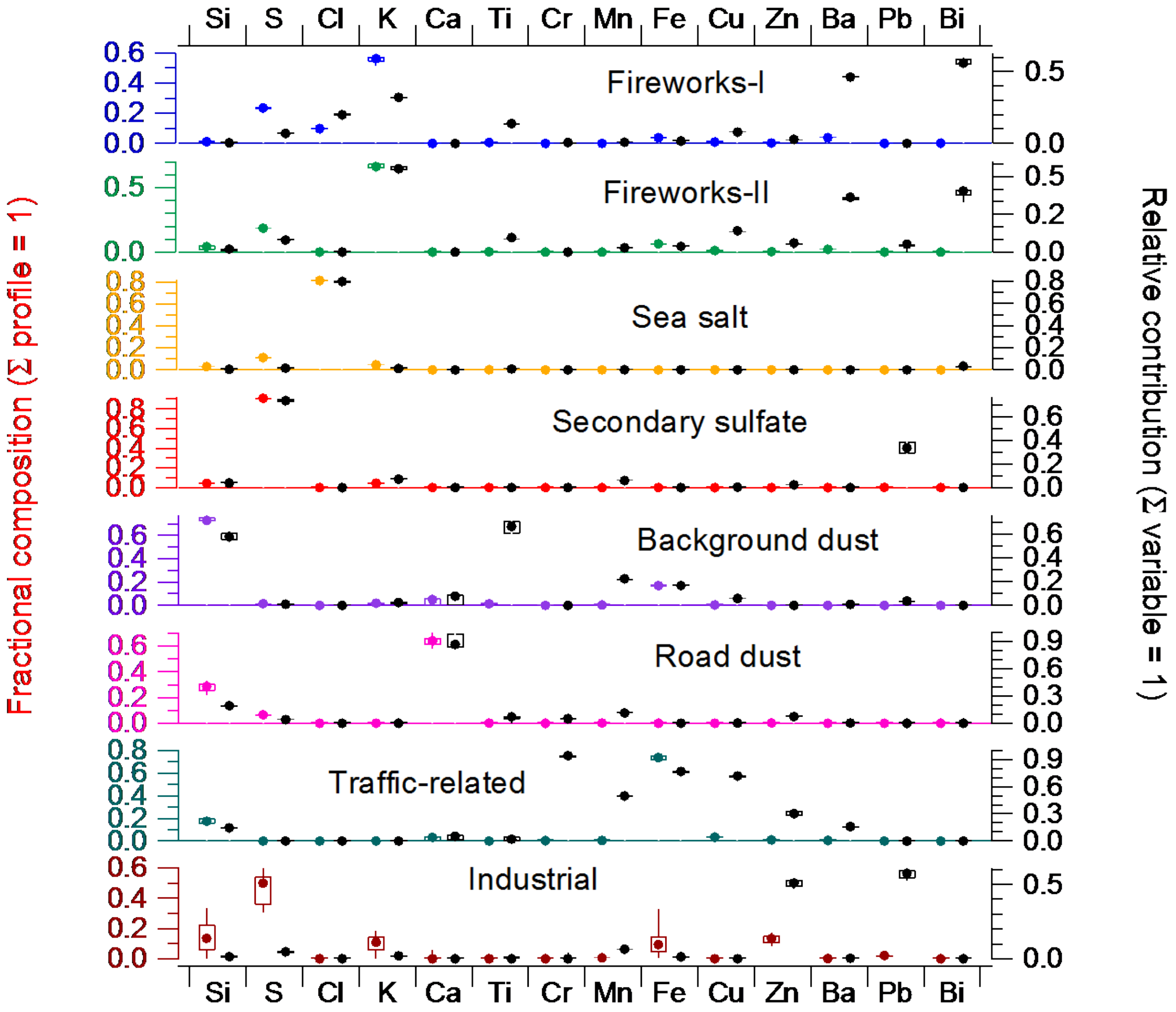
Si
S
Cl
K
Ca
Ti
Cr
Mn
Fe
Cu
Zn
Ba
Pb
Bi
Fireworks-I
Fireworks-II
Sea salt
Secondary sulfate
Background dust
Road dust
Traffic-related
Industrial
Fractional composition (Σ profile = 1)
Relative contribution (Σ variable = 1)
0.0
0.2
0.4
0.6
0.8
0.5
0.3
0.9

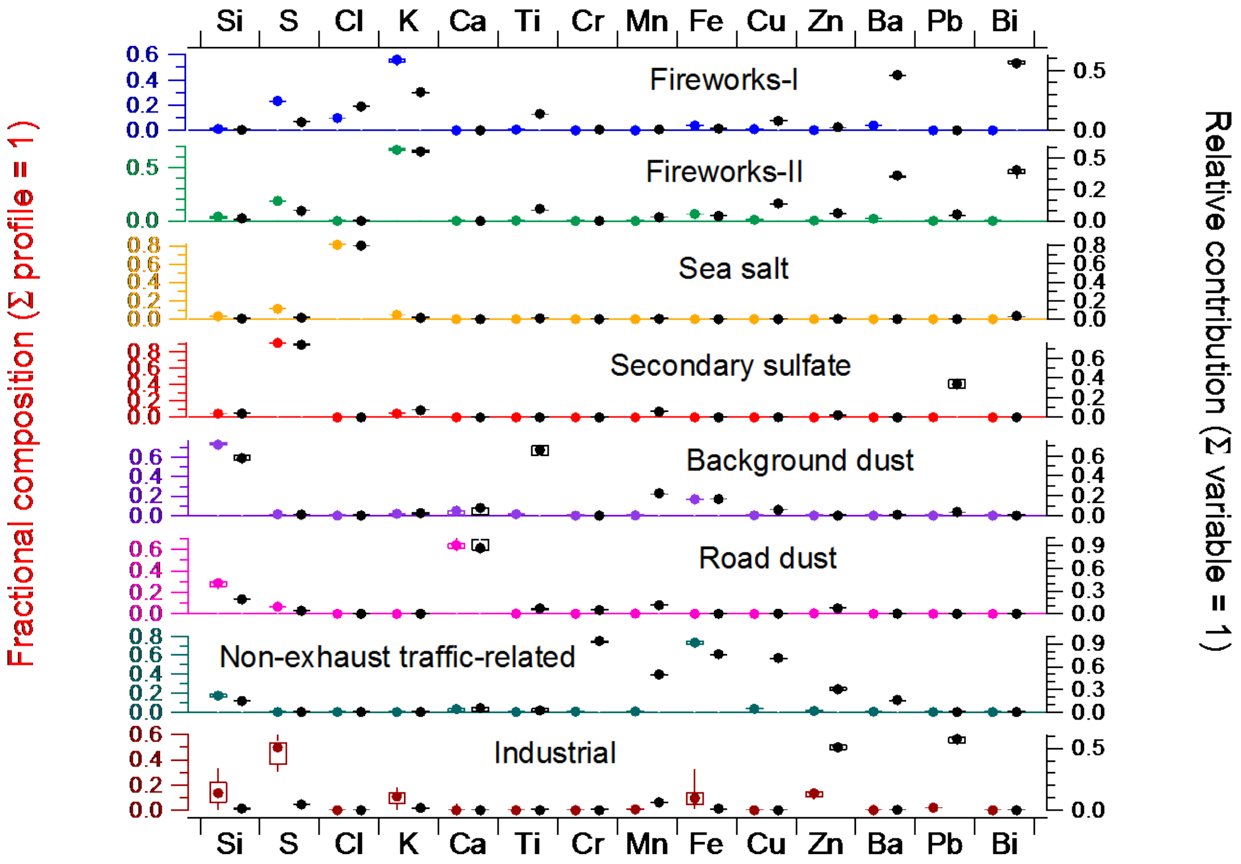

Figure 2: Source profiles of PMF results. The data and their corresponding uncertainty are given as box-whisker plot (bottom to top: p10-p25-p50-p75-p90) of good solutions from bootstrap runs. The left y-axis represents the fractional composition of the factor profile in row-wise (presented in coloured box whisker plot) for each factor in ng ng^{-1}, the right y-axis represents the relative contribution of each factor to each variable (indicated in black box-whisker plot).

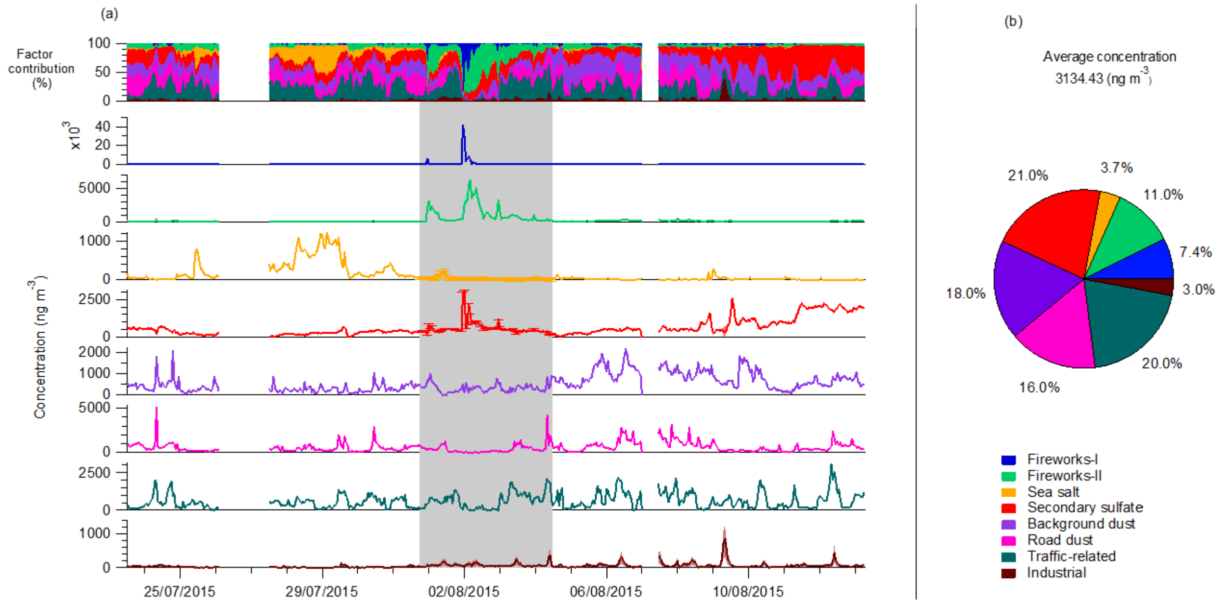

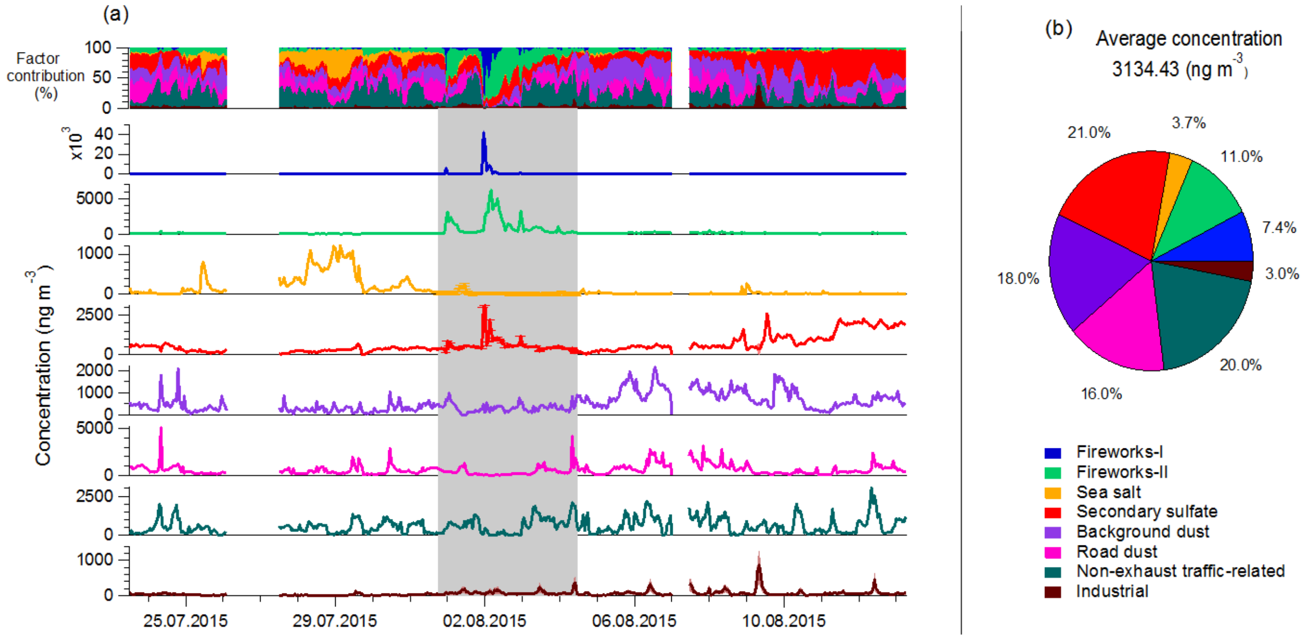

Figure 3: (a) Time series of the PM_{10el} sources and relative contributions of the different sources over time; shaded areas indicate the uncertainties (interquartiles) of selected bootstrap runs; grey background color represents the fireworks period; the estimated uncertainties of the secondary sulfate (± 5%) and the sea salt factors (± 42%) during the fireworks period are added as error bars; (b) Mean relative contributions of PM_{10el} sources. The average concentration represents the mean value of apportioned sources in PM_{10el} which is the sum of 14 elements.~~**Figure 3: (a) Time series of the PM_{10} elemental sources and relative contributions of the different sources over time; shaded areas indicate the uncertainties (interquartile) of selected bootstrap runs; grey background color represent the fireworks period; estimated uncertainty of the secondary sulfate (± 5%) and the sea salt factors (± 42%) during fireworks period are added as error bars; (b) Mean relative contributions of PM_{10} elemental sources.**~~

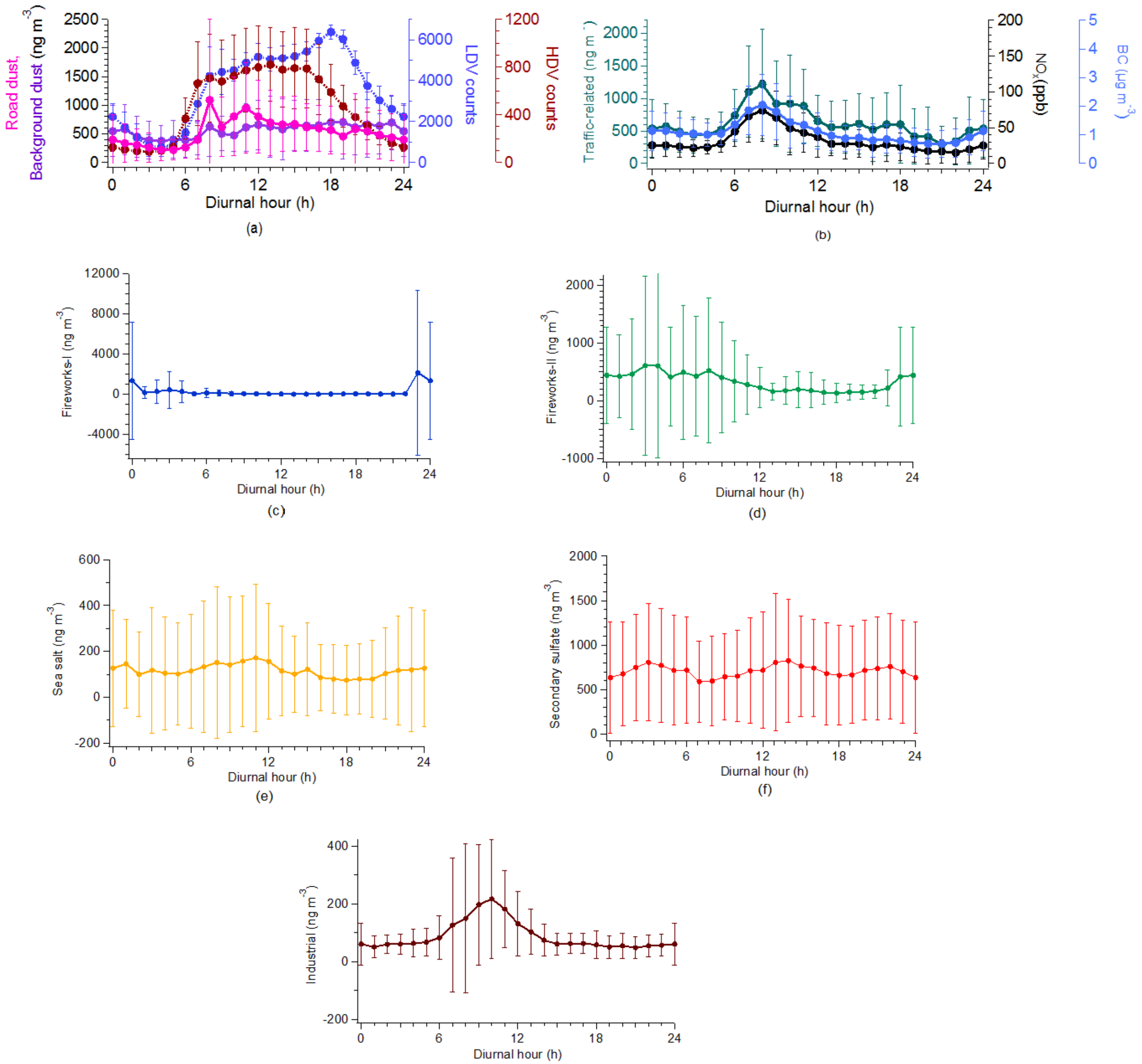
Road dust,
Background dust (ng m^{-3})
LDV counts
HDV counts
Diurnal hour (h)
Traffic-related (ng m^{-3})
NO$_X$ (ppb)
BC (μg m^{-3})
Fireworks-I (ng m^{-3})
Fireworks-II (ng m^{-3})
Sea salt (ng m^{-3})
Secondary sulfate (ng m^{-3})
Industrial (ng m^{-3})

(a) (b) (c) (d) (e) (f) (g)

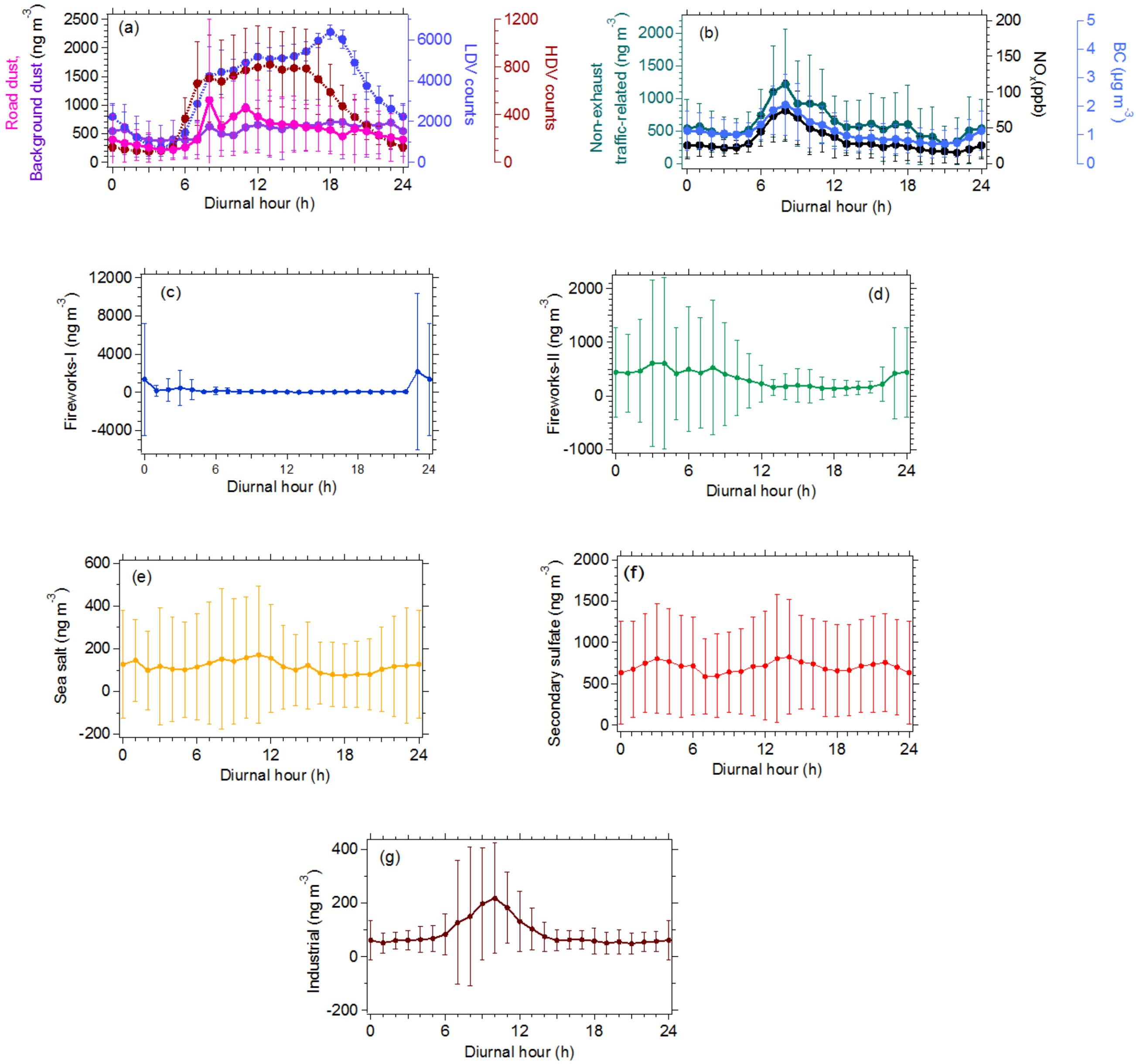

Figure 4: Mean diurnal patterns of the factors and of some corresponding external tracers with error bars (one standard deviation).

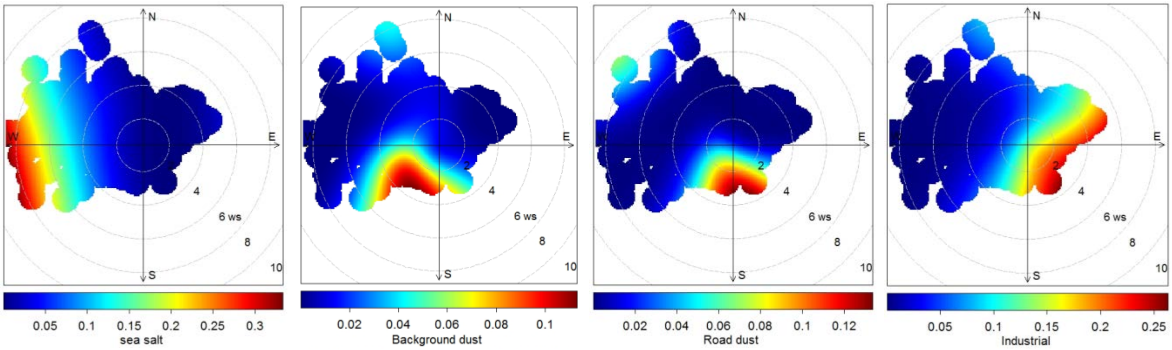

Figure 5: CBPF analysis (at 90th percentile) of factors in terms of wind speed (m s^{-1}) and wind direction. The color code represents the probability of the factor contribution.

Supplementary of

Source apportionment of highly time resolved ~~trace~~ elements during a firework episode from a rural freeway site in Switzerland

Pragati Rai et al.

Correspondence to: André S. H. Prévôt (andre.prevot@psi.ch) and Markus Furger (markus.furger@psi.ch)

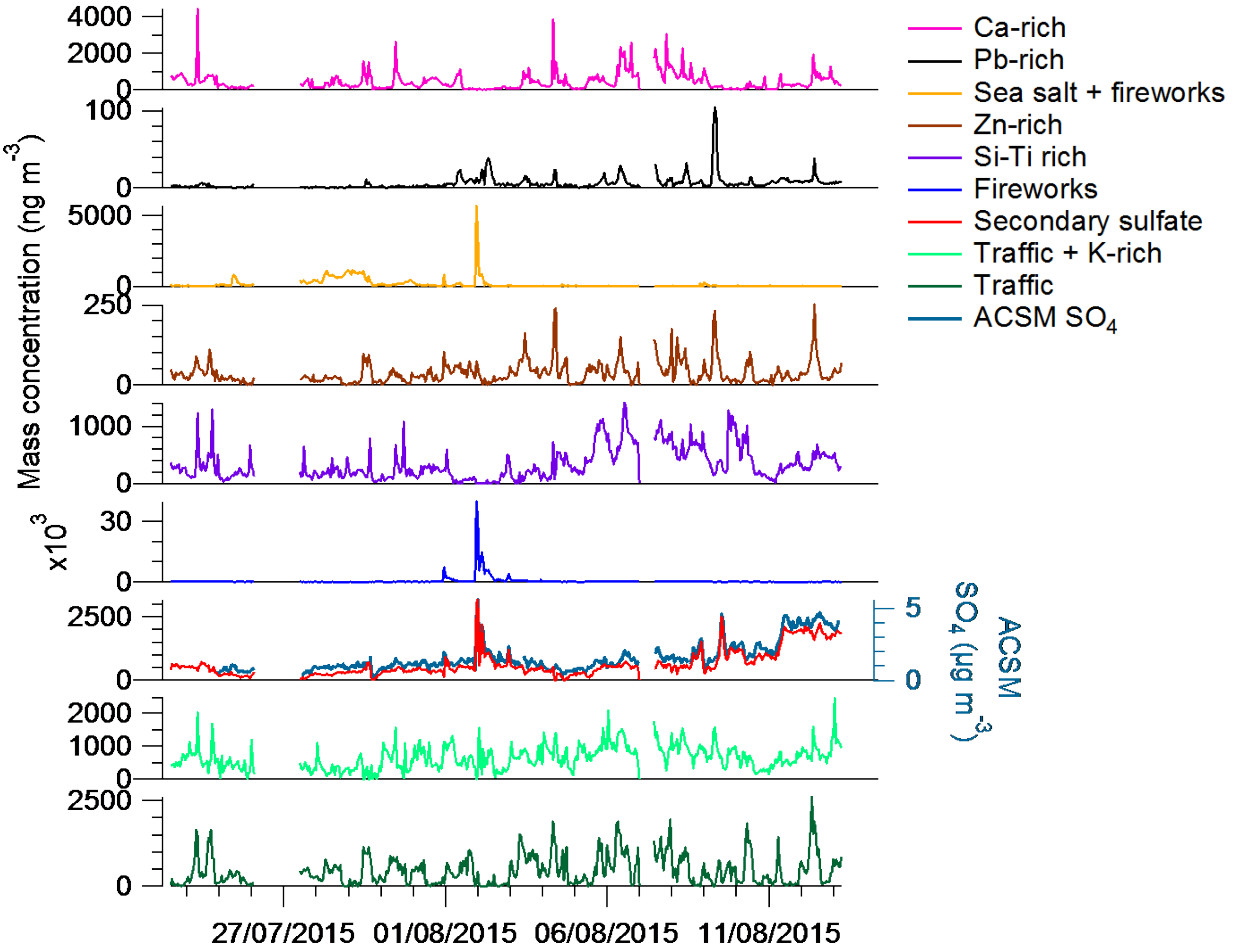

Figure S1: Unconstrained PMF with a nine-factor solution.

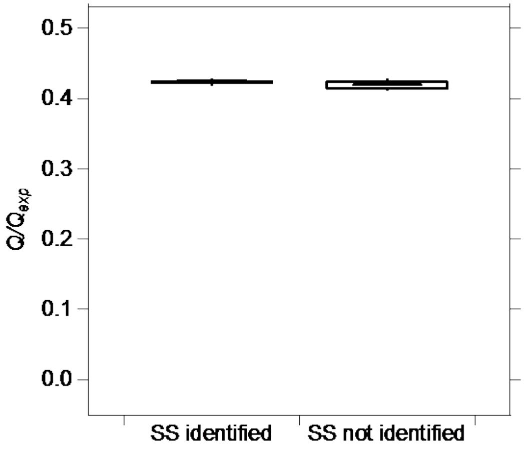

Figure S2: Box-whisker plots of *Q/Q$_{exp}$* for the seed analysis of the nine-factor unconstrained PMF on the full dataset. Shown separately are the 24 solutions in which a secondary sulfate (SS) factor was identified ("SS identified") and the 76 solutions where it was not ("SS not identified").

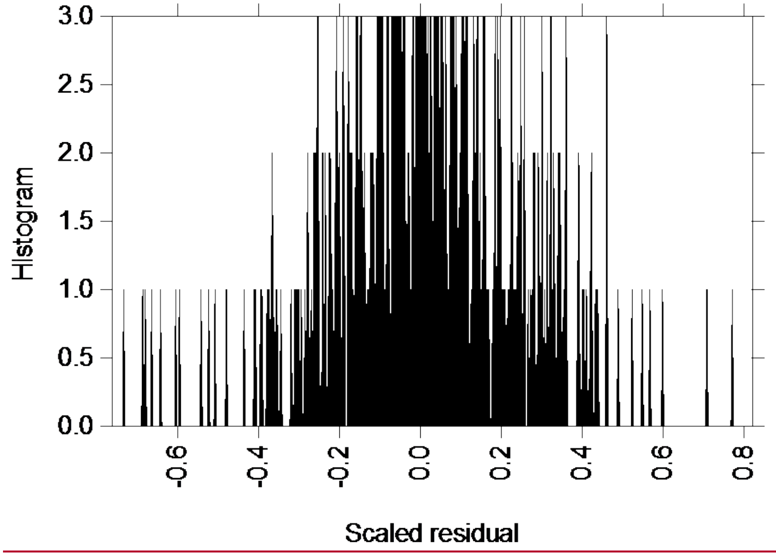

Figure S3: Histograms of the scaled residuals (e_{ij}/s_{ij}) for S in the nine-factor unconstrained PMF solution on the complete dataset.

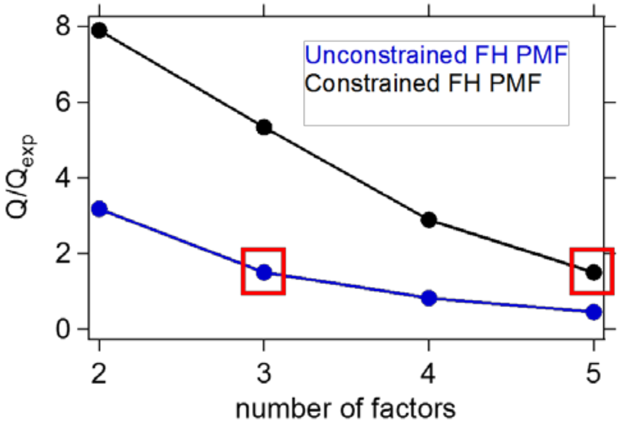

Figure S4: Q/Q_{exp} as a function of the number of factors for FH PMF analyses.

The unexplained variation (UEV, Paatero et al., 2004; Canonaco et al., 2013) which is a dimensionless quantity, describes how much of the measured variation (time or variable) is not explained by each PMF factor (Eq. S1, for variable *j*):

$$UEV_{j,k,real} = \frac{\sum_{i=1}^{n}\left(\left|e_{i,j}\right|/s_{i,j}\right)}{\sum_{i=1}^{n}\left(\left(\sum_{k=1}^{p}\left|g_{i,k}f_{k,j}\right|+\left|e_{i,j}\right|\right)/s_{i,j}\right)} \quad \text{for k} = 1, \dots\dots, \text{p for } \left(x_{i,j}/s_{i,j}\right) > 2 \qquad \text{(S1)}$$

Where $f_{k,j}$ are the factor profiles and $g_{i,k}$ represent their time-dependent contributions. The index *i* represents a specific point in time (up to *n*), *j* is the variable, and *k* is a factor (up to *p*). $e_{i,j}$ are the PMF-residuals, $x_{i,j}$ the input data and $s_{i,j}$ the measurement uncertainties. The UEV presented here is the real UEV for high S/N threshold >2, otherwise UEV will be considered as noisy UEV.

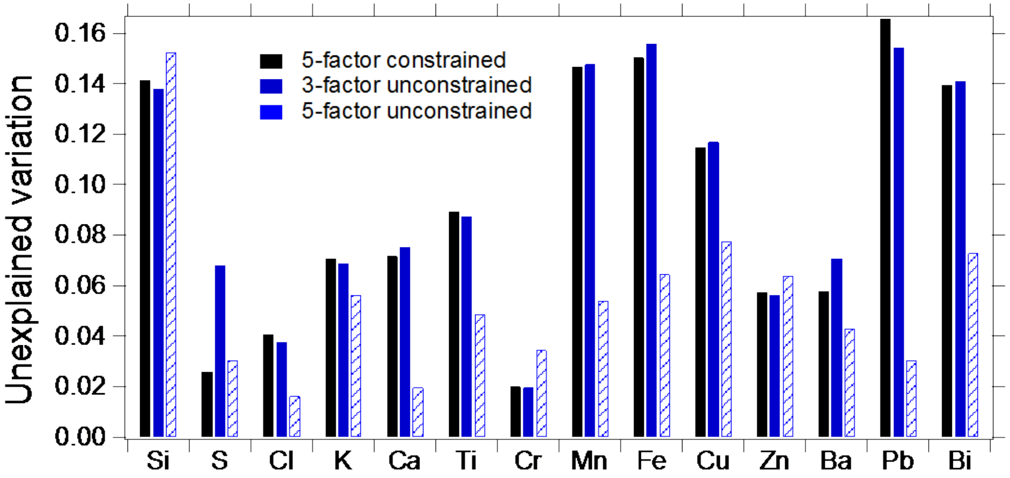

Figure S5: Unexplained variation for each variable in FH PMF solutions: (1) constrained five-factor (black color); (2) unconstrained 5-factor (semi filled blue color), and (3) unconstrained three-factor (blue color).

The stability of the fireworks factor profile was assessed by investigation of 1000 random BS runs on the FH dataset (see more details below). Solutions were accepted based on a K / S ratio in the fireworks factor of 2.76 ± 0.5, consistent with black powder composition (Dutcher et al., 1999) and the concentration peak between 40-45 µg m^{-3} on 1 August 23:00 LT in the factor time series. This criterion yielded an acceptance rate of 21.3 %, with an average Q/Q_{exp} of 1.3. The results of the BS analysis are provided in Fig. S6, where we show the fractional composition of the fireworks factor profiles from: (a) FH BS analysis (blue color); (b) 5-factor constrained FH PMF analysis (base case, in red color). The data and their corresponding uncertainty are given as box-whisker plot (bottom to top: p10-p25-p50-p75-p90) of selected 213 solutions out of 1000 BS runs. The displayed error bars for the base case correspond to the a-value of 0.1 used to constrain fireworks profile in the complete dataset PMF analysis. This figure shows that the variation in fireworks profiles retrieved from the bootstrap analysis is relatively stable despite the small number of data points; indeed, it generally denotes a smaller range of values than those allowed by the constrained fireworks profile in the full dataset PMF. Further, the resolved fireworks profile from FH BS solution agrees well with the base case, and the Q/Q_{exp} values are reasonable. Taken together, these results suggest that the FH dataset contains sufficient variability to allow retrieval of a robust fireworks profile.

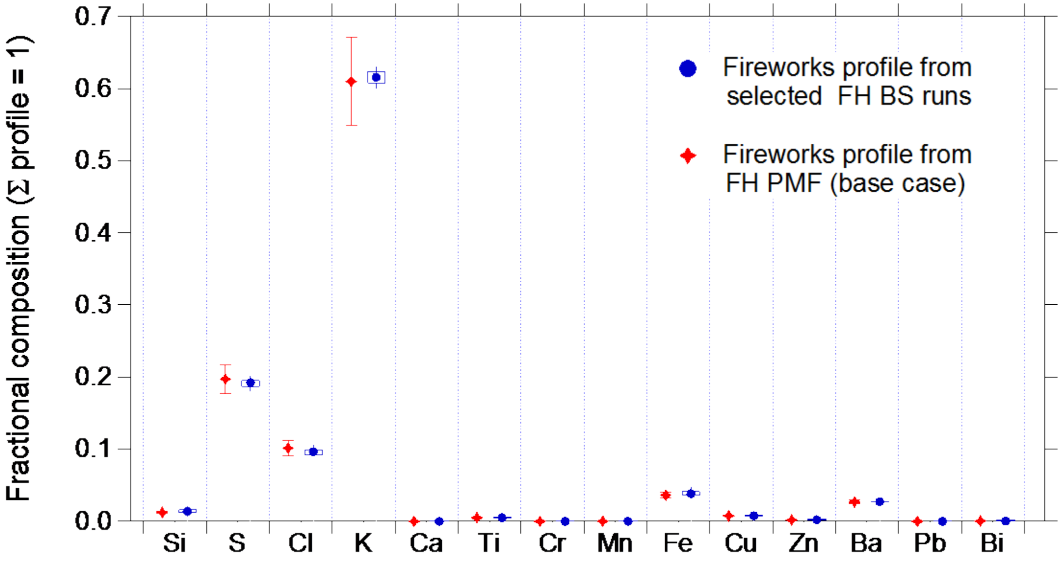

Figure S6: Fireworks factor profiles from: (a) FH BS analysis (blue color); (b) five-factor constrained FH PMF analysis (base case, red color). The data and their corresponding uncertainties are given as box-whisker plot (bottom to top: p10-p25-p50-p75-p90) of selected 213 solutions from 1000 BS runs in blue color. Base case uncertainties are given ± 10 % as error bar by considering that *a*-value 0.1 is applied to constrain fireworks profile in complete dataset PMF analysis. Y-axis represents the fractional composition of the factor profile in row-wise for each factor in ng ng^{-1}.

Based on Q_{avg}, defined as $\frac{\sum_{i=1}^{m}\sum_{j=1}^{n}\left(\frac{e_{ij}}{s_{ij}}\right)^{2}}{n*m}$ (*n*: sample time series, *m*: number of variables), the model explains the data variability very well when allowing for eight factors (Fig S7). Furthermore, we access the change in time-dependent $Q_{avg,i}$, $\frac{\sum_{i=1}^{m}\sum_{j=1}^{n}\left(\frac{e_{ij}}{s_{ij}}\right)^{2}}{n}$, when increasing the number of factors i.e., $\Delta Q_{avg,i}$; contribution to *Q* for the (*p*)-factor solution minus that of the (*p*+1)-factor solution (Fig S8~~3~~). A significant decrease in $\Delta Q_{avg,i}$ indicates that the structure in the residuals disappeared with the additional factor. The removed structure is evident up to eight factors. Increasing the number of factors to nine yields a new mixed factor of the traffic-related and background dust factors (Fig. S1). Overall, a best ME-2 solution was observed up to a number of factors equal to eight.

For the 8-factor solution, we assess how well the different variables are explained by PMF using the quantity $\Delta Q_{avg,j}$ $\frac{\sum_{i=1}^{m}\sum_{j=1}^{n}\left(\frac{e_{ij}}{s_{ij}}\right)^{2}}{m}$ (Fig S9~~4~~). $Q_{avg,j}$ shows that with 8 factors all variables are explained within their measurement uncertainty except Si and Pb. This might be linked to an underestimation of the measurement uncertainty itself.

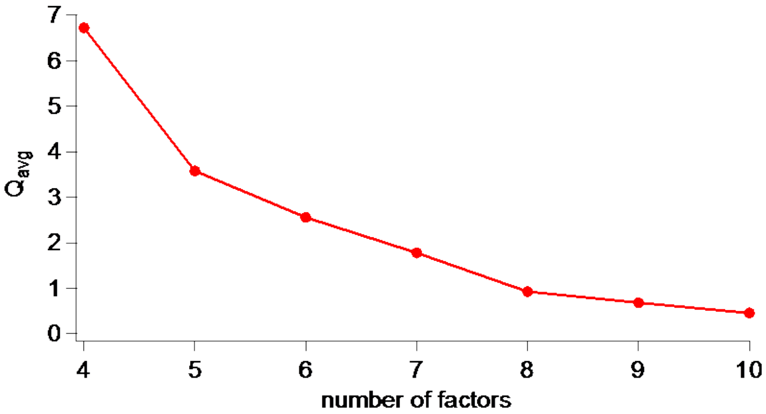

Figure S7~~2~~: Q_{avg} as a function of the number of factors.

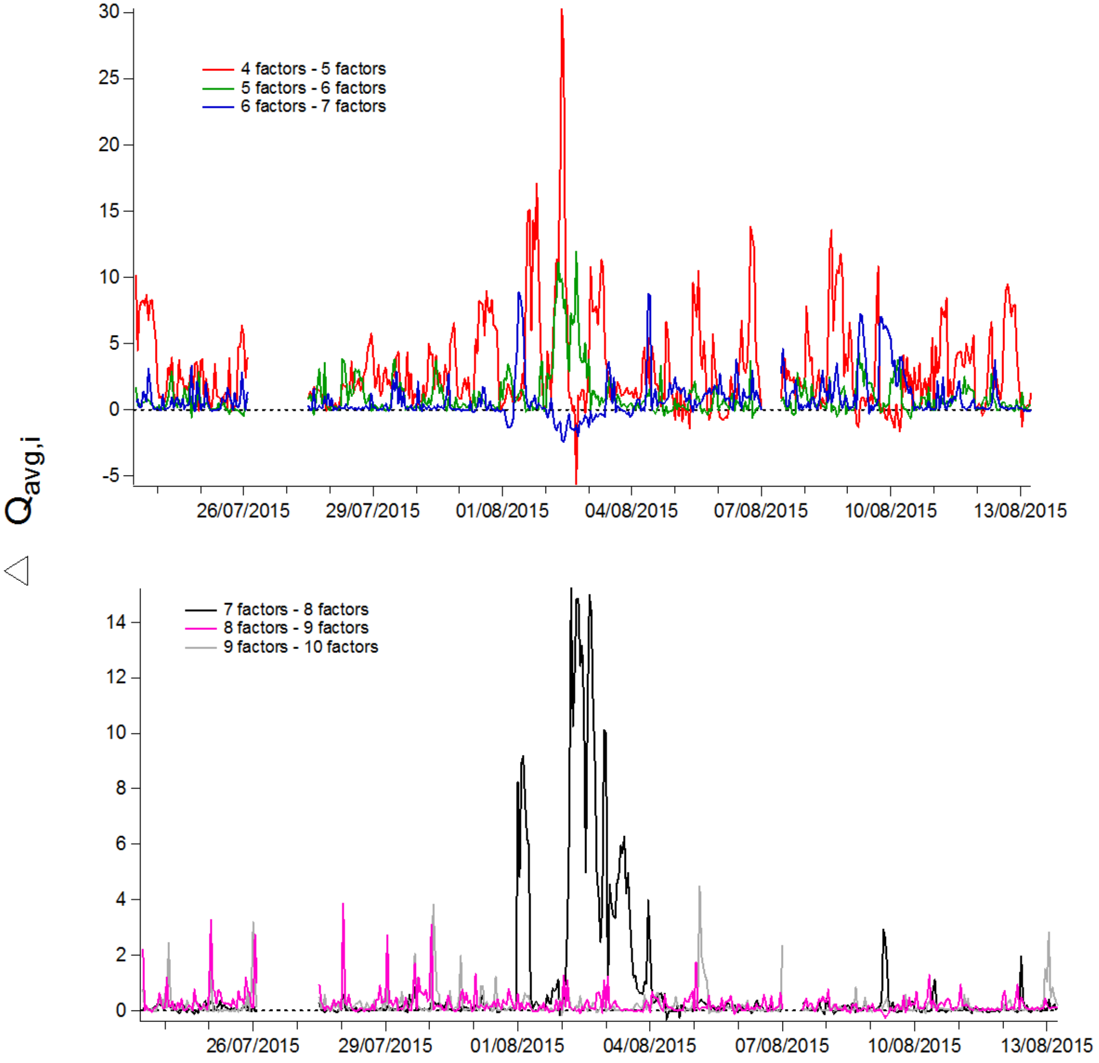

Figure S8~~3~~: Change in the time-dependent contribution of $Q_{avg,i}$ ($\Delta Q_{avg,i}$) as a function of the number of factors.

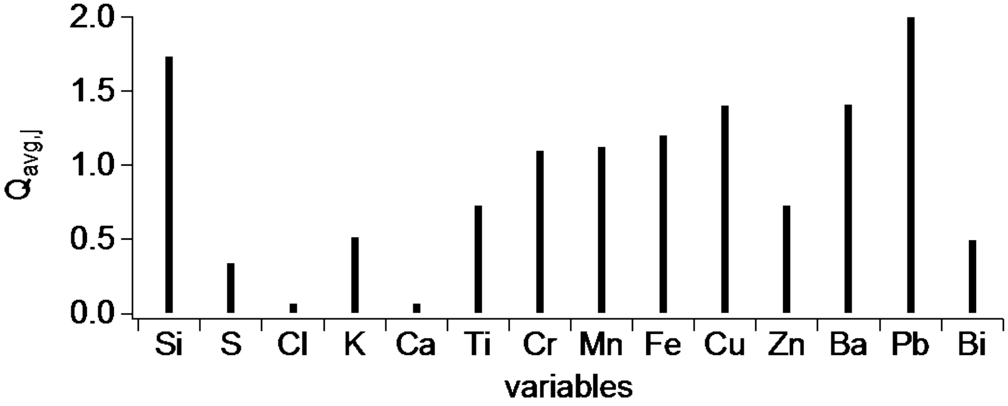

Figure S94: Q_{avg} as a function of variables for the eight-factor solution.

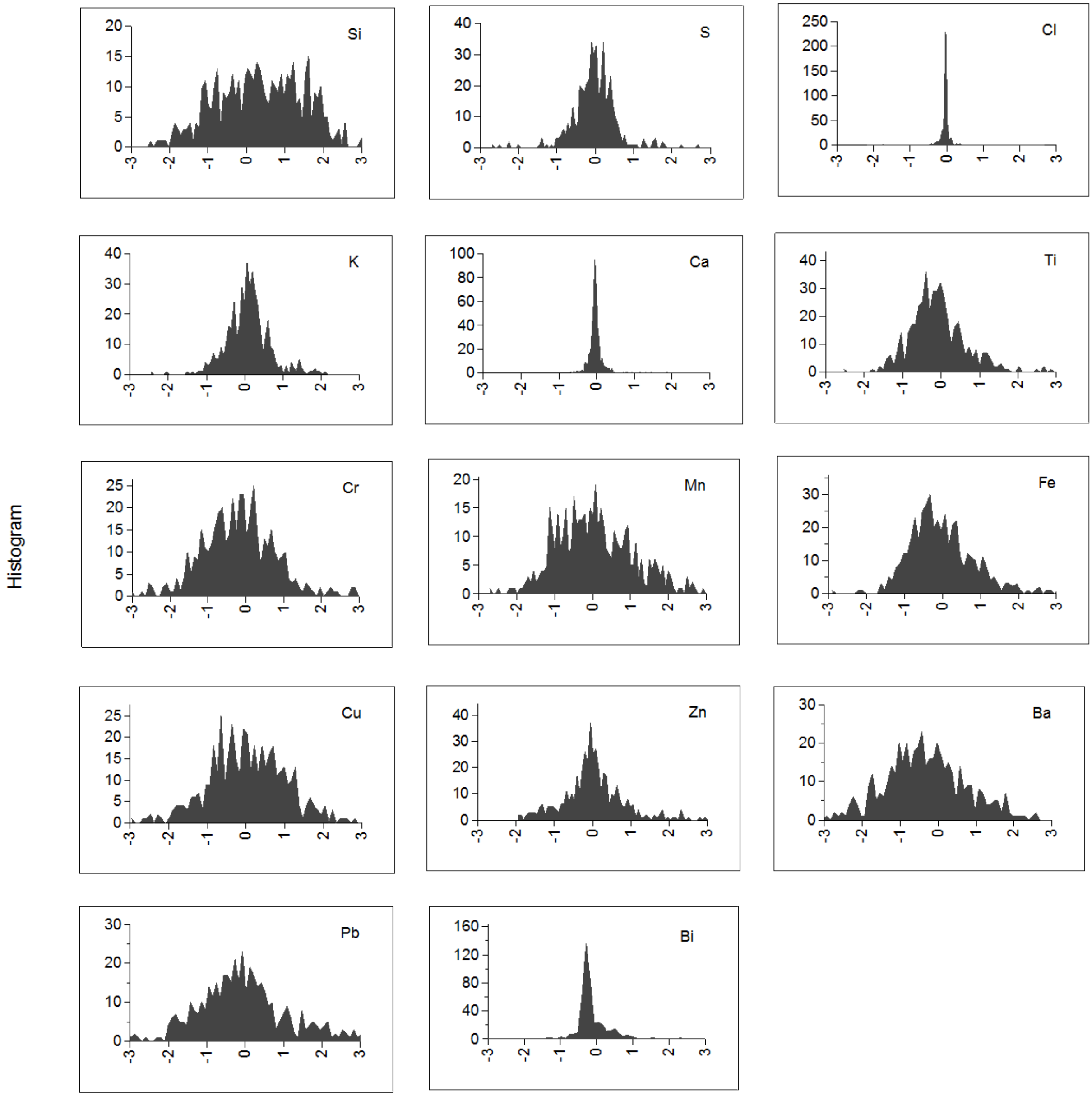

Figure S10~~5~~: Histograms of variables as a function of residuals weighted by the uncertainty (residual/uncertainty) for the eight-factor solution.

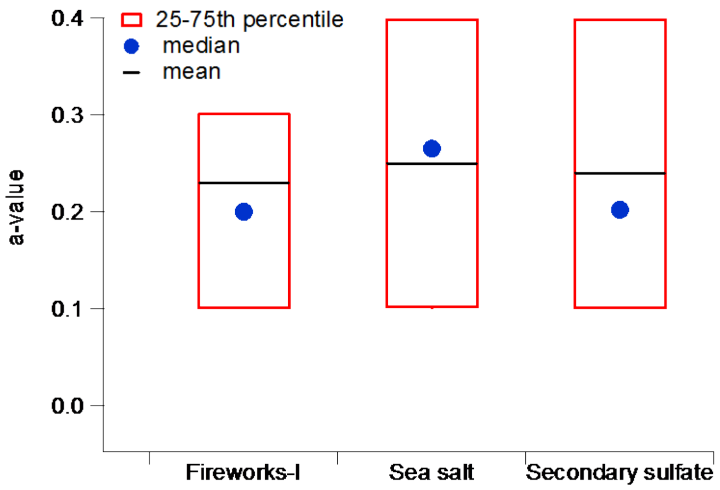

Figure S11~~6~~: *a*-value statistics of the accepted solutions. *a*-values between 0 to 0.5 were explored during BS analysis. The average *a*-value of the selected solutions was ranging from 0.2 to 0.3 for the constrained factors. The selected *a*-values were homogeneously distributed over that range.

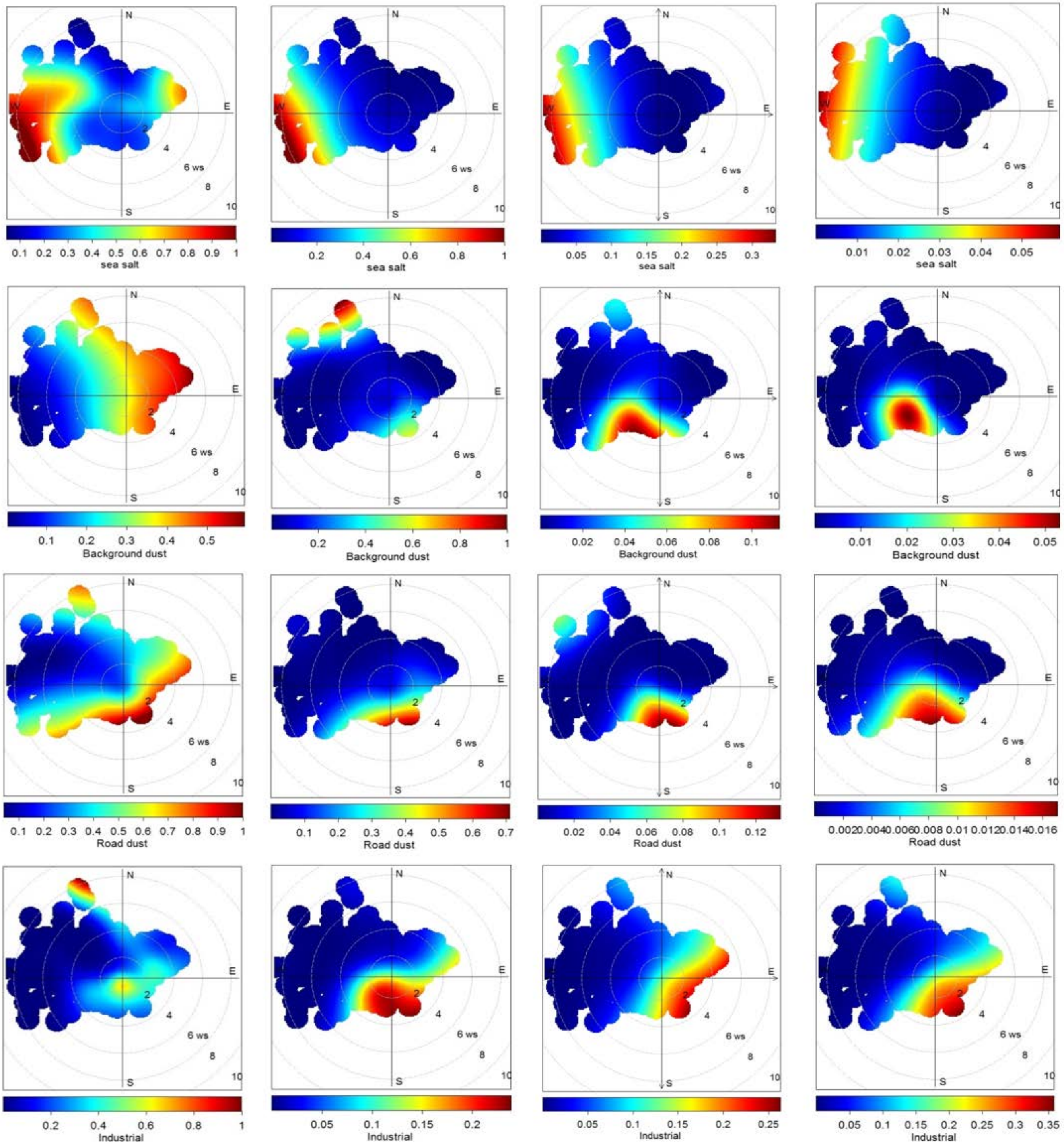

Figure S12~~6~~: CBPF analysis (from left to right: 50th, 75th, 90th, 95th percentiles) of factors (sea salt, background dust, road dust, industrial) in terms of wind speed (m s^{-1}) and wind direction. The color code represents the probability of the factor contribution.

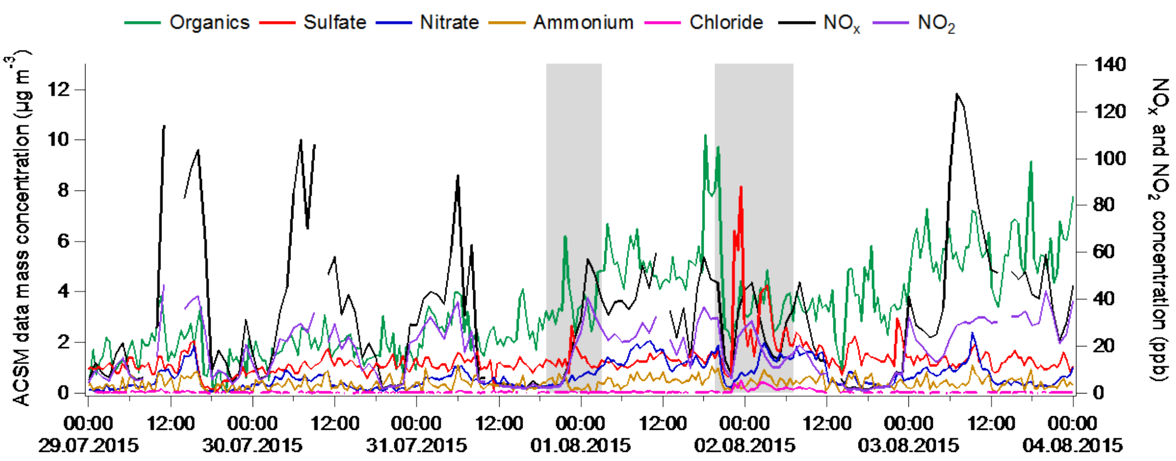

Figure S13~~7~~: Time series of the non-refractory aerosol components (measured with the ACSM), NO_2 and NO_x concentration. The fireworks episodes are underlain in grey color.

Fig. S14~~8~~ provides an estimate of the overall fireworks composition and temporal variability, complementing the PMF results (which are shown for reference). The figure is constructed in two stages. First, the time series of fireworks contributions to each element is estimated by subtracting the non-fireworks factors (NFF) from the original measurements. Then, the estimated fireworks contribution for each element is normalized by the total fireworks element contribution, and the displayed statistics are calculated. This is represented mathematically below, and the expression has been added to the main text. Note that the variation in fireworks profiles implied by this figure supports the representation of fireworks by 2 fireworks factors.

$$normalized\ concentration_{ij} = \frac{x_{ij} - \left(g_{ik} f_{kj}\right)_{k=NFF}}{\sum_j \left(x_{ij} - \left(g_{ik} f_{kj}\right)_{k=NFF}\right)} \qquad (S2\cancel{1})$$

where X represents the input data matrix for PMF, while G and F represent the factor time series and factor profiles driven by six non-fireworks factors (NFF). Here *i* and *j* denote time series and variables, respectively.

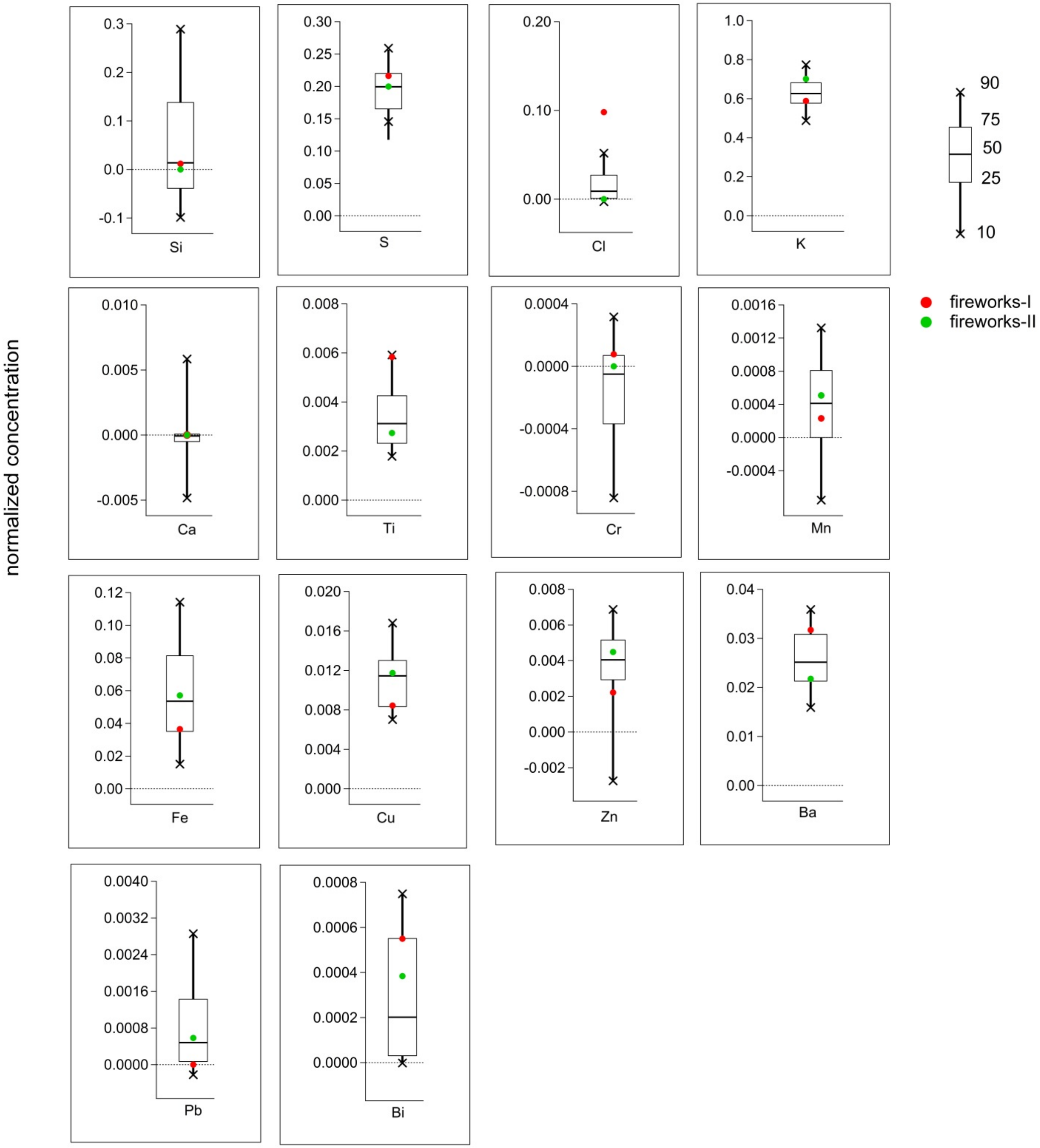

Figure S14~~8~~: Representation of fireworks data points (normalized concentration) in terms of median and 10-25-75-90th percentiles (bottom to top). Red and green dots denote the factor profiles of fireworks-I and fireworks-II, respectively.

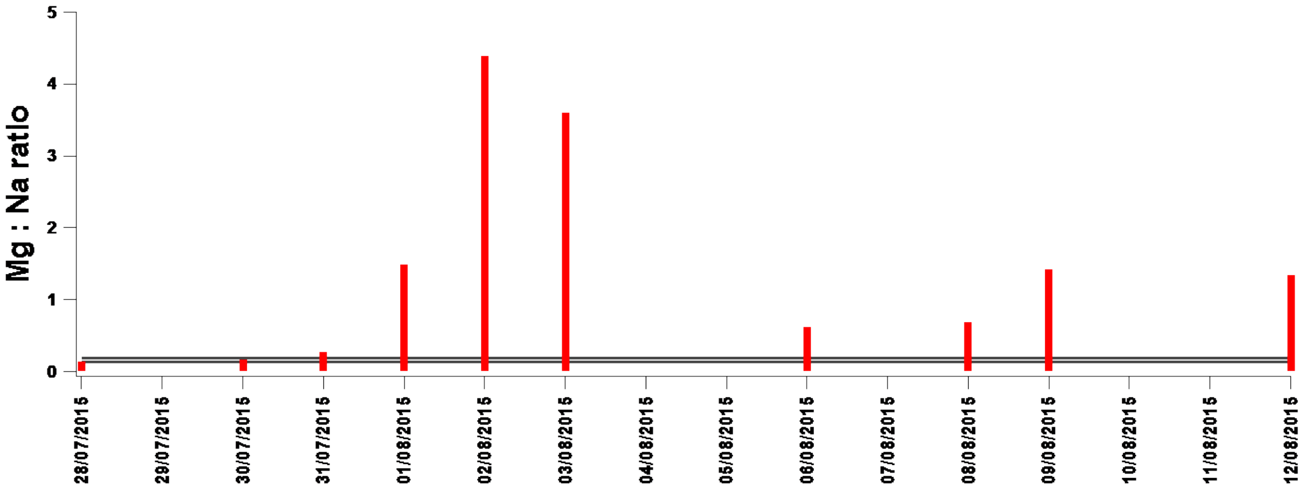

Figure S15~~0~~: Mg / Na ratio (red bars) for 24-h filter data analysed by ICP-OES. The gray lines represent the Mg / Na ratio range (0.132 -0.185) in marine aerosols. The Mg / Na ratio was 0.13 and 0.16 for 28 July and 30 July, respectively while for the rest of the days it was higher than 0.185.

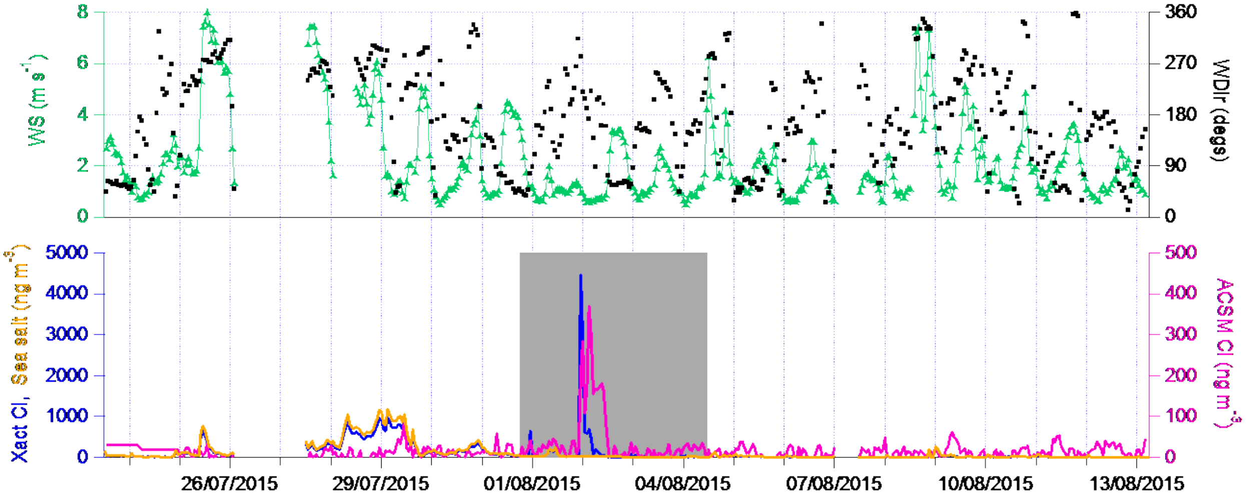

Figure S16~~1~~: Bottom panel: Time series of the Cl concentration from the Xact, sea salt factor (left y-axis) from the PMF solution, and ACSM chloride concentration (right y-axis). Top panel: Wind speed (WS in m s^{-1}) and wind direction (WDir in degree) during the measurement period. The grey area in the bottom panel represents fireworks days.

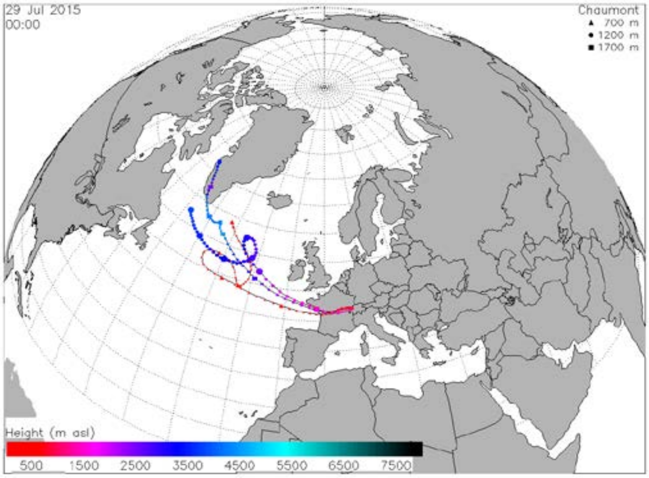

Figure S17~~2~~: Backward trajectory (produced from the FLEXTRA Trajectory Model; *https://folk.nilu.no/~andreas/flextra.html*) analysis at different heights during a sea salt event.

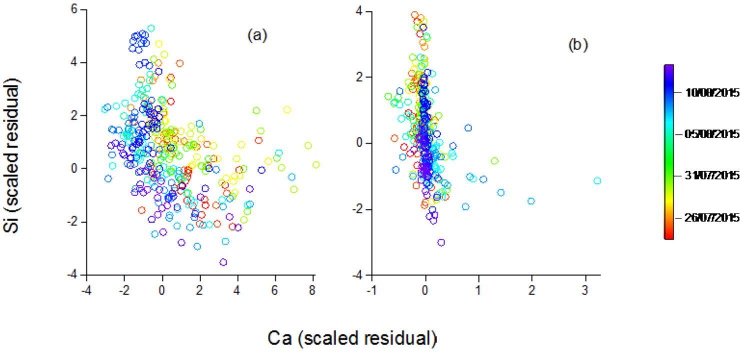

Figure S18~~3~~: Scatter plot of Si vs. Ca scaled residuals: (a) PMF solution with one dust factor; (b) PMF solution with two dust factors.

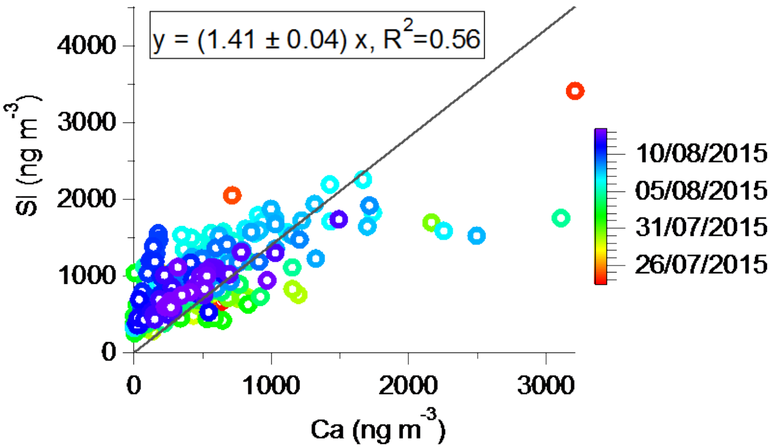

Figure S19~~4~~: Scatter plot of Si vs. Ca.

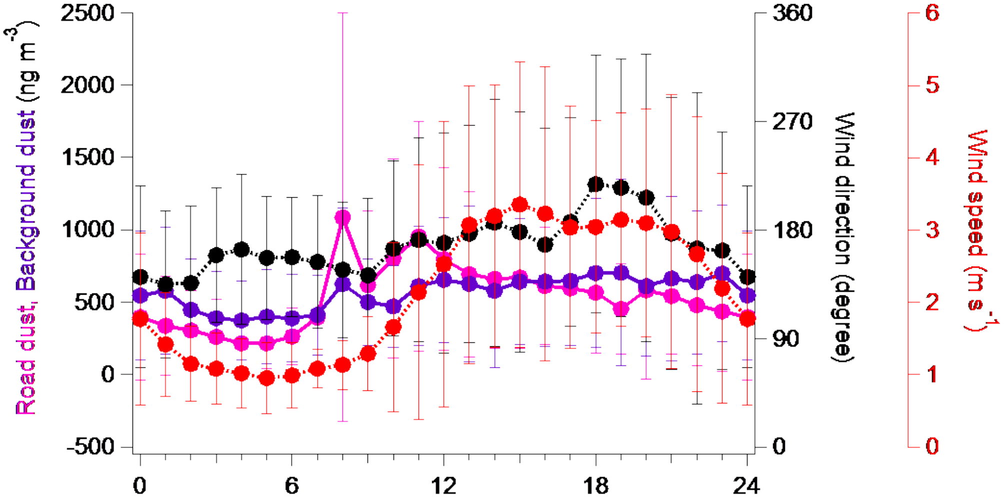

Figure S20~~15~~: Mean diurnal variations of the two dust factors (left-y axis) along with wind speed and wind direction (right y-axes) with error bars (one standard deviation).

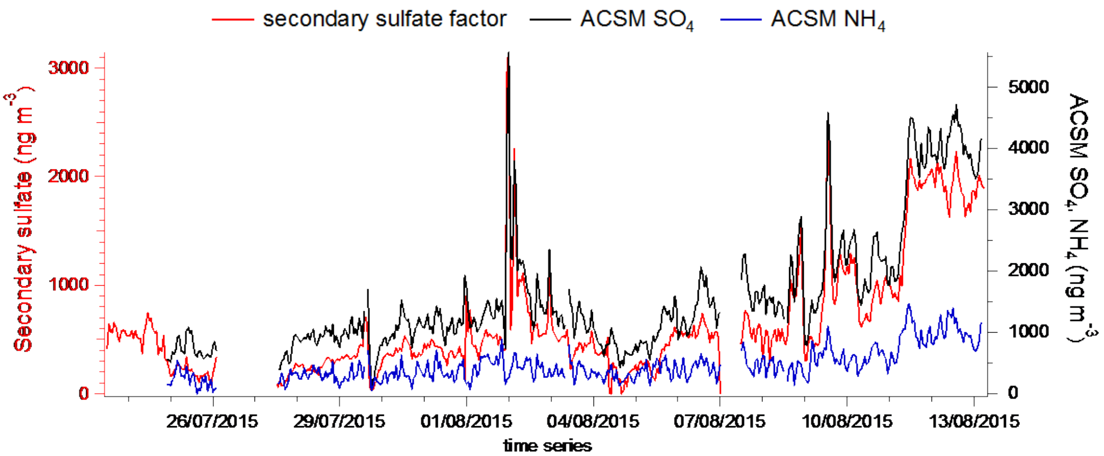

Figure S21~~9~~: Time series of the secondary sulfate factor (left y-axis) and mass concentration of SO$_4$, NH$_4$ from the ACSM (right y-axis).

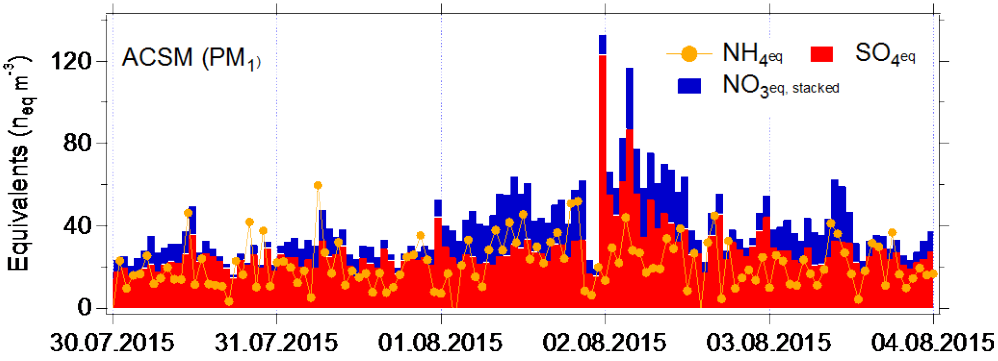

Figure S22: Time series of equivalent concentrations of the ACSM (PM$_1$) NH$_{4eq}$, and NO$_{3eq}$ and +2*SO$_{4eq}$. The NO$_{3eq}$ is stacked on 2*SO$_{4eq}$.

References

Canonaco, F., Crippa, M., Slowik, J. G., Baltensperger, U., and Prévôt, A. S. H.: SoFi, an IGOR-based interface for the efficient use of the generalized multilinear engine (ME-2) for the source apportionment: ME-2 application to aerosol mass spectrometer data, Atmos. Meas. Tech., 6, 3649–3661, https://doi.org/10.5194/amt-6-3649-2013, 2013.

Dutcher, D. D., Perry, K. D., Cahill, T. A., and Copeland, S. A.: Effects of indoor pyrotechnic displays on the air quality in the Houston Astrodome, J. Air Waste Manage. Assoc., 49, 156–160, https://doi.org/10.1080/10473289.1999.10463790, 1999.

Paatero, P.: User's guide for positive matrix factorization programs PMF2 and PMF3, 2004.